CHARACTERISING THE COMPOSITIONAL VARIATIONS OF THE MARTIAN NORTHERN LOWLANDS: INSIGHTS FROM CRISM AND OMEGA DATASETS

RACHAEL MARTINA FERNANDO MARSHAL
June,2020

SUPERVISORS:
W.H.Bakker, MSc
Dr. F.J.A. van Ruitenbeek
ADVISOR:
O.M Kamps, MSc

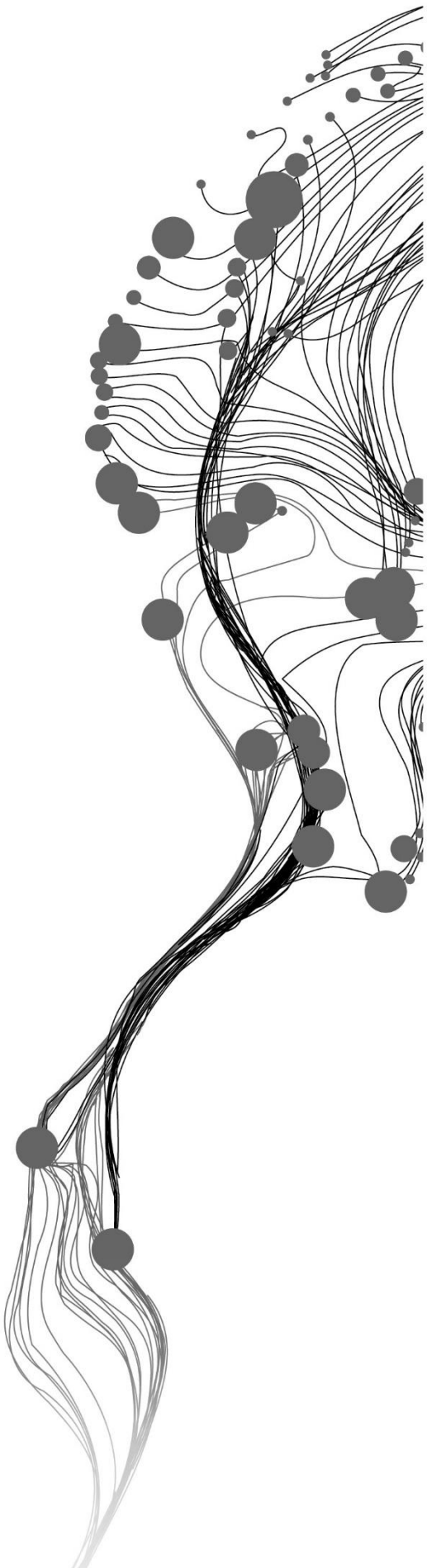

CHARACTERISING THE COMPOSITIONAL VARIATIONS OF THE MARTIAN NORTHERN LOWLANDS: INSIGHTS FROM CRISM AND OMEGA DATASETS

RACHAEL MARTINA FERNANDO MARSHAL
Enschede, The Netherlands, June 2020

Thesis submitted to the Faculty of Geo-Information Science and Earth Observation of the University of Twente in partial fulfilment of the requirements for the degree of Master of Science in Geo-information Science and Earth Observation.

Specialisation: Applied Remote Sensing for Earth Sciences

SUPERVISORS:

W.H.Bakker, MSc

Dr. F.J.A. van Ruitenbeek

ADVISOR:

O.M Kamps, MSc

THESIS ASSESSMENT BOARD:

Prof. dr. Mark van der Meijde (Chair)

Prof. dr. Kim Hein (External Examiner, emeritus & visiting professor at the University of the Witwatersrand, South Africa)

DISCLAIMER

This document describes work undertaken as part of a programme of study at the Faculty of Geo-Information Science and Earth Observation of the University of Twente. All views and opinions expressed therein remain the sole responsibility of the author, and do not necessarily represent those of the Faculty.

ABSTRACT

In the study of Kamps et al., (2019), Martian global surface types are classified based on the downsampled 5 °x 5° averaged CRISM multispectral summary product data. The surface type classification map indicated two units for the Northern Lowlands, i.e., the Northern Lowlands Unit and the Northern Transition Unit. Since subtle compositional variations may not be apparent in the averaged resolution, my research will investigate the findings of Kamps et al., (2019) in particular – the Northern Lowland and Transition Unit in the original data resolution of CRISM multispectral products. This thesis will focus on characterising the compositional variations prevailing over the Northern Lowlands of Mars, in particular, the region Acidalia Planitia. In addition to the regional characterisation of the study area using the CRISM dataset, my thesis also characterises local variations using the OMEGA dataset.

The composition of the Northern Lowlands has been studied before using data from the Thermal Emission Spectrometer and the Observatoire pour la Mineralogie, l'Eau, les Glaces et l'Activite – OMEGA but not using the multispectral dataset of the CRISM.

In my study, a principal component analysis (PCA) is carried out on the CRISM summary product data. Significant products contributing to the variance in the regions are identified, following which the regions exhibiting patterns in the PCA composites are demarcated. The mean spectra of the demarcated regions are analysed. A continuous downward negative spectral slope is identified as a ubiquitous characteristic of the Northern Lowlands. The parameter ISLOPE1 is designed to pick up this downward spectral slope, but the product ISLOPE1 has limitations that it only samples reflectances at two wavelengths: 1815nm and 2530nm. In order to improve the quantification of the spectral slope, an alternate refined spectral slope parameter that measures the slope of the regression line fitted through the wavelengths 1000nm – 2000nm is introduced in my study. The mean spectral slope of the CRISM reflectance strips shows an increase in absolute value as we move northward from the Transition Unit into the Northern Lowland Unit.

The mineralogical interpretation of the spectral slope is that it might be indicative of a weathering rind on basaltic glass or glassy basalt. This interpretation favours a weathered origin over an andesitic origin for the surface type associated with the Northern Lowlands.

Apart from the spectral slope, the Transition unit shows patterns of higher interpreted content of the olivine associated with crater ejecta, higher albedo, higher values for the dust products and shows an increase in elevation, in comparison to the Northern Lowland Unit.

Lastly, localised patterns are identified at the Highland-Lowland dichotomy and Mawrth Vallis using the OMEGA dataset. These regions indicate a presence of phyllosilicate minerals that may be remnants of an altered Noachian crust that is only locally exposed since much of the Northern Lowlands has been covered by younger Hesperian material. These localised regions may be indicative of a regional aqueous alteration of the Noachian crust in the ancient history of Mars. Following the Noachian period, the Northern lowlands have been extensively reworked by influx from the Highlands via the Circum-Chryse outflow channels and relatively recent weathering processes that could have been the reason for the ubiquitous spectral slope identified in this thesis.

ACKNOWLEDGEMENTS

I would like to thank my supervisors Wim Bakker and Frank Van Ruitenbeek for their thought-provoking questions, guidance, support, and encouragement throughout this research phase. I would also like to thank Oscar Kamps for the valuable discussions, suggestions, and insights since the early phases of my research.

I would like to extend my gratitude to the ITC Excellence Scholarship for financially supporting my education here. My gratitude to all the lecturers who taught me at ITC and to all my friends here.

My sincere gratitude to Dr S. Sanjeevi for his continued support and mentorship since my bachelor's degree. Thank you for also introducing me to the world of geosciences.

A big thank you to my parents and my brother for always motivating me, believing in me and making me see the brighter side of things even during the stressful times.

My heartfelt thanks to Jasim for always being my pillar of support. Many thanks to Keerthana for always being there through the many journeys of life.

Finally, but most importantly, I would like to thank the Almighty for the courage and the knowledge to carry out this study.

TABLE OF CONTENTS

LIST OF FIGURES

LIST OF TABLES

1. INTRODUCTION

Studying the Martian surface composition is essential to understand its history and current condition and pave the way to unveiling the nature of occurrences of detected minerals - be it weathering, precipitation, or of volcanic origin (Bandfield, Hamilton, & Christensen, 2000). The Martian crust is basaltic with variations occurring across its most striking feature – the dichotomy (Ehlmann & Edwards, 2014). The Martian dichotomy divides the Northern Hemisphere from the Southern Hemisphere (Watters, Mcgovern, & Iii, 2007) and its origin has been a long-standing question. The suggested hypotheses for the origin of the dichotomy include mantle convection or a large impact origin (Andrews-Hanna, Zuber, & Banerdt, 2008). Studies using orbital data from the VNIR-SWIR, and the TIR parts of the spectrum have indicated varying compositions on either side of this dichotomy.

As a part of an ongoing project, Kamps, Hewson, van Ruitenbeek, & Meer, (2019), study the surface of Mars using downsampled data products from the Compact Reconnaissance Imaging Spectrometer for Mars - CRISM (Murchie et al., 2007). My research will investigate the findings of Kamps et al. (2019) in the original data resolution of CRISM with a focus on characterising the compositional variations prevailing over the Northern Lowlands of Mars, in particular, the region Acidalia Planitia.

1.1. Background

In this section, I will briefly discuss the global surface studies on Mars using various instruments, following which I will introduce the background of my study.

1.1.1. Surface Studies on Mars – OMEGA, TES

Multiple instruments have been employed to carry out Martian surface studies. These include the Thermal Emission Spectrometer - TES (Christensen et al., 2001), Observatoire pour la Mineralogie, l'Eau, les Glaces et l'Activite - OMEGA (Bibring et al., 2004) and the Compact Reconnaissance Imaging Spectrometer for Mars - CRISM (Murchie et al., 2007).

On a global scale, multiple studies have been carried out using OMEGA data to investigate mineral occurrences (Carter, Poulet, Bibring, Mangold, & Murchie, 2013; Riu, Poulet, Bibring, & Gondet, 2019). One such example is the study to identify the distribution of anhydrous minerals on the Martian surface by Ody et al. (2012) using calculated spectral parameters or indices developed by Poulet et al. (2007) to generate global distribution maps for Olivine, Dust and Ferric oxides (see Appendix 2), that provide a useful resource for my study.

The Thermal Emission Spectrometer (TES) has been a critical instrument for global scale Martian surface studies. The study by Bandfield et al. (2000) utilised the TES data and primarily identified two distinct global surface types - Surface type 1 (ST1) being basaltic and concentrated in the Southern Highlands and Surface type 2 (ST2) being andesitic and concentrated in the Northern Lowlands, with the boundary between these two types occurring approximately around the planetary dichotomy.

The CRISM instrument onboard the Mars Reconnaissance Orbiter has also been useful in studying the Martian surface but on a localised scaled (Glotch, Bandfield, Tornabene, Jensen, & Seelos, 2010; Ehlmann et al., 2009) and for the first time on a global scale by Kamps et al. (2019).

1.1.2. Surface Studies using CRISM

The first study to employ the CRISM data for global surface mapping is the project by Kamps et al. (2019), namely the 'Defining Surface Types of Mars using Global CRISM Summary Product Maps'. The study of Kamps et al. (2019) aims towards a comprehensive mineralogical characterisation of the surface of Mars using CRISM multispectral mapping mode (MSP) summary products. These summary products are 'indices' generated by focussing on a specific spectral feature, from the entire spectrum, extracted using a parameter by utilising required mathematical operations (Pelkey et al., 2007).

The CRISM summary products are of two versions. The Pelkey et al. (2007) version (henceforth referred to as the 'Pelkey products') included 44 summary products to characterise different types of minerals, atmosphere constituents and aerosols. This set of summary products contains a few caveats, namely the abundance of false positives that occur even after reflectance corrections mainly due to instrument noise (Pelkey et al., 2007). Viviano-Beck et al. (2014) then updated the Pelkey products using corrected spectral reflectance at certain wavelength positions of the CRISM in its targeted observation mode, to map the heterogeneous nature of the Martian surface. These updated products are henceforth referred to as 'Viviano-Beck products' in this thesis. The Viviano-Beck products contain indices that have been derived to focus on recently acquired spectral information on new areas (Viviano-Beck et al., 2014). Products describing mafic mineralogy, i.e. OLINDEX, LCPINDEX, HCPINDEX have been refurbished extensively to include more wavelength channels to fine tune the parameters (Viviano-Beck et al., 2014).

Summary products have been vital in identifying various mineralogical associations and patterns over the surface of Mars. The identified minerals along with their type locality (on Mars) are compiled into a spectral library, that is useful for spectral studies as a reference, called the 'Minerals Identified through CRISM Analysis' (K. D. Seelos, Viviano, Ackiss, Kremer, & Murchie, 2019). Kamps et al. (2019) have employed both the versions of the summary products to generate a global map of surface types. For my study, I will focus on the surface types classifications generated by utilising the Viviano-Beck products.

The surface type map generated (Figure 1) using the Viviano-Beck summary products by Kamps et al. (2019), provides the base of my study. Kamps et al. (2019) identify two units in the Martian Northern Lowlands, i.e. the Lowland unit and the Transition unit. In my study, I will investigate in detail the surface type units classified within the Northern Lowlands and characterise the overall variance in this region

1.2. Research Problem

The main problem my research deals with is a comprehensive investigation of the compositional variations in the Northern Lowlands of Mars.

The global surface type map generated by Kamps et al. (2019) shown in Figure 1 is the result of a hierarchical clustering analysis done on 5° x 5° downsampled CRISM summary product data. After the clustering analysis, Kamps et al. (2019), carried out a partial least squares discriminant analysis to analyse the variation between identified clusters. The resulting classification of the low-

resolution dataset shows variations in the hemispherical composition similar to what has already been observed (Bandfield et al., 2000) i.e., the Northern Lowlands showing a decreased value for the pyroxene index, a high value for the ISLOPE1 product (interpreted as a ferric coating by Viviano-Beck et al. (2014)) whereas the Southern Highlands show an increased abundance of mafic minerals compared to the Northern Lowlands.

My study will focus on characterising the general variance observed in the Northern Lowlands and study in detail the transitions between the surface type units in the lowland region, using the original non-downsampled resolution. Since subtle variances are difficult to observe in the downsampled resolution used by Kamps et al. (2019), my study will characterise and map variations in this region using the original resolution CRISM MSP summary products and the CRISM MSP reflectance data. I also use secondary datasets and maps from OMEGA, TES to put in context the mapped variations.

To the best of knowledge, a detailed characterisation of the Northern Lowlands primarily using the CRISM multispectral mapping mode data in its original resolution has not yet been done before.

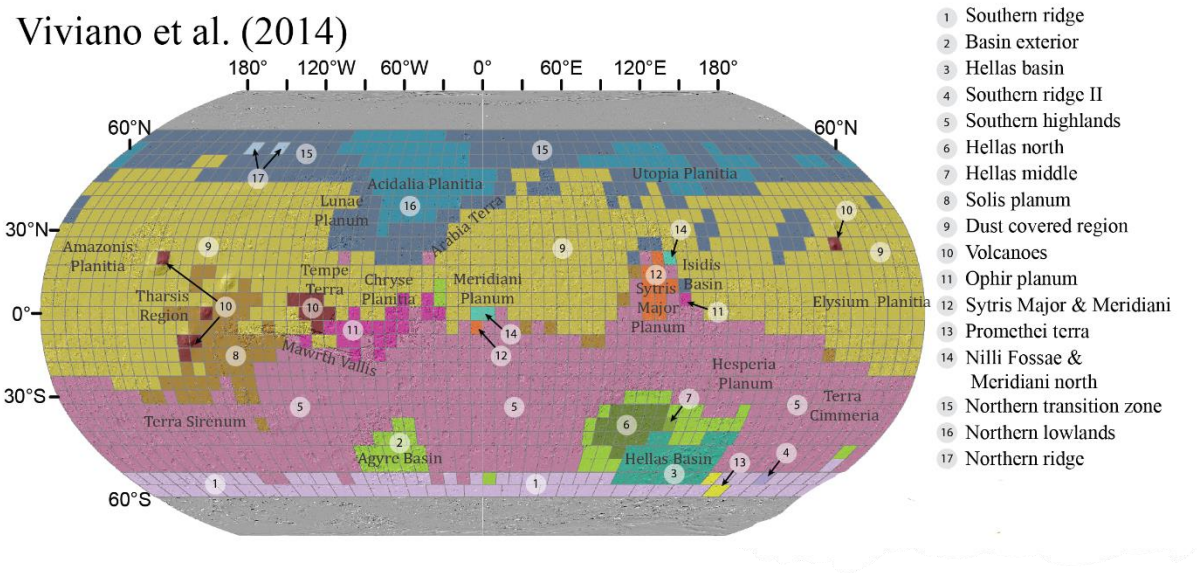

Figure 1: Surface type classification from the study of Kamps et al., (2019)

1.3. Research Objectives

The main objective of this project is to analyse and map the compositional variations in the Northern Lowlands of Mars. The specific research objectives include:

1) To study the surface composition variations in the Northern Lowland region and its immediate surroundings
2) To understand the characteristics of the observed variations – spatial and mineralogical.
3) To put the observed compositional variations in geologic context

1.4. Research Questions

1) What is the nature of the observed variations in the Northern Lowland region?
2) How does the regional geology relate to the area of observed compositional variations?
3) What are the summary products and associated mineral groups that primarily characterise the variations in the study area?
4) How does the integration of the OMEGA dataset, global maps and TES maps relate to the variations identified by the CRISM dataset?

1.5. Study Area

The study area for this research is the Northern Lowlands centred around Acidalia Planitia, as seen in Figure 2.

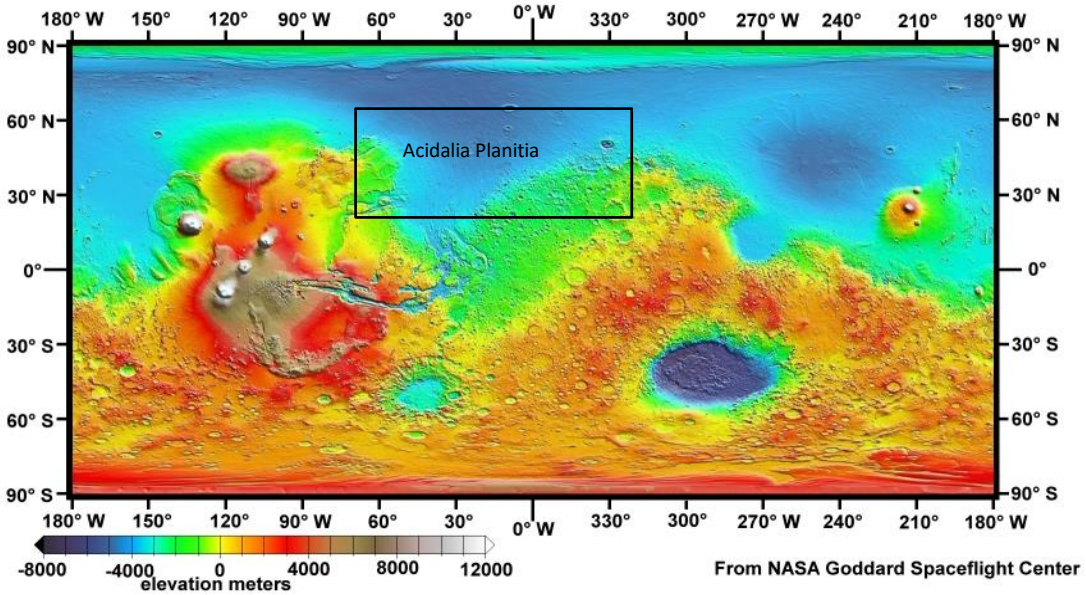

Figure 2: Study area indicated in the black square overlain on Mars Orbital Laser Altimeter - MOLA elevation layer (Smith et al., 1999)

The Northern Lowlands vary significantly in elevation with a difference of about 6km from the Southern Highlands across the dichotomy that likely formed as a result of an impact event (Marinova, Aharonson, & Asphaug, 2008). The Northern Lowlands have a much lower crustal thickness of ~35km when compared to ~75 km of the Southern Highlands (Pan, Ehlmann, Carter, & Ernst, 2017; Zuber, 2000). The Northern Lowlands appear to be smoother/less cratered and covered by Hesperian aged material implying a younger age than the Southern Highlands (Tanaka, Robbins, Fortezzo, Skinner, & Hare, 2014). But studies using data from the MOLA indicate that what is seen immediately is an overlaying sedimentary layer beneath which a much ancient Noachian crust is buried (Frey, Roark, Shockey, Frey, & Sakimoto, 2002)

The composition of the Northern Lowlands itself has been a subject of interest (Carr & Head, 2010) as it can furnish a better understanding of the complex processes that led to its formation. Multiple theories have been put forward regarding the composition on the Northern Lowlands. Bandfield et al. (2000) characterise the Northern Lowlands to be of andesitic volcanic origin (ST2) while Wyatt & McSween (2002) speculate after modelling the surface type spectra (from TES) to their tailored end member library, that the Northern Lowlands are more similar to weathered basalt

under submarine conditions rather than andesite. Such speculation hints the existence of a northern lowland ocean. However, a widespread ocean is again doubtful (Head et al., 2018) and has not yet been conclusively proven.

Nevertheless, studies show that the Northern Lowlands repeatedly received an influx of fluid or lava or sediments (Fishbaugh, Lognonné, Raulin, Des Marais, & Korablev, 2007) through the Circum-Chryse outflow channels that would have led to complex layering within the lowland basins. Studies of crater ejecta in the Northern Lowlands also show occurrences of mafic mineralogy (Section 4.1.1.1) , and this pattern strengthens the possibility that an ancient mafic crust is under the heavily altered surface of the Northern Lowlands (Ehlmann & Edwards, 2014). In summary, previous studies have shown that the Northern Lowlands seems to have developed from various complex surface processes, i.e. sedimentation, aqueous alteration, weathering, that have not yet been fully understood. This study will focus on characterising the region shown in Figure 2 using original resolution CRISM MSP data along with maps from TES, OMEGA and selected OMEGA scenes.

1.6. Dataset

The primary dataset for this study is from the CRISM instrument onboard the Mars Reconnaissance Orbiter. This instrument images the surface of Mars in two modes – multispectral mapping mode and the targeted mode. The multispectral mapping mode has a resolution of about 200-300m/pixel and consists of 73 bands . The hyperspectral targeted mode has a resolution of 18-20m/pixel and consists of 545 bands (Murchie et al., 2007).

Since this study investigates the units identified by Kamps et al. (2019) in detail, the dataset utilised is the same as on which the global mapping was carried out (see Figure 1). In this research, the non-downscaled CRISM multispectral mapping mode data and the corresponding summary products are employed. The multispectral mapping mode data are in the form of orbital strips that are then mosaicked into 5°x5° tiles and are available for download at the Mars Orbital Data Explorer portal. These mosaicked tiles provide broad coverage of about 87% of the Martian surface and make it suitable to be used for regional studies (F. P. Seelos, Murchie, & Hopkins, 2018). A major drawback of the mosaicked dataset is the radiometric levelling differences between strips that make adjacent strips look starkly different (F. P. Seelos et al., 2018).

Additionally, to investigate spatial patterns in detail, especially in regions of interesting local variations, the OMEGA hyperspectral dataset is utilised. The OMEGA instrument onboard the Mars Express offers global coverage of Mars because of the high degree of inclination of the orbit (Bibring et al., 2004). The OMEGA instrument images the surface of Mars in three channels spread across the wavelengths 0.38μm to 5.1μm (Bibring et al., 2004). The resolution of the imagery is altitude dependent and varies from 3km to 300m. The resolutions coupled with the highly inclined orbit, enable the OMEGA dataset to be utilised to study reasonably large regions and view spatial patterns in context (Bakker et al., 2014). However, a drawback of the OMEGA scenes used in my study do exhibit spatial misregistration across the merged channels.

2. METHODOLOGY

In this chapter, I will outline the main steps taken in order to answer the research questions presented in Chapter 1.
This thesis aims to characterise the compositional variations in the Northern Lowlands of Mars. Since the study area is large, the demarcation of regions exhibiting variations is done to streamline the study. The region demarcation is done by visualising composites of the Principal Component Analysis. After demarcating regions, they are characterised spectrally by extracting mean spectra from the regions of interest.
Apart from characterising the regional compositions, local variations are also studied using the OMEGA scenes.

2.1. Data Preprocessing

As mentioned in section 1.6, my study mainly utilises data from the CRISM and selected scenes from OMEGA. In the following subsections, the various pre-processing steps taken before the data analysis is described.

2.1.1. CRISM Dataset

In this study, I only employ the Viviano-Beck products. The multispectral mapping mode CRISM orbital strips are mosaicked into 5°x5° tiles and are called MRDR – Multispectral Reduced Data Records (Murchie et al., 2007). The summary products have been calculated onto the atmospherically and photometrically corrected albedo MRDR dataset (Kamps et al., 2019) and then mosaicked into an extent covering the region Acidalia Planitia and its immediate surroundings as shown in Figure 5. The spatial resolution of this dataset is ~200m per pixel (Pelkey et al., 2007). A limitation of the CRISM MRDR dataset is the presence of outliers for the summary products. To minimise the effect of these extreme values on our study, I calculate thresholds to find outliers for each of these summary products for the study area extent using Tukey's fences (Tukey, 1977) with an interquartile distance of 1.5, similar to what was done in the study by Kamps et al. (2019). These outliers beyond the defined thresholds are then masked out, and maps for each summary product were made to visualise the values for each summary product in the region. The maps produced for my study area, along with the global averaged maps by Kamps et al. (2019) played an important factor in selecting which of the summary products would be utilised for the exploratory data analysis. Another factor that played a role in making a selection of the summary products was the grouping of the summary products into categories (dust cover, atmosphere thickness, mafic mineralogy, hydrated mineralogy, ferric minerals) by Kamps et al. (2019) based on the interpretations by Viviano-Beck et al. (2014).
The summary products after being pre-processed were subject to a principal component analysis, as described in Section 2.2.1. Patterns exhibited in the PCA composites, as highlighted in Section 3.2, are required to be characterised spectrally as well to understand the compositional variations better. Since summary products are indices calculated onto the spectra, heterogeneities identified in the summary products would also reflect back in the spectra. These heterogeneities would play a key role in characterising the regions spectrally. Hence for this purpose, the orbital reflectance data was utilised. After identifying zones of interest from the PCA (see section 2.2.1), reflectance

orbital strips (MSP) data crossing these regions are downloaded from the Mars Orbital Data Explorer. These MSP data strips are the parent data which has been mosaicked and on which the summary products described previously have been calculated. The selection of orbital strips was made systematically to ensure strips of good quality with a minimum presence of outliers. The selection was made by first drawing polygons on the summary product mosaic in regions that showed variations/patterns. These polygons were then imported into JMARS(Java Mission-planning and Analysis for Remote Sensing) and then the CRISM MSP stamps that overlap these polygons were chosen. The IDs of these stamps were noted (Appendix 6) and then downloaded from the Mars Orbital Data Explorer.

After downloading these strips, the pre-processing was done, as indicated in Figure 3. It is important to note that the VNIR-SWIR is split between data cubes when downloading data from Mars ODE. S- refers to the VNIR range, and L refers to the SWIR range. The CRISM MSP data have already been solar corrected and is available in I/F units (radiance/irradiance) (Murchie, Guinness, & Slavney, 2016). For my thesis, the I/F data is atmospherically corrected (SWIR set), photometrically corrected, map projected (using CRISM Analysis Toolkit - CAT) and then layer stacked.

Further, due to the noisy nature of the CRISM MSP strips for the study area, a spectral mean filter (using HypPy) was also applied to the dataset. Miscellaneous data pre-processing techniques, including spectral subsetting, masking background values were also carried out for my research. Summary products were also calculated on the individual MSP strips using the CAT ENVI plugin.

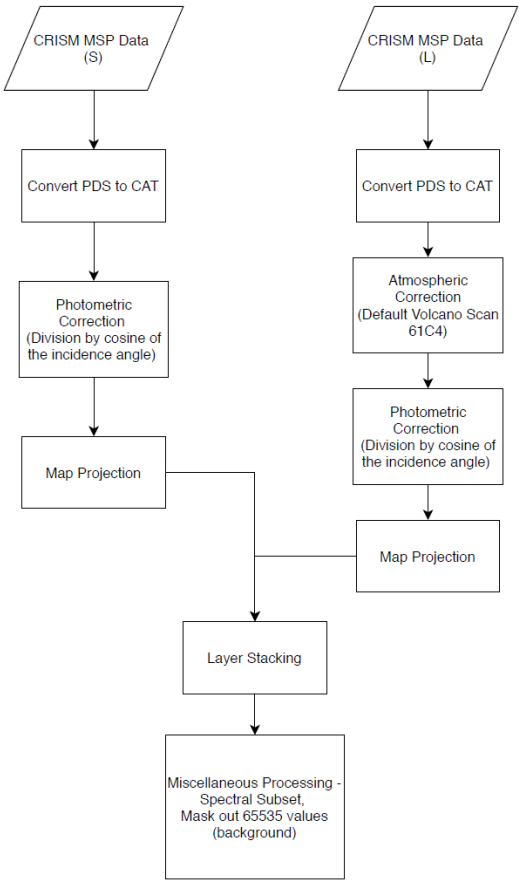

Figure 3: Flowchart showing CRISM MSP orbital I/F data pre-processing

2.1.2. OMEGA Dataset

The OMEGA dataset having a larger field of view and offering a more extensive image area makes it better suited to put in context the variations visible in the CRISM MSP dataset. The OMEGA dataset is downloaded from the Planetary Science Archive and pre-processed using the steps prescribed by (Bakker, 2018). A simplified flowchart of the prescribed pre-processing steps is shown in Figure 4.

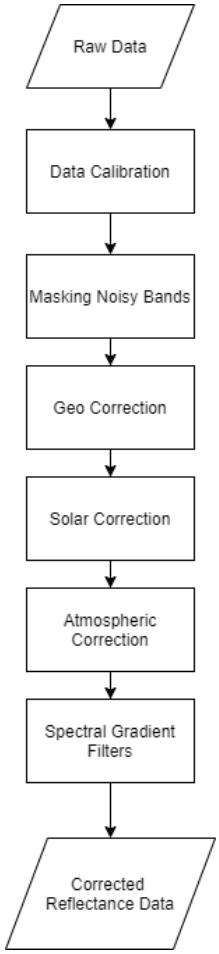

Figure 4 : Simplified flow chart indicating the main pre-processing procedures (Bakker, 2018)

2.2. Data Exploration

Since the study area is quite large, there was a need for demarcated regions of interest to align the analysis. Hence, a method to visualise the overall regional variance was utilised. In this case, it was the principal component analysis (PCA).

2.2.1. Principal Component Analysis

2.2.1.1. Theory

The PCA is a data transformation method utilised to minimise redundancy, i.e. reduce correlations within the dataset (Lillesand & Kiefer, 1979). It can be used for multiple purposes like dimensionality reduction, classification, choosing variables (Wold, Esbensen, & Geladi, 1987). In the context of remote sensing, PCA has often been used to reduce dimensions and reduce

correlations between bands in the image data. The PCA transforms the data cloud in directions that exhibit maximum variance. The transformation is done by by identifying axes within the data cloud that explain the most variance and projecting the data cloud onto these axes. The new values for these transformed data points is a linear combination of the principal components and coefficients known as eigenvectors (Lillesand & Kiefer, 1979).

For this study, the PCA was used as a data exploratory technique to identify and visualise the variance within the region that can then be studied further. An additional reason for choosing to analyse variance using the PCA was that it was a simple and efficient method to visualise the evident and subtle variances in a large dataset. For my study, the PCA was done utilising the scikit-learn package from Python, after standardising the dataset by subtracting the average and dividing by the standard deviation of the summary product for the study area. Since the summary product data layers had different data ranges, it was required to standardise the dataset before any statistical analysis.

2.1.1.1 Application to the dataset

A mosaicked set of MRDR tiles covering the study area is utilised for the PCA. Maps were generated for the study area for each summary product with the outliers masked out (as described in section 2.1.1) to give an idea on the patterns exhibited by the summary products. A sample of the subset summary product map of the study area is indicated below in Figure 5. This map shows the distribution of values for the summary product R770 that is reflectance at 770nm, where high values highlight dusty and icy surfaces (Viviano-Beck et al., 2014).

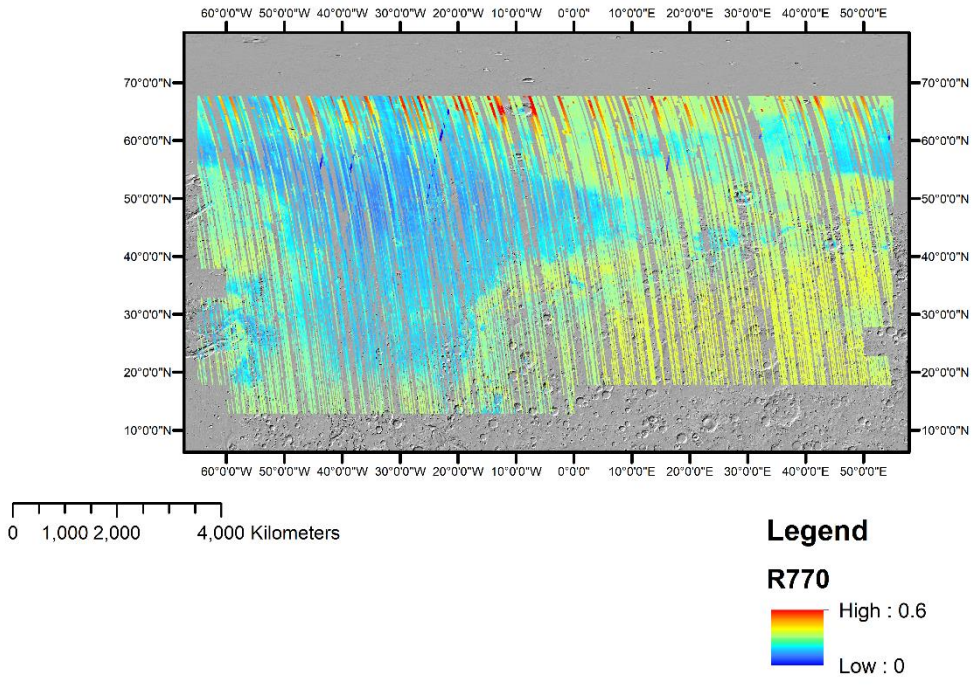

Figure 5: Map showing the summary product R770 for the study area

After visualising such summary product maps for the region, only those summary products were chosen which did not contain many outliers in the region of interest and contained coherent patterns. In addition to this filter, the grouping of summary products according to what information

they captured, i.e. dust, atmosphere, mafic, ferric (Kamps et al., 2019; Viviano-Beck et al., 2014), is also referred to while selecting summary products.

Since the major variations in the data were the difference between the data strips and the background 65535 values, it was necessary to eliminate the 65535 values from the PCA. Apart from the 65535 background values, outliers beyond the threshold defined (section 2.1.1) are also excluded from the PCA. This was done to minimise the effects of outliers and the background 65535 values, so the patterns exhibited were meaningful variances in the summary product. Hence, the approach was to completely ignore and exclude the 65535 values and the outliers beyond the defined thresholds. The next step was to transfer the valid data values into a 1D array, perform the PCA transformation and project it back into a 2D format. Concerning outliers, the PCA employed in my study was made to accept a pixel only if it was not an outlier in any of the summary product layers. There are two sides to this approach; the positive side is that it made the data manageable since a layer stack of 20 (and later 13) summary products was memory intensive and challenging to process. The downside is that, if a pixel is only an outlier in one of the layers, it still gets excluded from the analysis, thus resulting in a loss of information.

Another point to keep in mind is that this PCA also considered negative band depth values for the band depth parameters. A negative band depth is could be due to a lack of absorption feature or a noise peak (section 4.1.1.1). It may not be of mineralogical significance. To combat this, after the PCA was performed, the band depth products were analysed individually with only the non-negative values present since negative values were not describing the mineral group intended to be described. The distribution of the non-negative band depth products was plotted with a motive to identify trends in the occurrence of positive band depths with latitude (section 3.3).

The first trial of the PCA was employed using the summary products shown in Table 1. This PCA was then refined since products describing atmosphere and dust cover were still included, it was of interest to filter them out and visualise patterns that were not directly attributed to dust and atmosphere but rather indicated mineralogical variation. Hence, a second (final) trial of the PCA was employed with only a subset of the products from Table 1, i.e. products describing dust and atmosphere were excluded.

The summary products utilised are shown in Table 1, with the products excluded in the second (final) trial highlighted.

Table 1 Table indicating selected summary products. Products highlighted in beige were excluded in the second trial

Name	Type
R770	Dust
BD530_2	Dust
SH600_2	Ferric
SH770	Ferric
RPEAK1	Dust
BDI1000VIS	Dust/Mafic
OLINDEX3	Mafic
R1330	Dust
BD1300	Mafic

LCPINDEX2	Mafic
HCPINDEX2	Mafic
VAR	Dust
ISLOPE1	Ferric
ICER1_2	Dust
BD1900_2	Phyllosilicates
MIN2200	Phyllosilicates
BD2210_2	Phyllosilicates/Sulfates
SINDEX2	Sulfate
BD3400_2	Carbonate
CINDEX2	Carbonate

Next, individual components were visualised (see Appendix 1), and RGB composites (Figure 6) of the principal components were also visualised. The composites helped demarcate interesting zones of variance that were essential to help focus the spectral analysis. Additionally, the loadings and the variable contribution to the variance captured in the component were also calculated to facilitate a better understanding of what summary product is majorly responsible for the zonation we see.
The employed PCA does have certain limitations as described earlier, but it facilitated an analysis of the variance in the region that streamlined the study further. Based on the patterns visualised in the PCA, regions of interest were delineated. Some of these regions reappeared on the mafic browse product (Figure 9). All the visualised zonations demarcated were investigated further using the orbital reflectance data.

2.3. Spectral Analysis

As mentioned in Section 2.1.1, in order to complement the variations identified from the PCA composites with the spectral properties of the region, it was essential to spectrally chracterise the demarcated regions.

2.3.1. CRISM MSP Data

The multispectral reflectance data orbital strips were chosen within the zones demarcated from the PCA and browse product composites.
Large regions of interest of approximately 10000-12000 pixels were drawn on the MSP strips. The reason for the choice of large ROIs was because I wanted to focus on regional variations and not on describing the within-strip local patterns. The ROIs were chosen on either side of the zone demarcations (wherever zones were adjacent with each other). To ensure that relatively homogenous pixels were selected for a ROI, PCA composites of the individual strips were also utilised. After the ROIs were drawn, the mean ROI spectra are extracted and saved as a record in a spectral library.

2.3.2. Refined Spectral Slope Parameter

In my study, it is seen that the spectral slope is a dominant character exhibited by the Northern Lowlands. This slope was designed to be highlighted by the ISLOPE1 parameter (Viviano-Beck et al., 2014). However, the ISLOPE1 parameter only considers reflectance values at two wavelengths

1815nm and 2530nm while the slope begins ~1 μm. Hence, in my study, we introduce a new parameter that accounts for the slope of a fitted regression line between wavelengths 1 μm – 2 μm. This is done using the Spectral Slope tool in HypPy.

2.3.3. Region Spectra Extraction

To spectrally quantify the difference between the regions within Acidalia (see Figure 10) a mean regional spectrum for regions A, B and C is extracted from the set of MSP strips processed (see Appendix 6 for the list of IDs). From the extracted mean spectra, two values are computed – 1) average absolute value of the slope of the fitted regression line for the spectrum within wavelengths between 1 μm -2 μm (new ISLOPE parameter Section 3.4.3) and 2) the spectral angle between the mean spectra.

2.3.4. OMEGA Data

Fewer OMEGA images (Figure 21) were chosen than the CRISM MSP strips. The OMEGA images are mostly employed to study in better detail and spectral quality, the patterns exhibited at the transition between demarcated regions.

The processed OMEGA scenes are 353_3,314_4,1000_4,4357_6,2398_4. The scenes were chosen based on the demarcated regions of interest (Figure 10).

Scenes 314_4 and 2398_4 lay on the dichotomy of the Southern Highland – Northern Lowland transition, while 353_3 and 4357_6 were chosen based on the highly localised zonations shown in those areas in the PCA (Figure 6). Scene 1000_4 was chosen to study in detail the region North Acidalia/Region C (Figure 10).

A similar procedure of choosing large regions of interest (13000-15000 pixels) within demarcated zones to analyse the overall spectral characteristic of the region, is employed. Apart from that, local patterns were also studied using wavelength maps and browse products – as described below.

An overview of absorption features in the image is obtained by employing the Wavelength Mapping technique (Bakker, 2018). This technique identifies the wavelength of the deepest absorption feature within a section of the spectra as specified by the user. The final output is a map combining the information of the wavelength of the deepest feature and the depth of the deepest feature, along with a legend indicating the same. This wavelength mapping technique is useful in identifying spatial patterns and the association of mineral groups present in the image.

Additionally, the Viviano-Beck products are also calculated onto the OMEGA scenes. These summary products are also combined to form composites known, i.e. browse products to indicate the minerals/mineral groups present (Viviano-Beck et al., 2014).

In order to study local variations, regions showing patterns in the wavelength map and the browse products are selected as regions of interest, and the mean spectra are extracted.

3. RESULTS

3.1. Principal Component Analysis

In this section, the results of the final PCA will be elaborated. The PCA, as mention in section 2.2.1, was done with a subset of 13 products out of a total of 60 summary products. The main purpose of utilising a PCA was to have a visualisation of the area and the variance it exhibits. Since the data is voluminous, i.e. each summary product layer is 3.3GB and handling a stack of the summary product data becomes cumbersome. A quick method to understand the variance was utilised.

Shown below are the results from the principal component analysis that was carried out using 13 summary products. The first individual components show visible patterns (Appendix 1), while subtle patterns are observed in the last components that contribute less to the variance description. Colour composites of the components are chosen to demarcate regions of interests for further spectral analysis. The RGB colour composite of the first three principal components is shown in Figure 6a and the RGB composite of the Principal components 11,12,13 is shown in Figure 6b. The clearly visible and subtle patterns I see in these composites are elaborated on in section 3.2.

a)

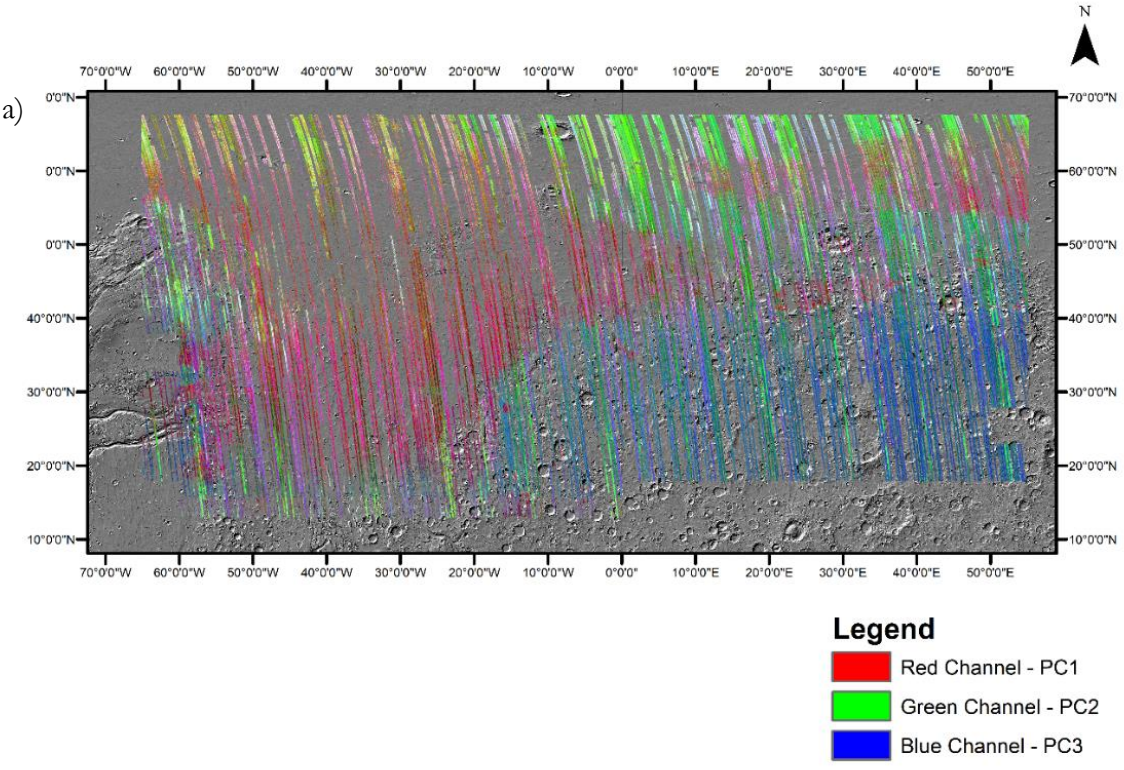

b)

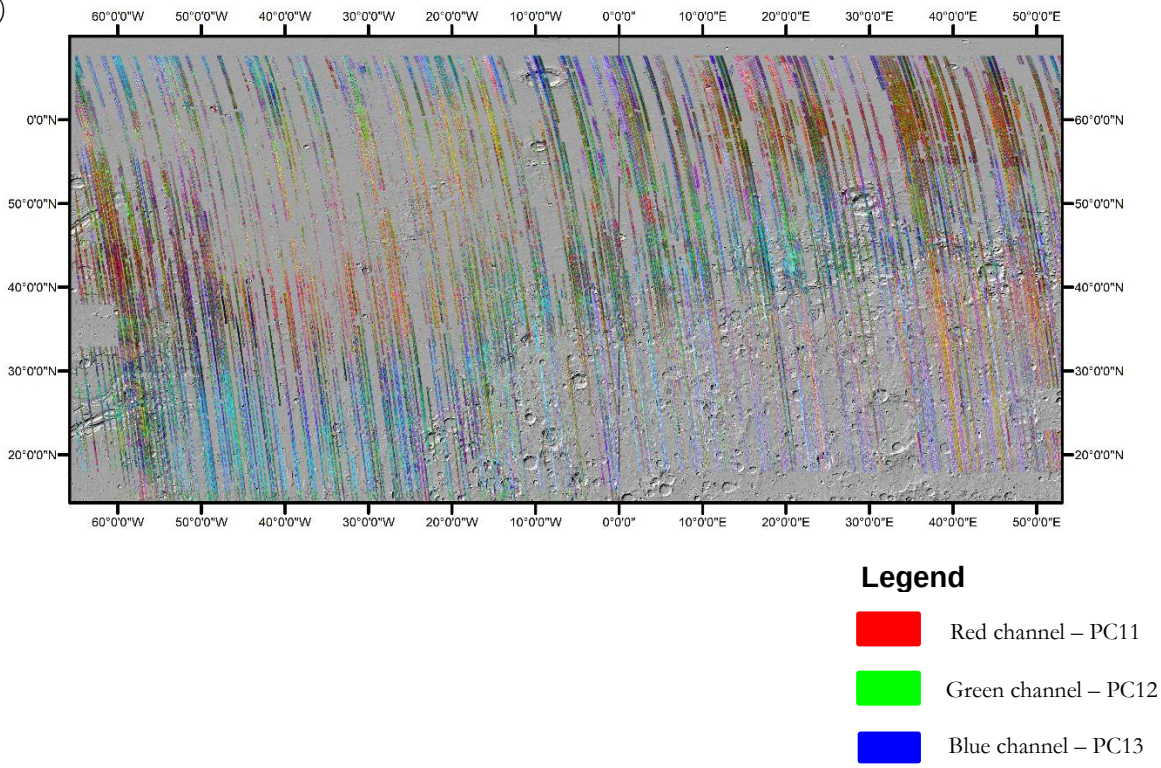

Figure 6: PCA RGB Composites a) RGB Composite of the principal components 1, 2 and 3 b) RGB composite of the principal components 11,12,13.

As seen in Figure 6a and b, patterns are discernible as delineated in Figure 10. In order to facilitate easier interpretation of the composites, graphical visualisation of the loadings and the percentage contribution of the variables to the variance captured by each principal component is shown in the Figure 7a and 7b & c respectively.

7a.

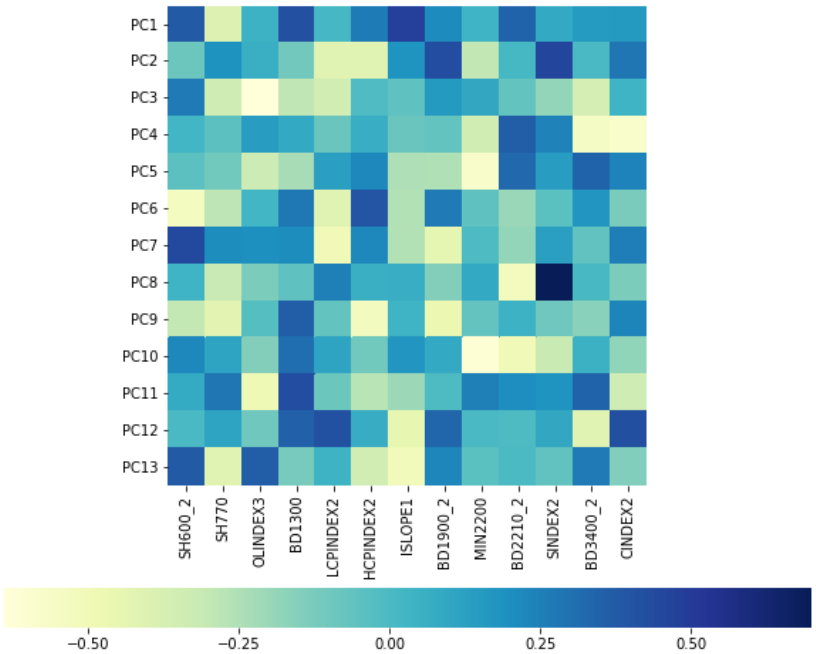

7b

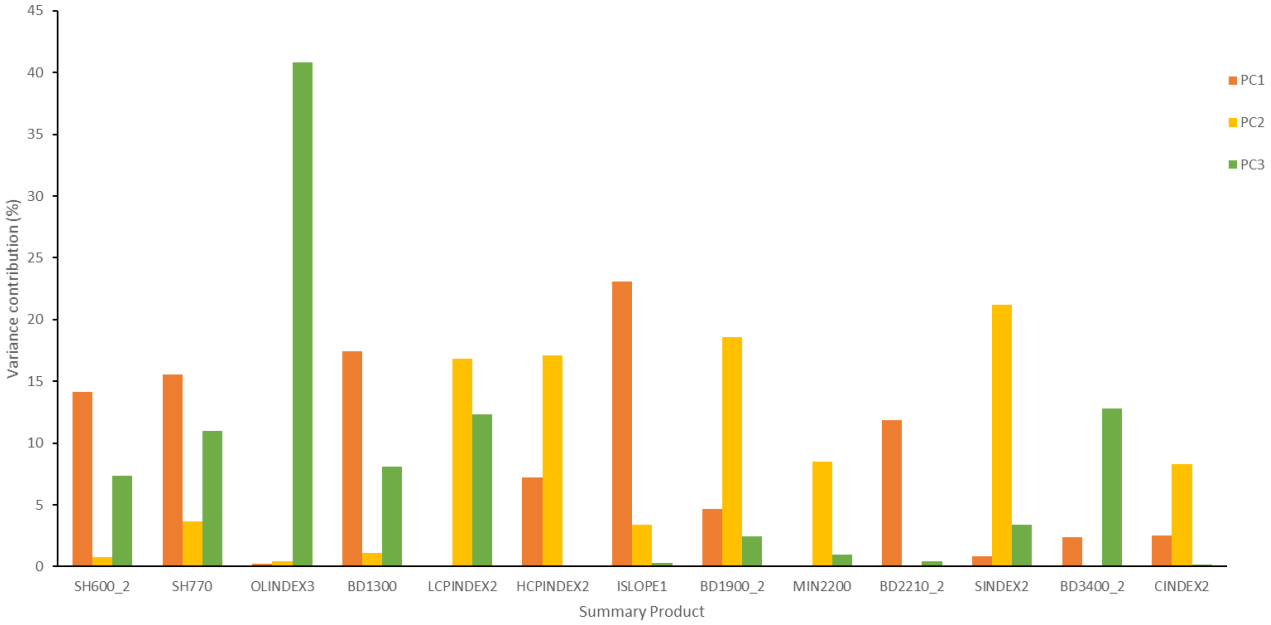

7c

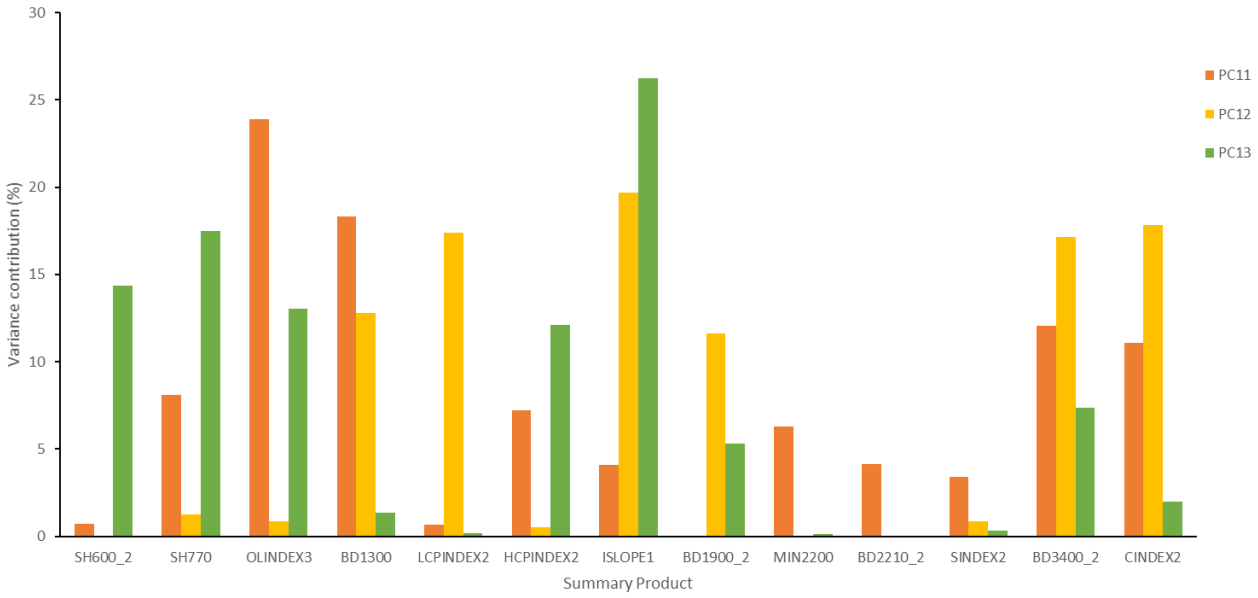

Figure 7 : a) Matrix showing the loadings for the first five principal components, b) bar graph showing the contribution of each variable to the variance captured by the principal components 1,2 and 3 c) bar graph showing the contribution of each variable to the variance captured by the principal components 11,12 and 13.

A summary of the positive and negative variance contributions, for each component of the composites shown in Figure 6a and 6b, is shown in Table 2.

Table 2 Summary of positive and negative contributions to the components by summary products

Component	Products contributing positively	Products contributing negatively
PC1	ISLOPE1 (23.05%) BD1300 (17.46%) SH600_2 (14.12%) BD2210(11.84%)	SH770(15.53%)
PC2	SINDEX2 (21.23%) BD1900_2 (18.55%)	HCPINDEX2 (17.12%) LCPINDEX (16.85%)
PC3	SH600_2(7.37%)	OLINDEX3 (40.798%) BD3400_2(12.82%) LCPINDEX2 (12.32%)
PC11	BD1300(18.3%) BD3400_2(12.05%)	OLINDEX3 (23.9%), CINDEX2 (11.1%)
PC12	CINDEX2 (17.84%) LCPINDEX2(17.35%) BD1900_2 (11.59%)	ISLOPE1 (19.7%) BD3400_2(17.12%
PC13	OLINDEX3(13.05%) SH600_2(14.4%)	ISLOPE1(27.26%), SH770(17.5%) HCPINDEX2 (12.11%)

A key observation from the PCA composite in Figure 6a is that the patterns exhibited are quite comparable to the patterns exhibited in the TES Dust Cover Index map as shown in Figure 8 that coincide with the Highland - Lowland dichotomy. This could be since the products describing the variance in the first components, namely ISLOPE1 and SH600_2 (See Appendix 3 for maps) highlighting the ferric phase, might be highlighting the ferric component of the dust. In my study, I find that the ISLOPE1 parameter that measures the spectral slope shows variations with dustcover.

Moreover, the PCA is known to capture albedo in the first components since albedo explains a significant portion of the variance in an image dataset, and in the case of Mars spectral studies, the albedo is influenced by the nanophase ferric oxide, i.e. dust cover (Ruff & Christensen, 2002; Poulet et al., 2007). Hence it could be that the first few components that describe the larger variances are influenced heavily by the albedo. The patterns of low and high dust coverage are also visible in the maps produced by OMEGA (see Appendix 2: Ferric Oxide and Dust cover maps) and evident from the BD530_2 map (see Appendix 3) generated from my study which measures the band depth at 530 nm indicating fine-grain hematite (Viviano-Beck et al., 2014)

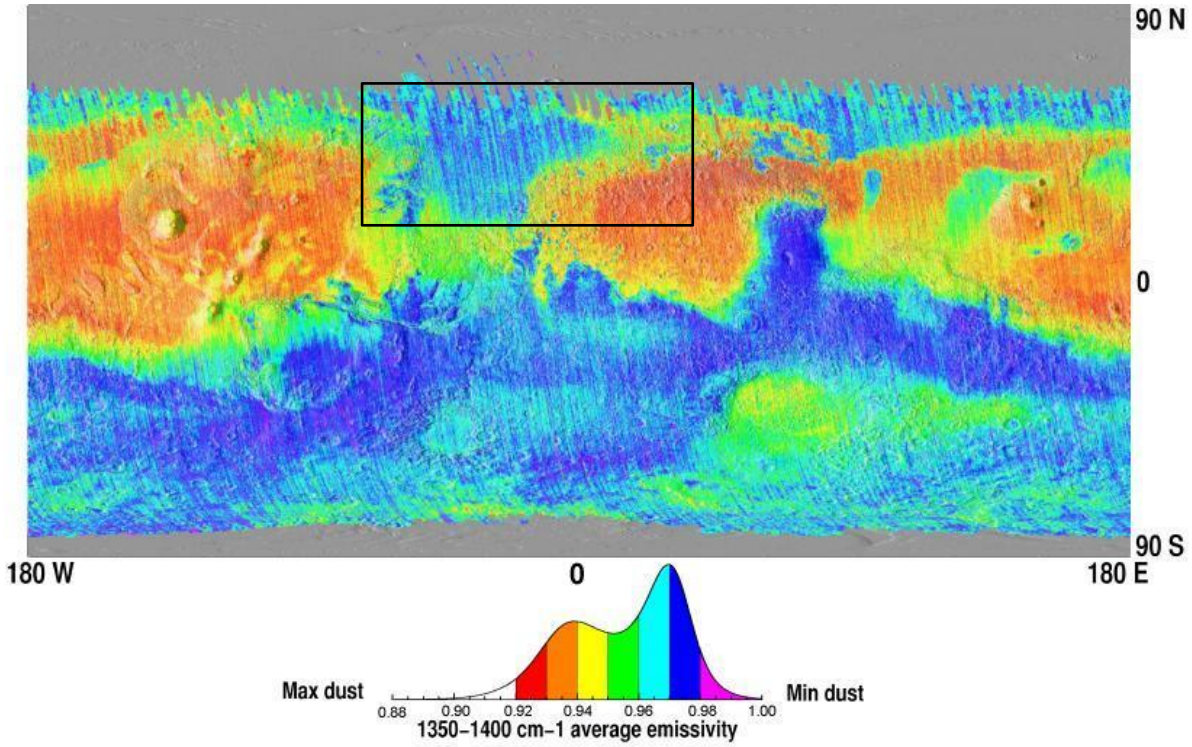

Figure 8: Dust Cover Index map produced by data from the Thermal Emission Spectrometer (Ruff & Christensen, 2002) with the study area indicated.

The reddish regions in Figure 6a indicate higher scores for the summary products ISLOPE1, BD1300, SH600_2, while SH770 contributes negatively to the first component. ISLOPE1 values being high in the region Acidalia Planitia indicating a downward/negative slope in the region 1.8 μm to 2.5 μm, do play a key role in discriminating regions in the study area. The spectral slope and the associated parameter is discussed in detail in section 3.4.3. The greenish regions in Figure 6a indicate higher scores for the products SINDEX2 and BD1900_2, while LCPINDEX2 and HCPINDEX2 contribute negatively to the second component. The blueish region in Figure 6a contains significant contributions from SH600_2, while OLINDEX3 and BD3400_2 contributes negatively to this component.

From the PCA Composite seen in Figure 6b, subtler patterns are captured especially for the region between 20-30°N and 30-50°W, where the colour changes from red/magenta to blue. The reddish regions in Figure 6b contain major contributions from the summary products: BD1300, and BD3400_2, while OLINDEX3 contributes negatively. The greenish regions contain major contributions from the summary products LCPINDEX2, CINDEX2, BD1900_2 while BD3400_2 contributes negatively. The bluish regions contain major contributions by the products OLINDEX3 and SH600_2 while ISLOPE1 and SH770 contribute negatively to the 13th component. The described contributions are summarised in Table 2.

The limitations in this analysis are that the values of negative band depths were also considered (See Section 3.3) and not masked out. This was done mainly to reduce the number of masked out pixels and to provide a quick method to visualise overall variance in this region. The patterns exhibited by Band Depth products can be studied by visualising the individual summary products and stretching from 0 to the maximum value. In my study, I also analyse the distributions of the non-negative band-depths, as discussed in section 3.3.

3.2. Regions of Interest Delineation

As seen in Figure 6a and 6b obvious and subtle patterns are visible from the PCA composites. In addition to this, the mafic browse product (Viviano-Beck et al., 2014) shown in Figure 9, which is a composite of OLINDEX3, LCPINDEX2, HCPINDEX2 is also used here to visualise patterns in the study area. This product shows a horizontal banding pattern confirming patterns seen in Figure 6a &b, with a zonation at ~35°N that appears cyan with higher values in the blue and green channel, i.e. LCPINDEX2 and HCPINDEX2. Individual maps of these mafic products are shown in Figure 11,12 and 13. Summary products LCPINDEX2 and HCPINDEX2 have relatively low values in the study area when compared to the global distribution, as shown in Figure 12 and 13.
Regions of interest are made around the observed patterns (from PCA composites as well as the Mafic browse products) and are then subject to further study. Since the area of study is large, and handling a large dataset becomes tedious, these manually defined zones helped streamline the study and focus attention on regions of interests.
Shown in Figure 10 is the preliminary delineation of zones/regions overlain on a MOLA hillshade map, labelled for further reference.

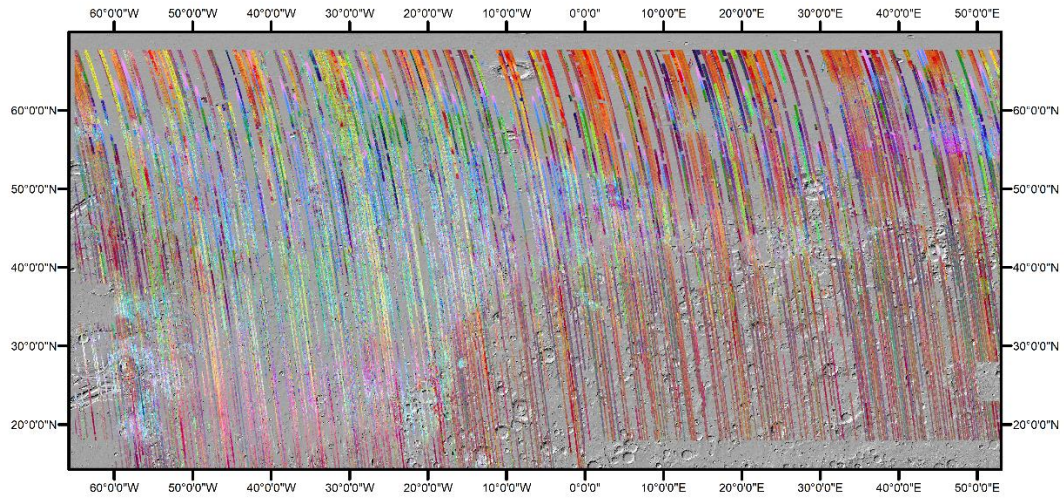

Figure 9: Mafic Browse Product with OLINDEX3, LCPINDEX2, HCPINDEX2 in RGB

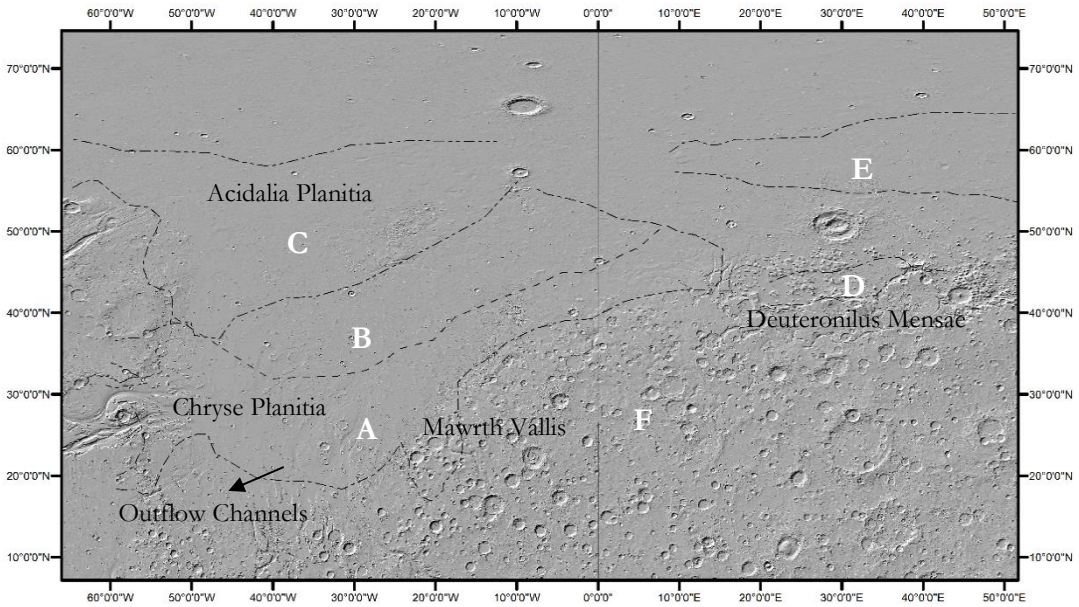

Figure 10 : Regions of interest (white text) delineated overlain on the MOLA Hillshade. Regions A, B, C are referred to as South Acidalia, Middle Acidalia and North Acidalia, respectively in the density plots of Figure 14. The geographically important regions are labelled in black text.

a.

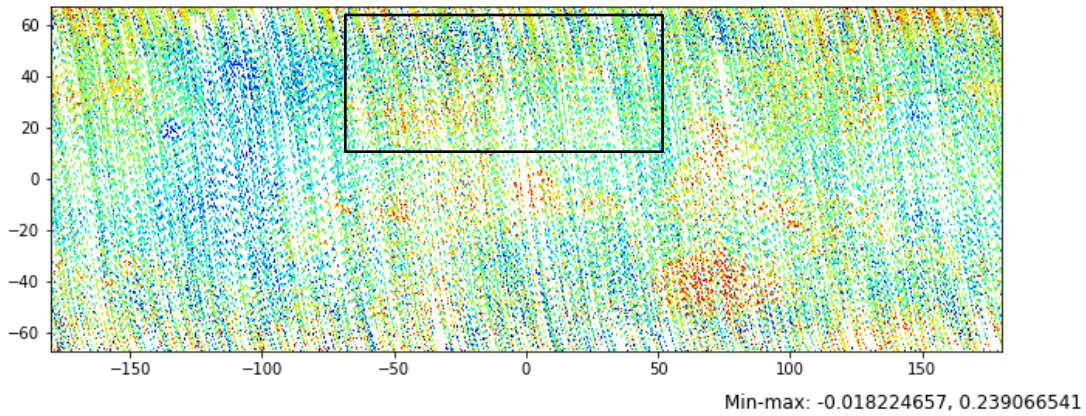

b.

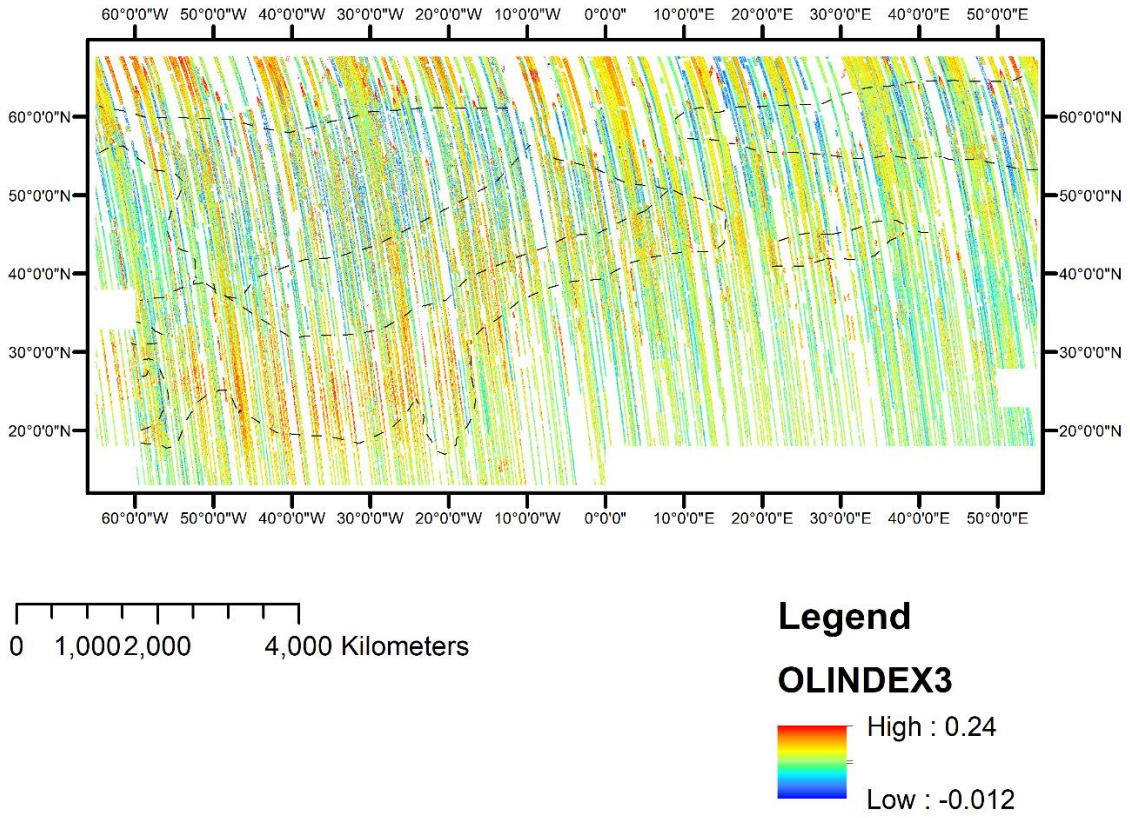

Figure 11 : a) Global OLINDEX3 map generated by Kamps et al. (2019) with study area indicated b) OLINDEX3 map generated for my thesis showing the study area extent.

a.

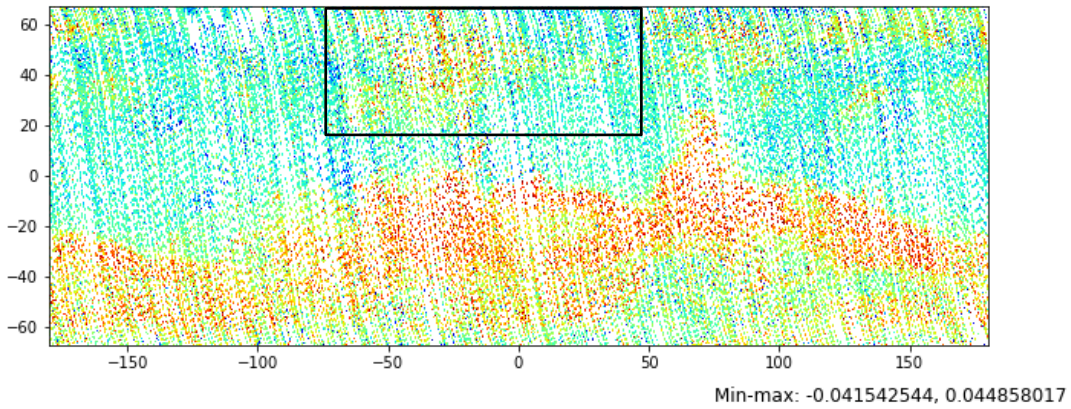

b.

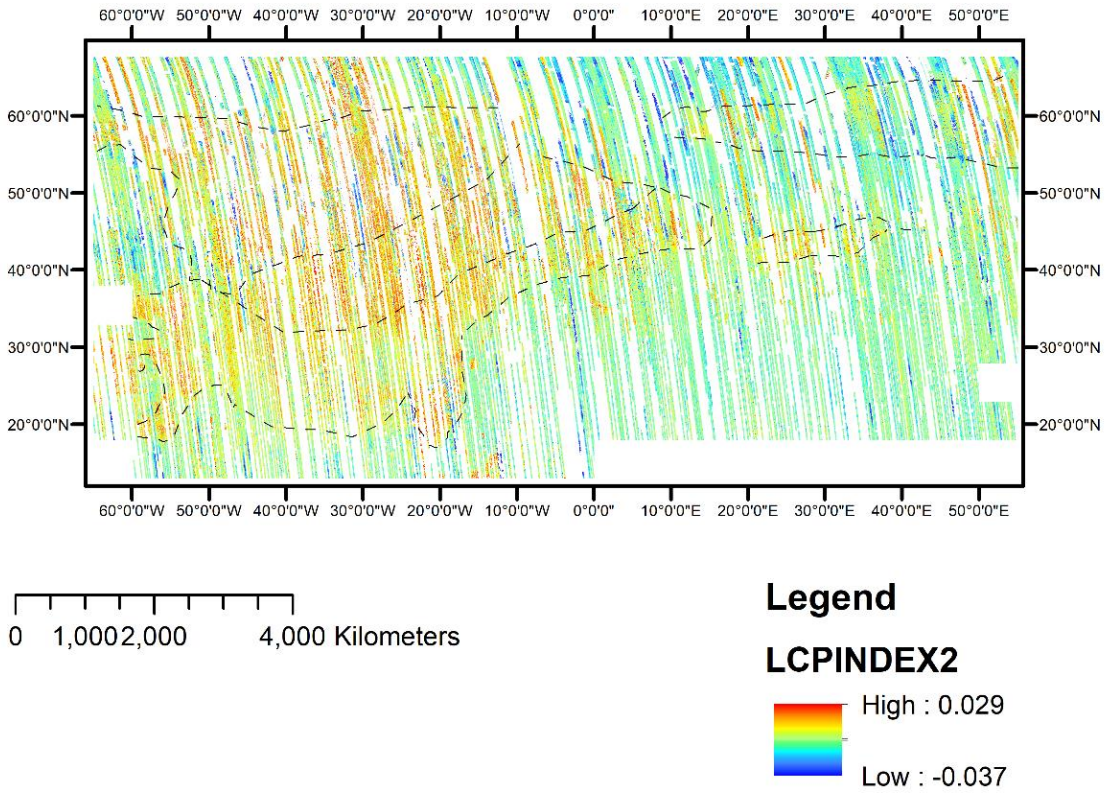

Figure 12 : a) Global map for LCPINDEX2 generated by Kamps et al. (2019) with study area indicated b) LCPINDEX2 map for my thesis showing the study area extent.

a.

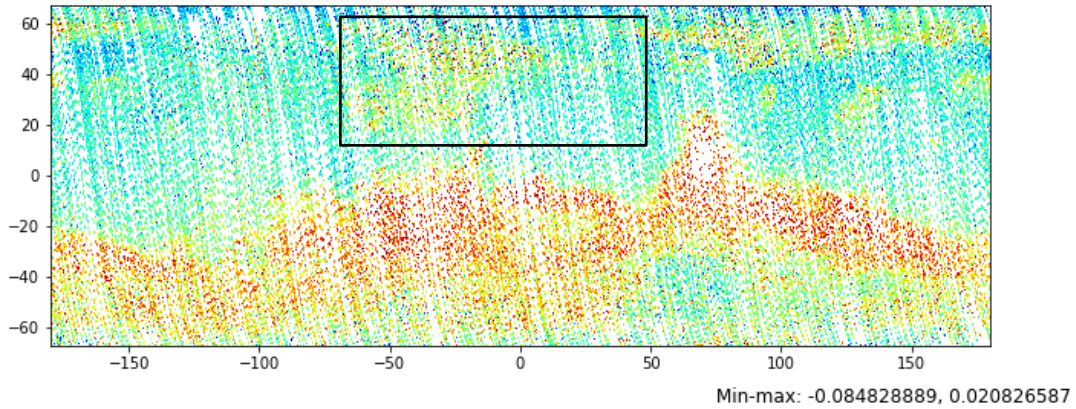

b.

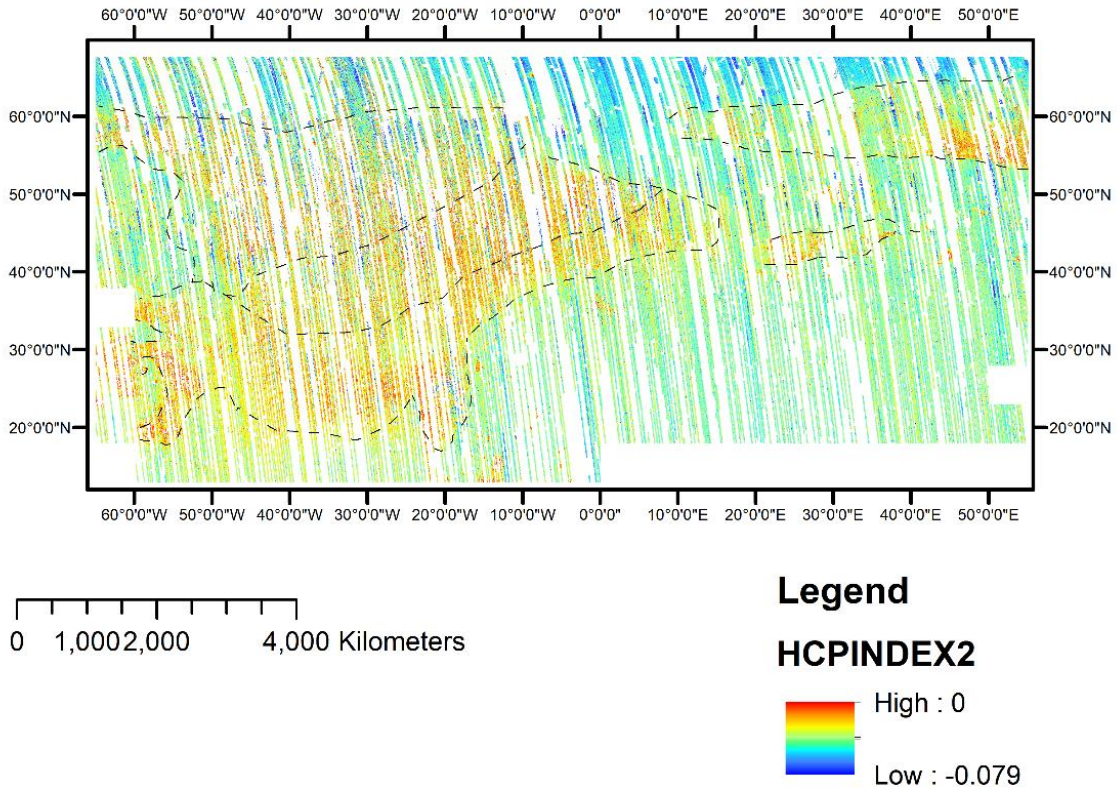

Figure 13 : a) Global map for HCPINDEX2 generated by Kamps et al. (2019) with study area indicated b) HCPINDEX2 for my thesis showing the study area extent.

OLINDEX3 shows higher values in region A, both in the regional map in Figure11b and the global map in Figure 11a. Whereas HCPINDEX2 (Figure 13 a and b) shows consistently negative values throughout the defined zones while LCPINDEX2 (Figure 12 a and b) shows relatively higher values in Regions B and C.

It is also interesting to note that the 'U' shaped region (20N,20W)- Mawrth Vallis, that shows extremely defined and localised patterns in the Mafic Browse product in Figure 9, in magenta (red

– OLINDEX3 and blue- HCPINDEX2) that also occur around the craters. These localised patterns are elaborated on in section 3.4.4.

3.3. Summary Product Distributions

Only few hydrated summary products, i.e. BD1900_2, MIN2200,BD2210_2, had been utilised for the exploratory PCA analysis. The BD1900_2 shows overall low values in Acidalia Planitia with a few pixels of higher values in Region C (Appendix 3)

However, for the PCA, band depths below zero were also considered. Hence it was of interest to revisit the hydrated summary products and visualise the patterns for only the pixels with a value greater than 0. Since effectively a negative band depth might be noise or an absence of an absorption feature, it may not be indicative of the mineral/mineral group it is designed to highlight and might be highlighting a different mineral group.

The summary product BD2210_2 which is designed to pick up absorption feature at 2210nm due to Al-OH absorptions (Viviano-Beck et al., 2014), seemed to contribute significantly to the distribution of K, Th enrichment in the Northern Lowlands, while modelling the Gamma Ray Spectrometer data (Kamps, personal communication, 10th Feb 2020). The summary product BD2210 did show a higher number of pixels exhibiting relatively high values in Regions B and C, as shown in Figure 14e. Hence, I decided to analyse the distribution of the non-negative values for other sulfate indicating products for this region as well, i.e. BD1750_2, BD2100_2.

Apart the products indicating sulfates, the product BD 3400_2 shows relatively high values in the order of ~0.20, and I wanted to investigate the patterns exhibited by the non-negative values for the product since for the PCA this product was included(but the negative band depths were also considered for the PCA). However, this product BD3400_2 must be interpreted with great caution since the CRISM instrument shows a signal to noise ratio four times less in this wavelength region than in the regions <2.7 μm (Viviano-Beck et al., 2014). Additionally, it may be erroneous to conclude the presence of carbonates using the BD3400_2 since widespread indications of carbonates have not been previously observed except for localised occurrences in the Southern Highlands (Ehlmann & Edwards, 2014). The products for which the distributions of their non-negative values are analysed are described in Table 3.

Table 3 Description of evaporite indicating summary products (Viviano-Beck et al., 2014)

Product	Rationale
BD1750_2	H_2O Band Depth to detect sulfates
BD2100_2	H_2O in monohydrated sulfates
BD2210_2	Al-OH absorption feature (Caveat: gypsum, alunite)
BD3400_2	Carbonates

The maps themselves (Figure 14) do show more number of pixels having high values within the region C however visualising these pixels is unclear due to the prevalence of zero and low values. Hence density plots were created to visualise if there is a latitude dependent trend and shown in Figure 14. The density curves were drawn only taking into consideration the pixels that have a physical meaning, i.e. the non-negative band depth pixels. These density plots indicate a subtle

trend that the probability of finding a pixel with higher values in the distribution is slightly higher within the Regions Northern Acidalia (Region C) and Middle Acidalia (Region B) compared to South Acidalia (Region A).

Similar visualisations of the distributions only for the positive band depths of the products shown in Table 3 was done for the OMEGA scenes as well, by selecting large regions of interest that fall within the regions A,B,C. The density curves for the OMEGA datasets are shown in the Appendix 7.

a)

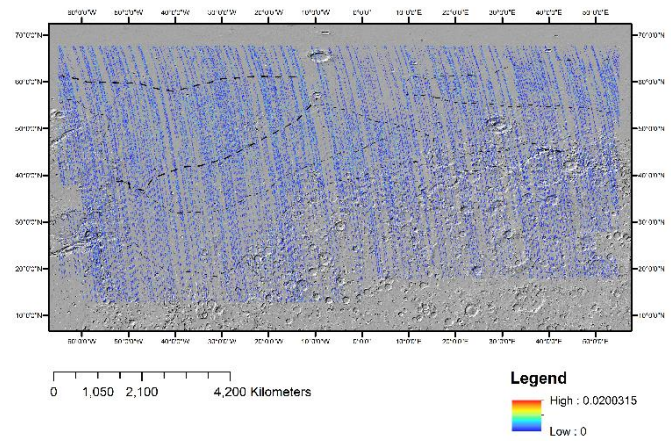

b)

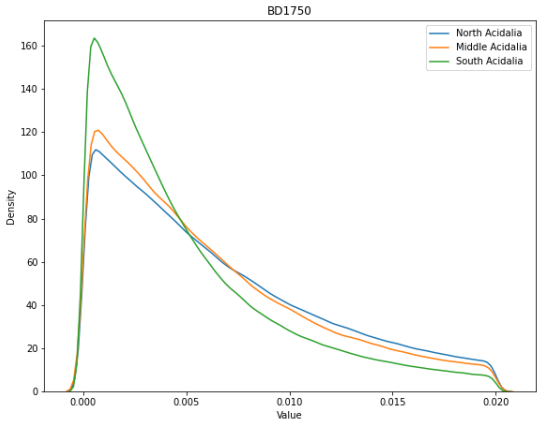

c)

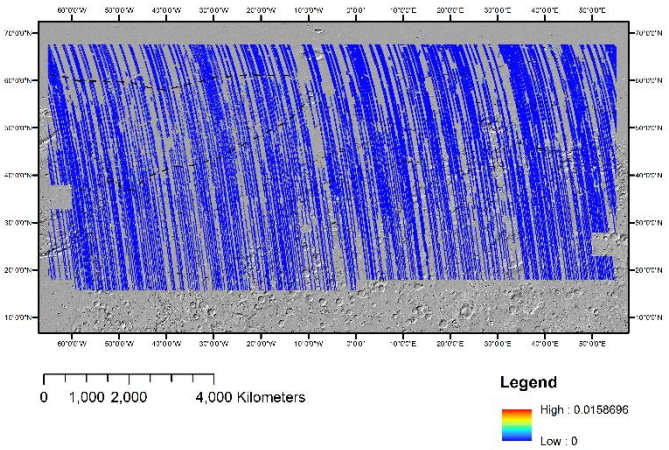

d)

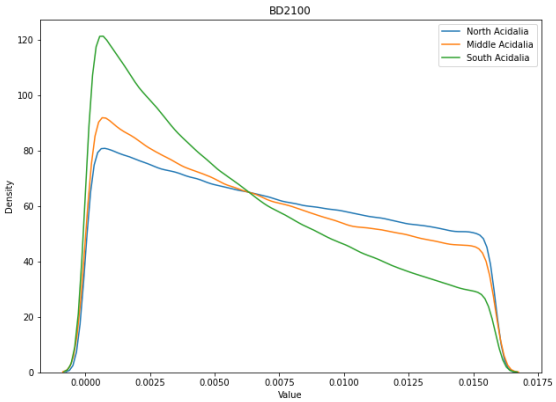

e)

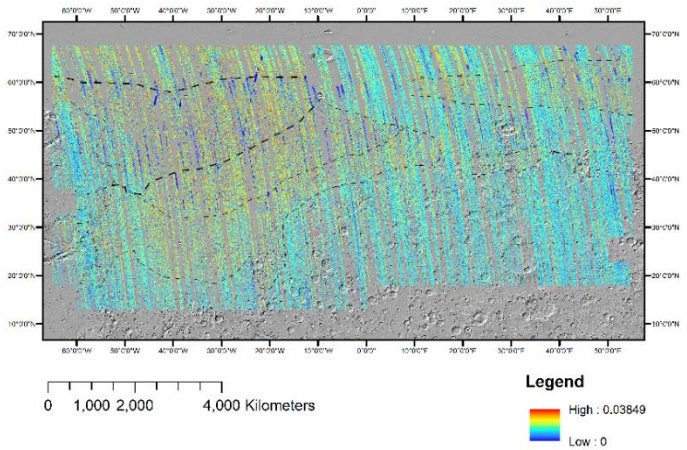

f)

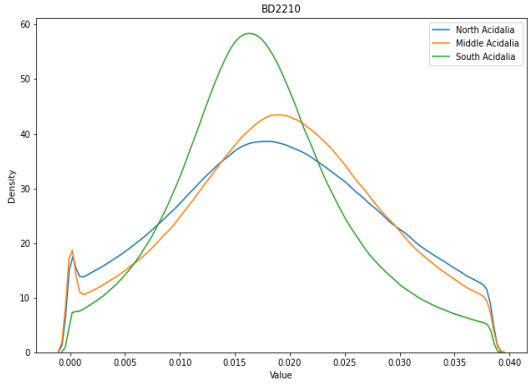

g)

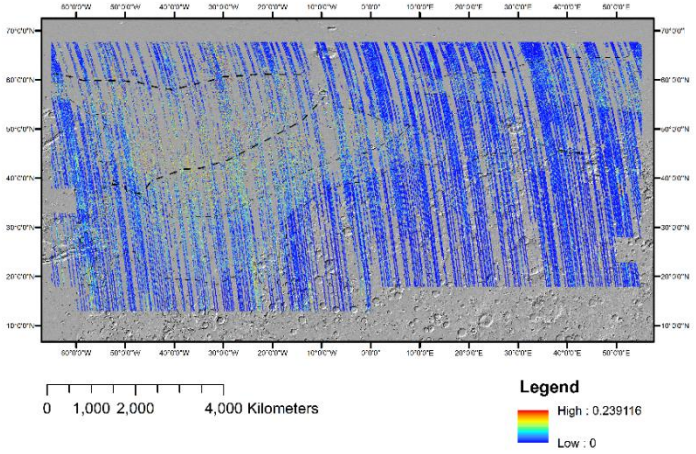

h)

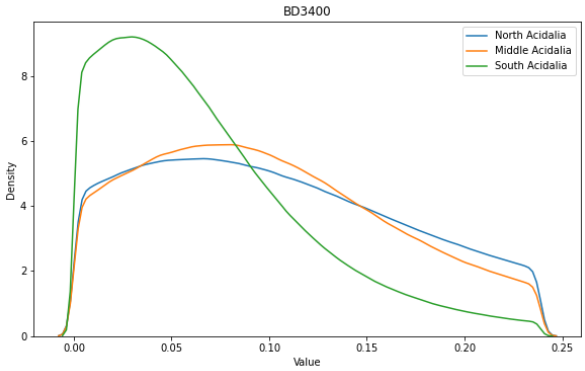

Figure 14 : Figure set of summary product distributions a) Summary product maps of BD1750_2 b) Density plot indicating the distribution of pixels having relatively high values for BD1750_2 for regions South Acidalia – Region A, Middle Acidalia -Region B, North Acidalia – Region C. c) Summary product maps of BD2100_2 d) Density plot indicating the distribution of pixels having relatively high values for BD2100_2. e) Summary product maps of BD2210_2 f) Density plot indicating the distribution of pixels having relatively high values for BD2210_2. g) Summary product maps of BD3400_2 h) Density plot indicating the distribution of pixels having relatively high values for BD3400_2

3.4. Spectral Analysis

The principal component analysis and the browse product map do show zonations as seen in Figure 6 a,b and Figure 9. However, it is essential to understand that these are indices calculated on to the spectra and the differences seen in these maps must be confirmed spectrally too (Section 2.1.1) . The spectral analysis was done for both the CRISM MSP spectral strips as well as for the OMEGA dataset.

3.4.1. Mean Spectra -CRISM

In order to identify variations across boundaries, large regions of interest were selected across CRISM MSP strips, and the mean spectra of these large regions were then analysed.

The regions of interest were consistently around 10000-12000 pixels. An overview of the selected CRISM strips is shown in Figure 15. A list of the image IDs are included in the Appendix (See Appendix 6)

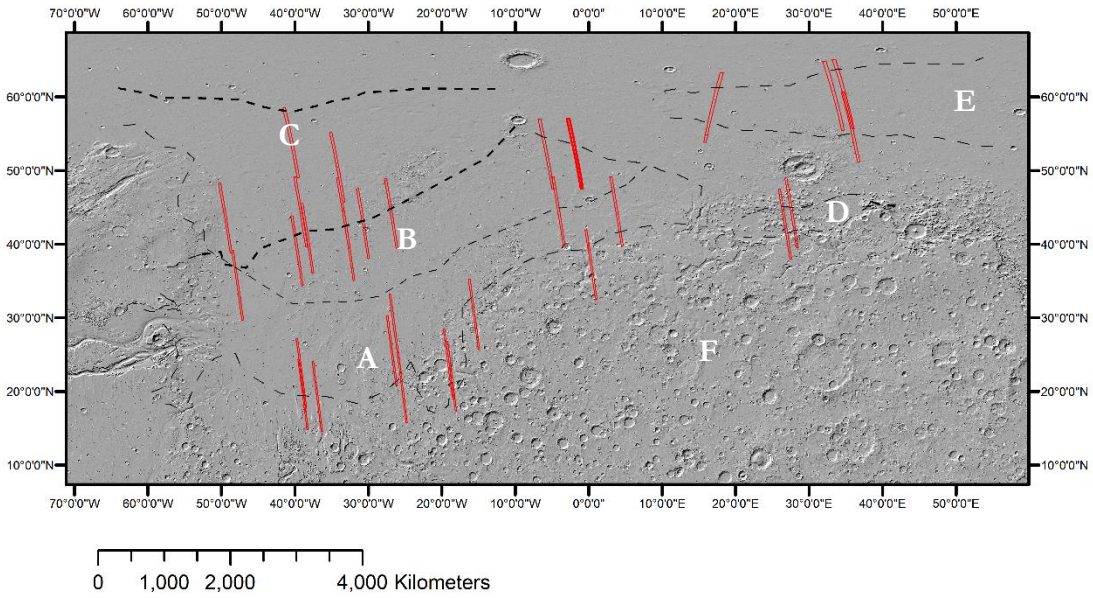

Figure 15 : Overview of chosen CRISM MSP strips shown in red overlaid on MOLA hillshade base map.

3.4.1.1. Region A

Spectra from region A show a downward sloping trend as shown in Figure 16. These spectra are from the large regions of interest (Section 2.3.1) chose on orbital MSP strips falling within the Region A.

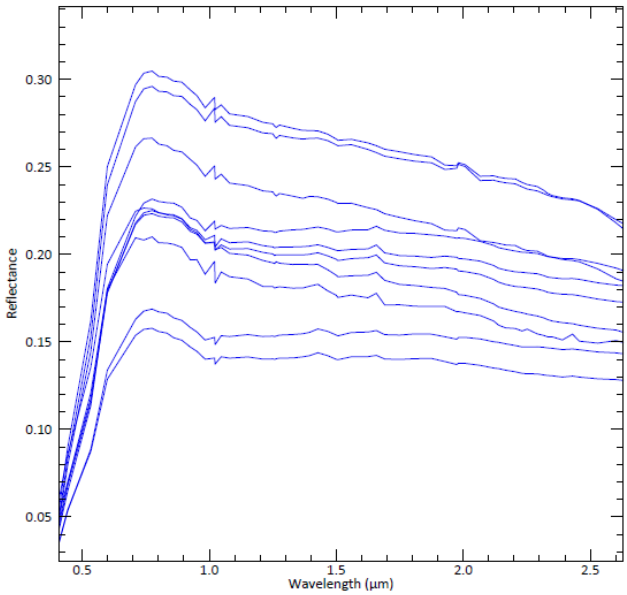

Figure 16 : CRISM MSP spectral plots from regions of interest chose on orbital strips, within Region A

This pattern is also further confirmed with the values of the summary product ISLOPE1, which effectively quantifies the spectral slope from 1.815 to 2.530 μm. However, local variations within this region are also identified. Illuminated and shaded slopes show higher and lower ISLOPE1 values; however, this cannot be the sole reason for the spectral slope as it is ubiquitous in Region A, B and C. This will be elaborated on in the section 3.4.3 as well as in chapter 4.

3.4.1.2. Region B

Mean spectra from large regions of interest (section 2.3.1) in CRISM MSP strips that fall within the Region B are shown in Figure 17. These spectra also have similar characteristics of the downwards spectral slope as in Region A

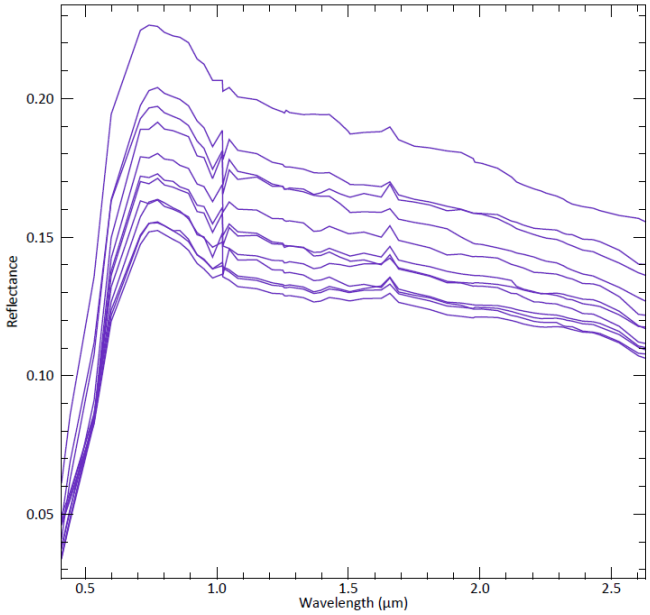

Figure 17 : CRISM MSP Spectral Plot from Region B from the large regions of interest chosen on the orbital strips, falling within the Region B.

3.4.1.3. Region C

Since many pixels from this region have been masked out while carrying out the PCA (section 2.2.1), it was of interest to see if the spectra do show absorption features. This region also shows a characteristic downward sloping trend in the spectra.

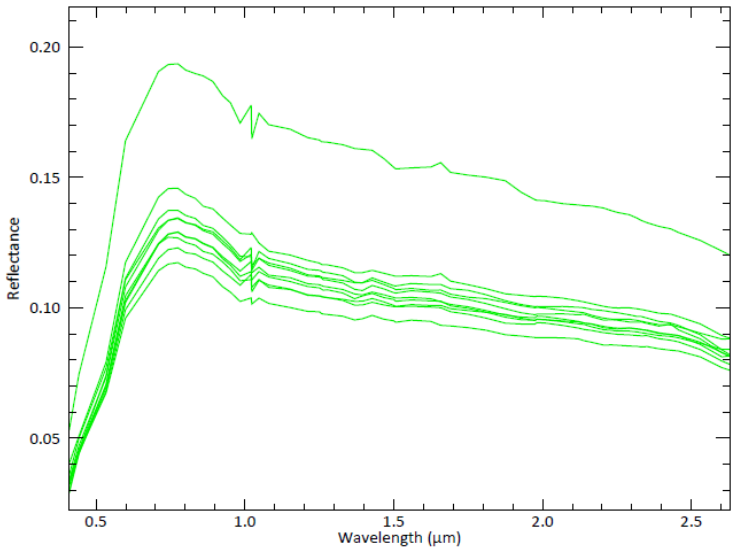

Figure 18 : CRISM MSP Spectral Plot from Region C from the large regions of interest chosen on the orbital strips, falling within the Region C.

3.4.1.4. Region D and E

The figure 19a and 19b show the mean spectra of large regions of interest falling within the Regions D and E. The region D shows a flat spectrum varying in albedo within the region, as shown in Figure 19a, whereas spectra from region E show a strong absorption at 1.5 μm and 2.0 μm as seen in Figure 19b.

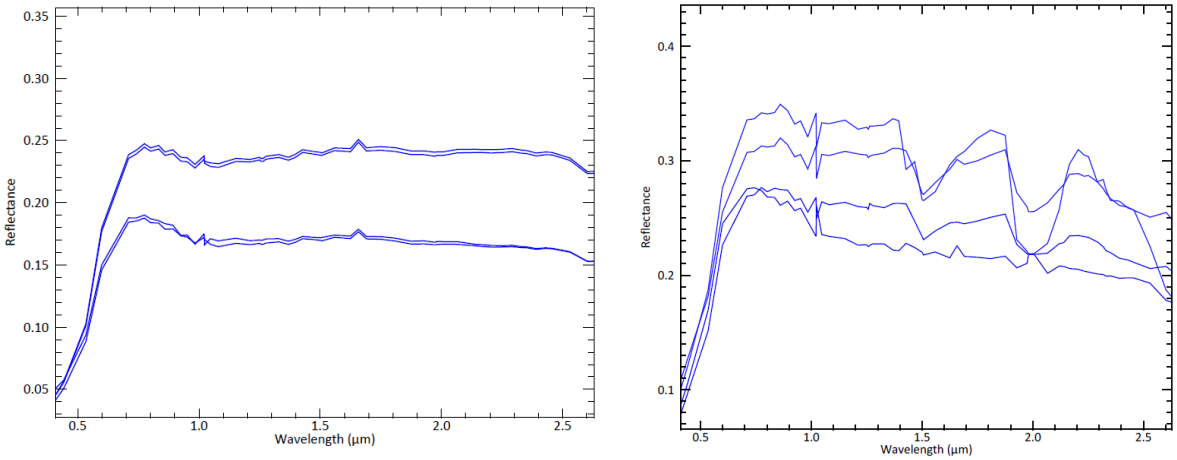

Figure 19 : CRISM MSP spectral plot extracted from large regions of interest selected on MSP strips falling within the a) Region D and b) Region E

3.4.1.5. Region F

Most of Region F lies on the Highland unit. Region F though spread out show a characteristic upward sloping trend that is an effect of dust (Horgan & Bell, 2012). Spectra from Region F are shown in Figure 20.

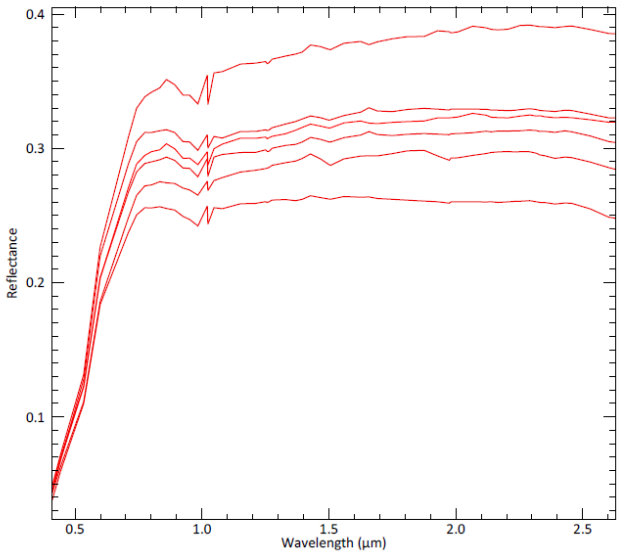

Figure 20 : CRISM MSP spectral plot extracted from large regions of interest selected on MSP strips falling within Region F.

3.4.2. Mean Spectra – OMEGA

An overview of the OMEGA scenes chosen is shown in Figure 21.

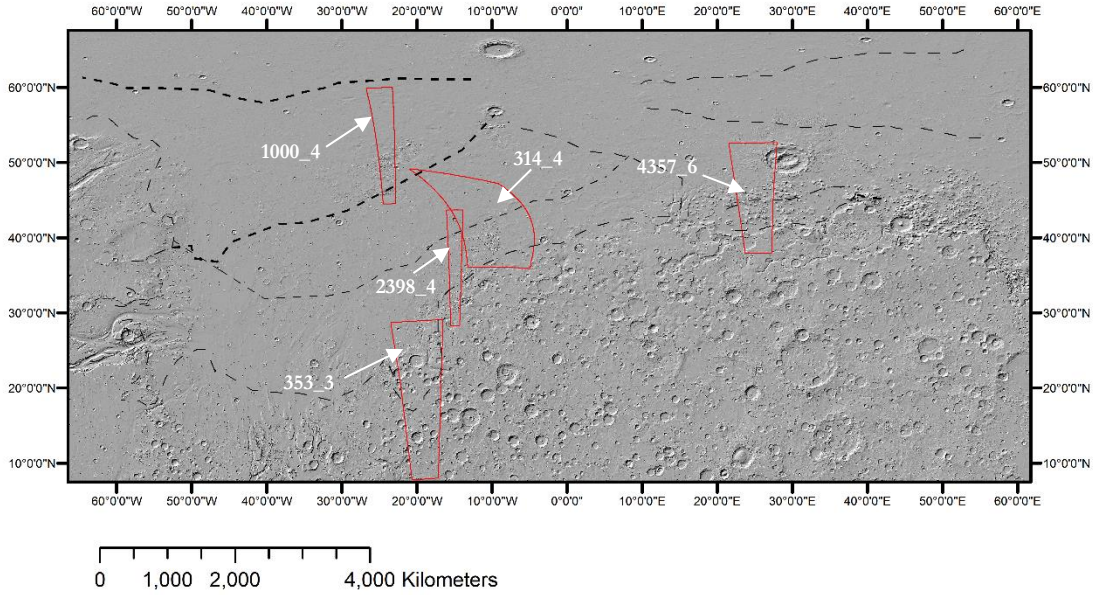

Figure 21 : Overview of chosen OMEGA scenes shown in red overlaid on MOLA hill shade base map with the image IDs indicated.

Large regions of interest were selected across the boundary of regions to observe mean spectral differences. The primary variation in the spectral slope is again observed to show the same patterns for regions A, B, C and F. The spectra of the dust-covered Region F is shown in Figure 22a and the spectra from Regions A, B, C with relatively less dust cover compared to F, is shown in Figure 22b.

a)

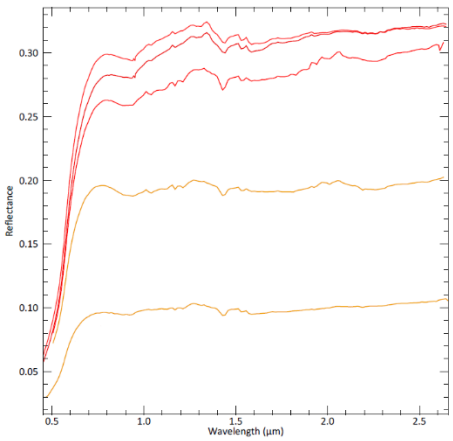

b)

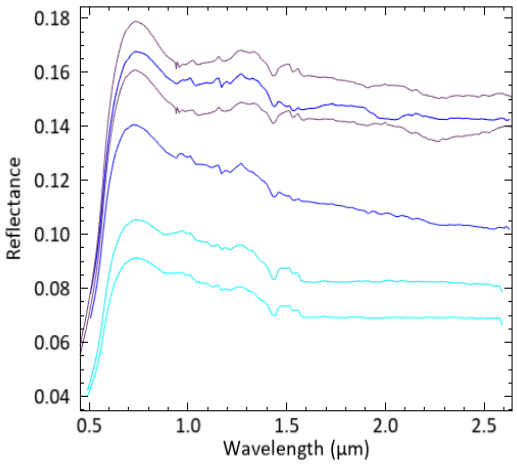

Figure 22 : OMEGA spectral plot for large regions of interest lies within a) Region F where orange spectra are closer to the dust-free regions, and red spectra are well within the dusty regions b) Region A spectra in purple, Region B in blue and Region C in cyan showing flatter spectrum towards longer wavelengths.

The region D also shows a similar downward sloping trend, as shown in Figure 23 with an artefact at the joining of the two channels of the OMEGA instrument around 1.0 μm.

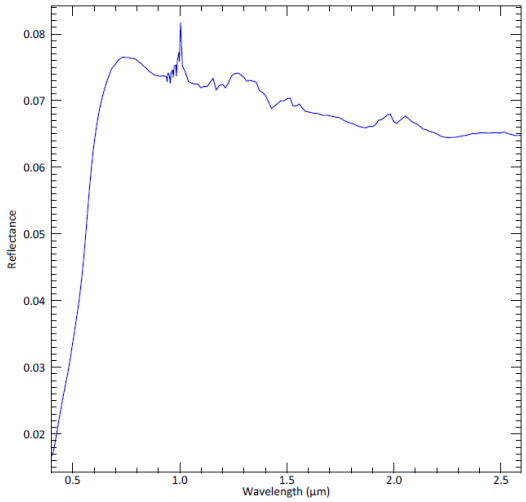

Figure 23 : OMEGA spectral plot from the large region of interest extracted from Region D, indicating a downward spectral slope from ~1.5 μm. An instrumental artefact is seen at ~1 μm, which is the region at the join of the two sensors.

3.4.3. Refined Spectral Slope Parameter

The significant observation of my study from the spectral analysis of the CRISM MSP and OMEGA scenes is the spectral slope. Although the demarcated regions except Region F show high values of the parameter ISLOPE1 thereby indicating a negative/downward slope(See Appendix 3), on taking a closer look at the MSP strips, it is seen that this product is noisy (Figure 24a). The ISLOPE1 parameter only considers a small portion of the spectrum, i.e. from 1815nm to 2530nm, when on closer observation of the spectrum, it is noticed that the slope begins from ~1000nm. The new spectral slope parameter is engineered, as mentioned in section 2.3.2. The new spectral parameter also has the advantage of utilising all reflectances between the wavelengths 1 μm to 2 μm, instead of only considering the reflectance at the start and end wavelengths. The results for both the MSP strips and the OMEGA strips are shown in Figure 24. Here the left images are the old ISLOPE1 parameter while the right images are the new refined parameters. Here the red colours indicate a downward slope typical of Region A, B and C while blue regions indicate the upward slope typical of the dusty surface Region F. The new slope parameter is much less noisy for the CRISM MSP strips and shows more defined patterns than the ISLOPE1 parameter. The ISLOPE1 parameter performs better on the OMEGA dataset in comparison to the CRISM dataset; the new spectral slope parameter does not show much improvement.

a)

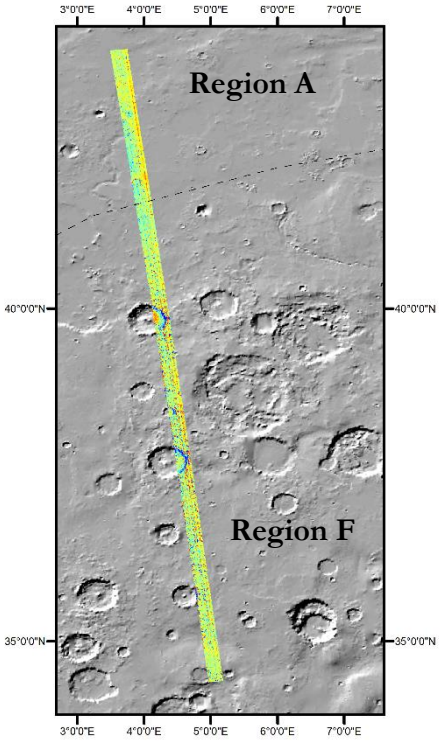
3°0'0"E
4°0'0"E
5°0'0"E
6°0'0"E
7°0'0"E
Region A
Region F
40°0'0"N
35°0'0"N

b)

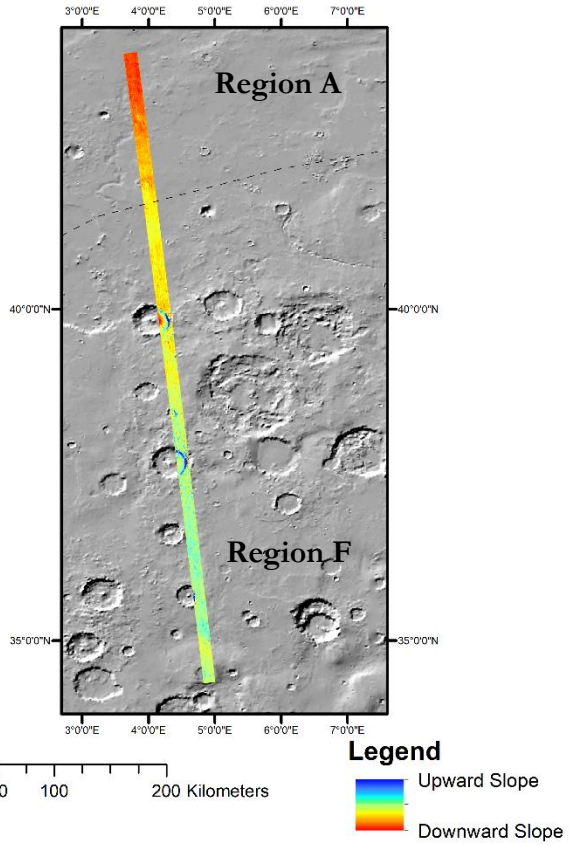
3°0'0"E
4°0'0"E
5°0'0"E
6°0'0"E
7°0'0"E
Region A
Region F
40°0'0"N
35°0'0"N
0
50
100
200 Kilometers
Legend
Upward Slope
Downward Slope

c)

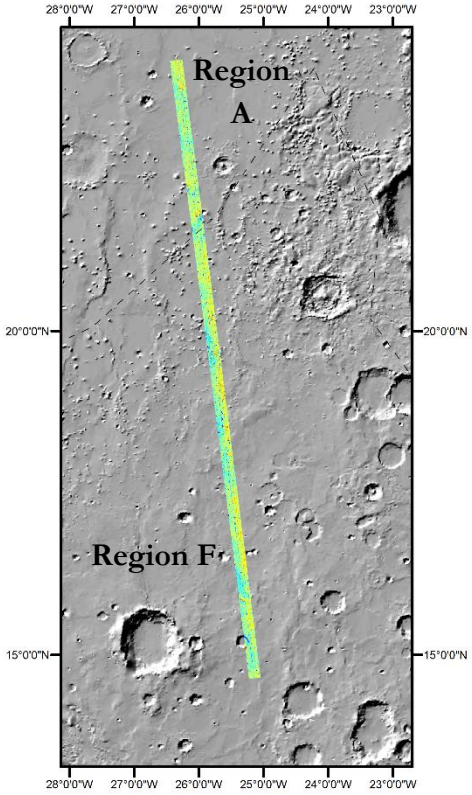
28°0'0"W
27°0'0"W
26°0'0"W
25°0'0"W
24°0'0"W
23°0'0"W
Region A
Region F
20°0'0"N
15°0'0"N

d)

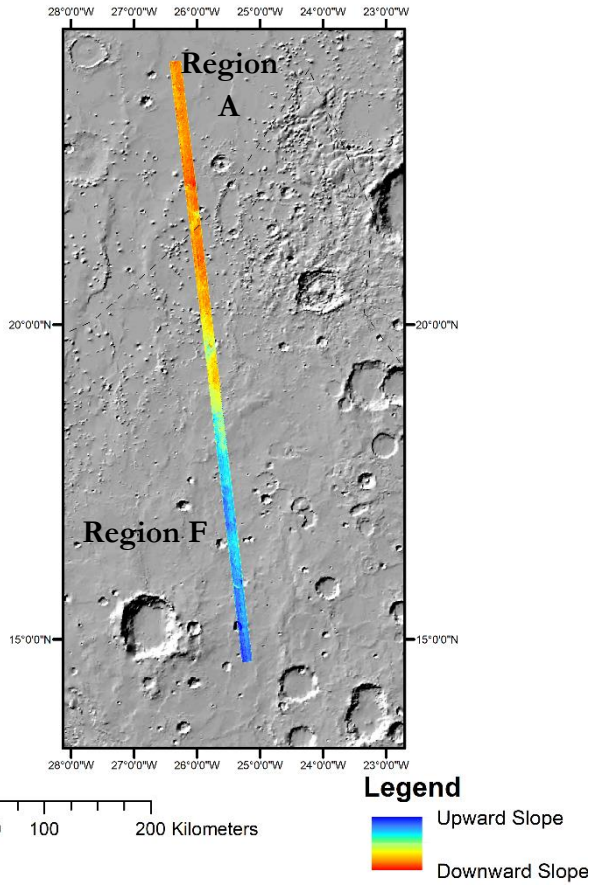
28°0'0"W
27°0'0"W
26°0'0"W
25°0'0"W
24°0'0"W
23°0'0"W
Region A
Region F
20°0'0"N
15°0'0"N
0
50
100
200 Kilometers
Legend
Upward Slope
Downward Slope

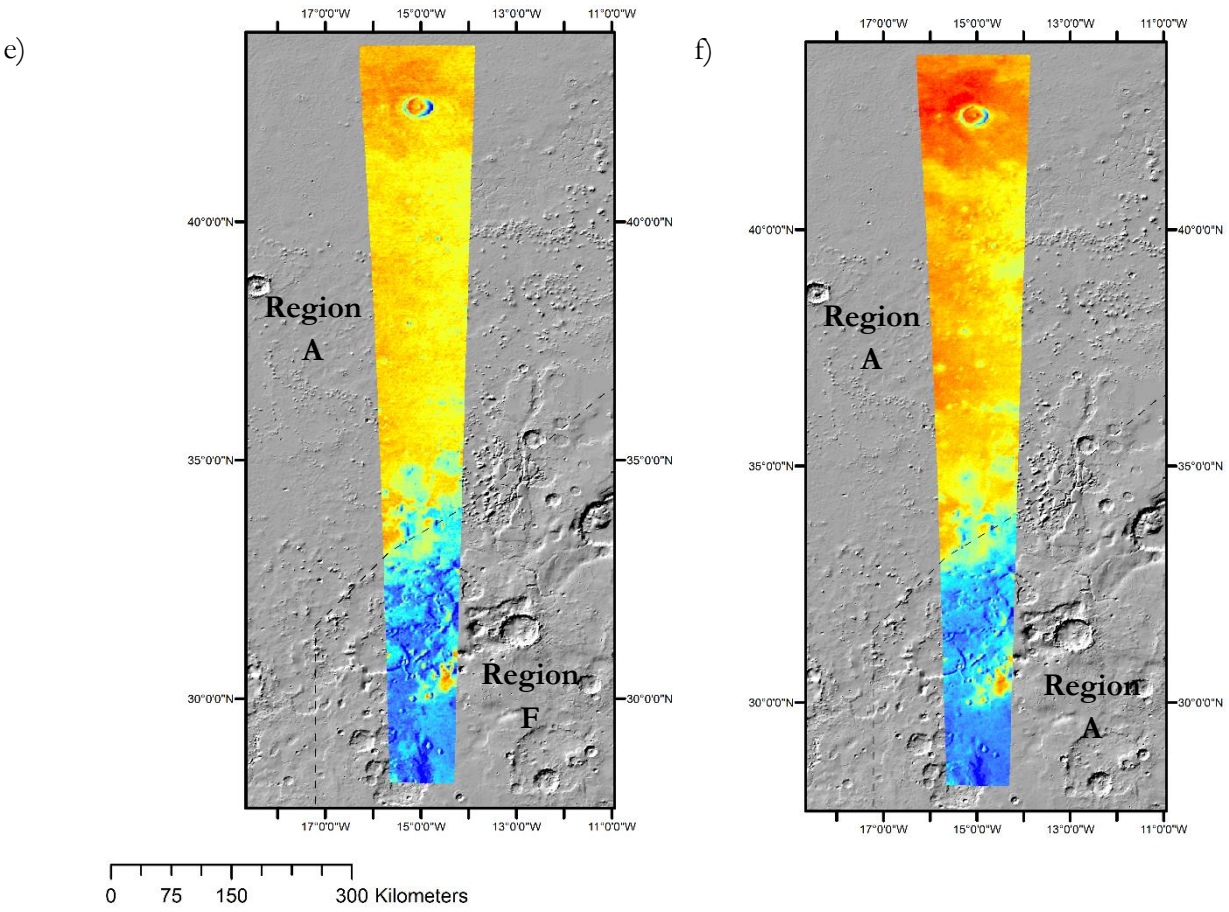

Figure 24: Comparison between the ISLOPE1 parameter and the refined spectral slope parameter a) and c) ISLOPE1 product for CRISM MSP strip b) & d) New spectral slope calculated for the same scenes e) ISLOPE1 parameter calculated for OMEGA scene 2938_4 f) New spectral slope parameter calculated for the same scene. Black line indicates the boundary between Region A and F. It is seen that the for the CRISM MSP strips, refined spectral slope parameter is less noisier (b & d) in comparison to the ISLOPE1 parameter. The noise reduction is not very clear in the OMEGA scene.

3.4.4. Localised Patterns

3.4.4.1. OMEGA Scene 353_3

Apart from regional variations in the summary products, localised patterns were observed in my study in the region Mawrth Vallis. The mafic browse product for the OMEGA scene 353_3 and overlapping CRISM MSP strips is shown in Figure 25a. High values for OLINDEX3 associated with the Oyama crater (indicated in Figure 25a) both for the OMEGA (353_3) and overlapping MSP strips, as shown in Figure 25 a and b. Browse products, namely False Colour, Phyllosilicates with Al and Phyllosilicates with Fe and Mg are shown in Figure 25c,d & e respectively. The browse products are explained in Table 4.

Table 4 : Table describing browse products (Viviano-Beck et al., 2014)

Browse Products	Rationale
FAL (R -R2529, G- R1506, ,B-R1080)	False-colour where Red/Orange indicates olivine-rich units, blue/green may indicate clay units
PFM (R-BD2355,G-D2300,B-BD2290)	Phyllosilicate with Fe and Mg where cyan colours indicate Fe/Mg Smectite or Mg carbonate, red/yellow colours indicate chlorite, prehnite, epidote.
PAL (R-BD2210_2,G-BD2190, B-BD2165)	Phyllosilicate with Al where Al smectites are red/yellow, cyan colours indicate alunite, white colours – kaolinite minerals

Faint cyan colours (indicated by yellow arrows) can be seen in Figure 25c, indicating clay minerals (Viviano-Beck et al., 2014). Yellow zonations are seen in Figure 25d indicating Al-smectites, while cyan zonations in Figure 25e are indicating Fe/Mg smectites (Viviano-Beck et al., 2014).

The same scene shows the presence of absorption features from 2.2-2.25μm in the wavelength map, as seen in Figure 26a. It is also seen from the wavelength map that the yellow unit possibly Fe/Mg phyllosilicates with absorption at longer wavelengths (~2.28 μm) encircle the units that are in green that have absorptions in shorter wavelengths (~2.22 μm) that may indicate Al-OH absorptions.

Figure 26b shows that the browse product indicates a yellow zonation on the flanks – northeast of the crater, the mean spectra for this region is shown in Figure 26c indicating the presence of Fe/Mg smectites (K. D. Seelos et al., 2019).

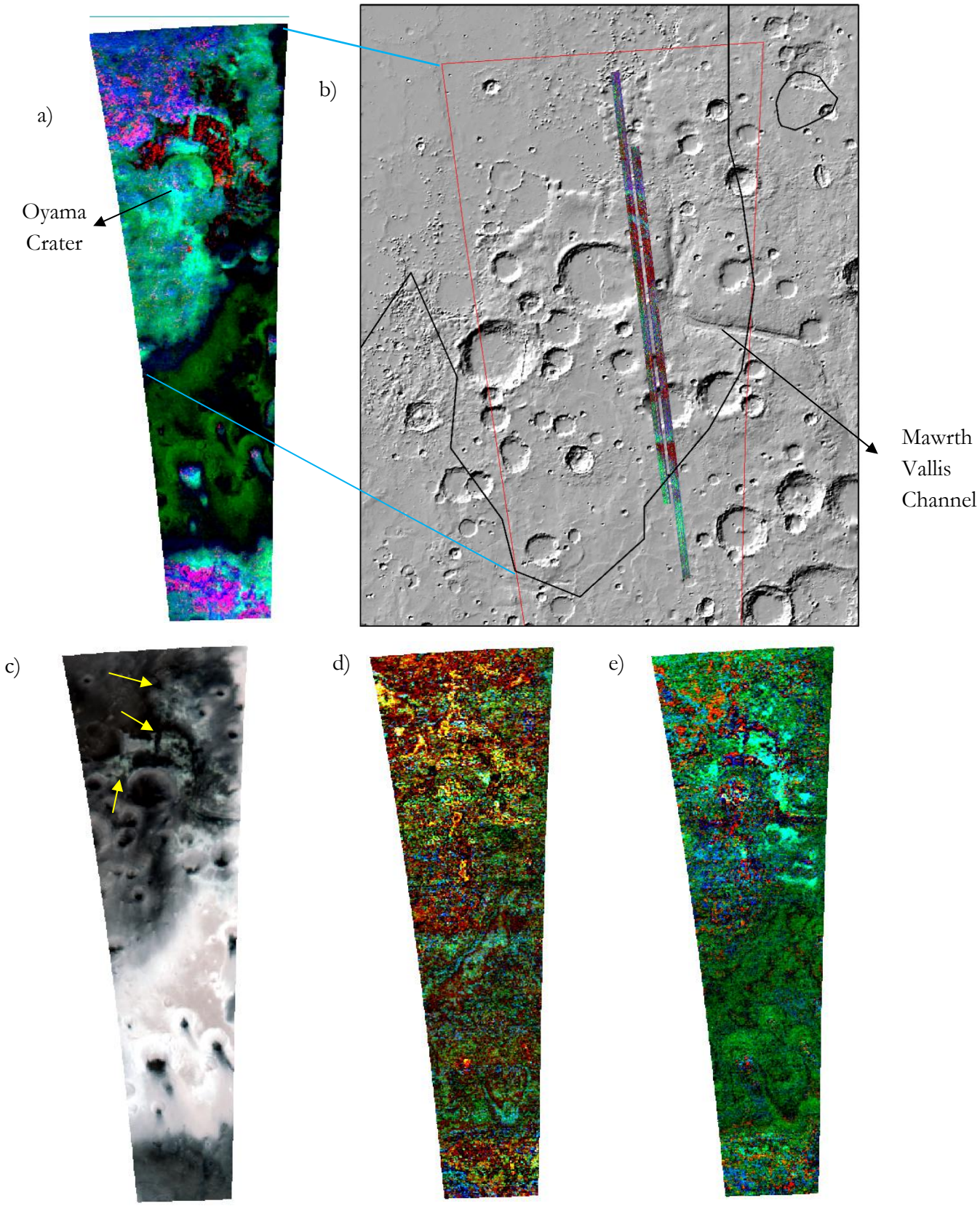

Figure 25 : Browse products of Mawrth Vallis a) Mafic Browse product RGB -OLINDEX3, LCPINDEX2, HCPINDEX2 for OMEGA scene 353_3 b) Overlapping CRISM MSP scenes showing the Mafic Browse product with the OMEGA scene outlined in red. c) FAL browse product with RGB-R2529,R1506,R1080 – cyan regions are indicated in yellow arrows d) PAL Browse product with RGB- BD2210_2,BD2190,BD2165 e) PFM Browse Product RGB-BD2355,D2300,BD2290

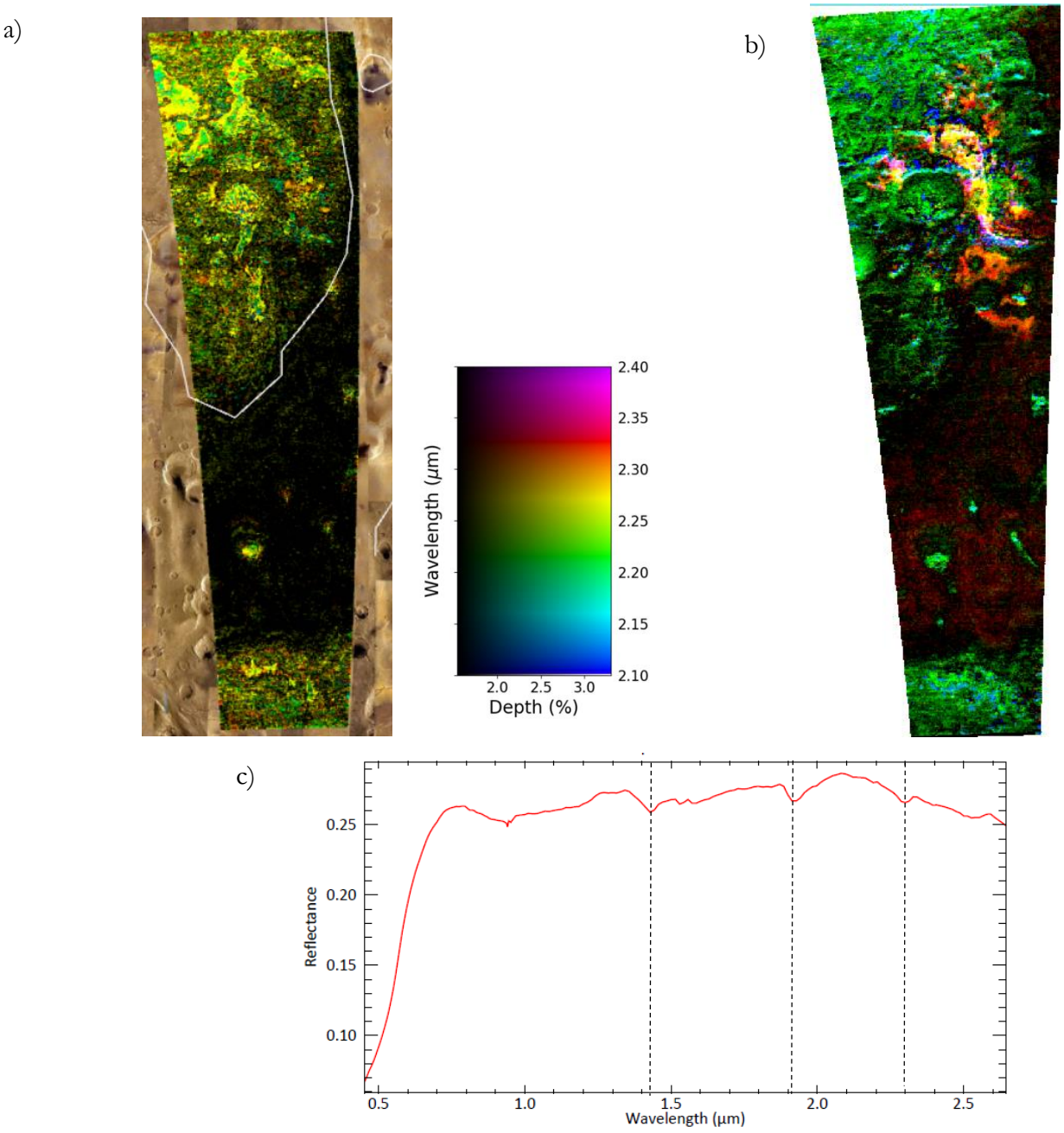

Figure 26 : a) Wavelength map for OMEGA scene 353_3 with the boundary of Region A indicated in white b) Browse product with R-1900, G-D2300, B-2400 using the old version of the products (Pelkey et al., 2007), c) Mean spectra of the yellow region from the browse product shown in b) with absorption features at ~1.4um, ~1.9 μm and 2.3 μm. Collectively, it is seen that phyllosilicates are abundant in Mawrth Vallis – in specific Fe/Mg and Al phyllosilicates.

3.4.4.2. OMEGA Scene 314_4

The OMEGA scene 314_4 lies on the boundary between Region A and F. Zonations near the boundary exhibit an absorption feature at 2.18-2.20 μm, as shown in Figure 27a. The spectra from this zonation are also shown in Figure 27 b. The spectrum shows absorption at ~1.42 μm, and 1.91 μm indicating OH and H_2O features respectively. A faint absorption at ~2.19 μm is also seen in the spectra and in the wavelength map Figure 27a, that indicate Al-OH absorptions roughly occuring in proximity of the proposed shoreline (Parker, Gorsline, Saunders, Pieri, & Schneeberger,

1993). The 1.428 μm feature is resolved in most OMEGA scenes; this might be the presence of the OH feature that occurs from 1.38 μm to 1.42 μm (K. D. Seelos et al., 2019) or the indication of CO_2 ice absorption at 1.435 μm.

a)

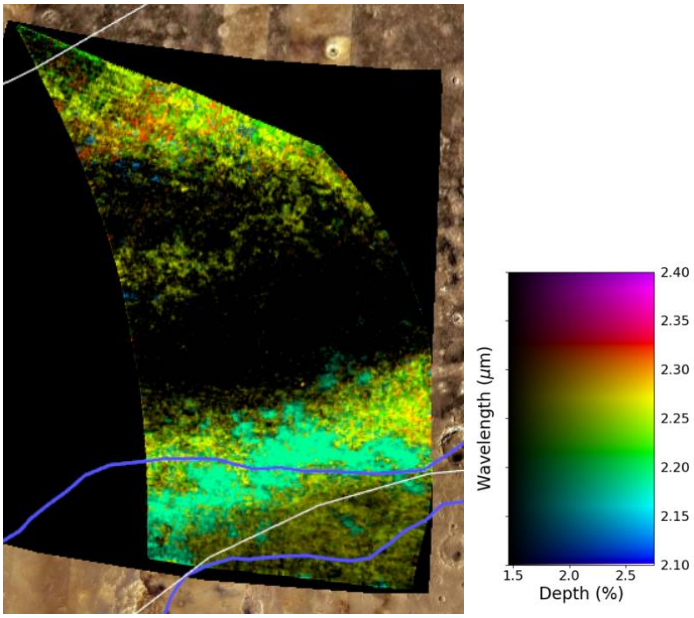

b)

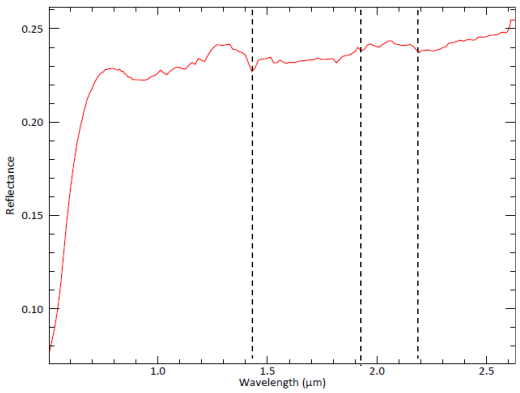

Figure 27 : Localised variations identified at the Highland-Lowland dichotomy a) Wavelength map of OMEGA scene 314_4 with boundaries between Region A and F indicated in white and the proposed shoreline (Parker et al., 1993)b) Mean spectra of green zonation indicating absorptions ~2.19 μm seen near the boundary

3.5. Summary

In summary, the results of my study include the regions demarcated upon visualising patterns in the PCA composites, the mean spectra extracted from the reflectance CRISM strips for each of the demarcated regions and the primary characteristic of the spectra from Regions A, B, C is the difference in the spectral slope. Additionally, a new refined spectral parameter is introduced to quantify the spectral slope between 1 μm and 2 μm by fitting a regression line between these two wavelengths. Finally, the spectral slope variations are again identified on the OMEGA scenes while more interesting local variations are also identified.

4. DISCUSSION

4.1. Discussion regarding the demarcated regions

The identified regions of interest from my study are overlaid on to the global surface type classification produced by Kamps et al. (2019) as shown in Figure 28a. Figure 28a shows that the surface type units defined by Kamps et al. (2019) are identified at the original non-downsampled resolution of the CRISM summary products. Concerning the surface type studies of Rogers & Christensen (2007) using the TES data, Region C from my study spatially relates to the 'Northern Acidalia' indicated as RC Group 1 from their study as shown in Fig 28b.

a)

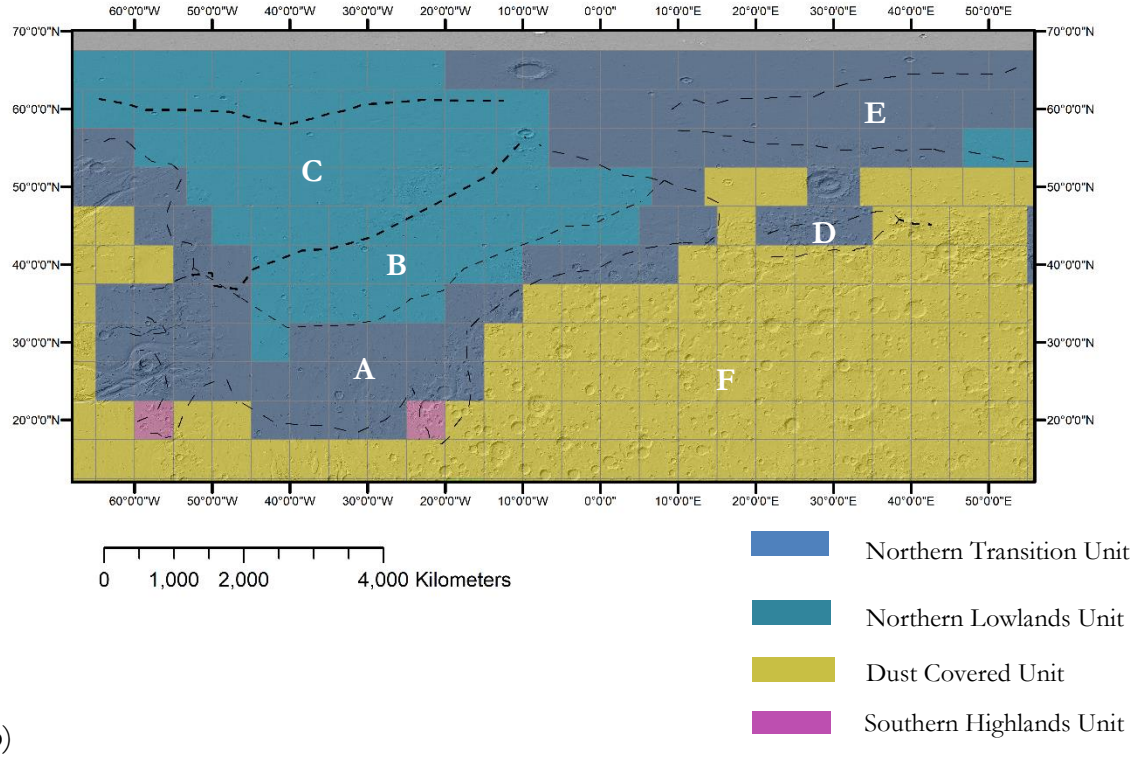

b)

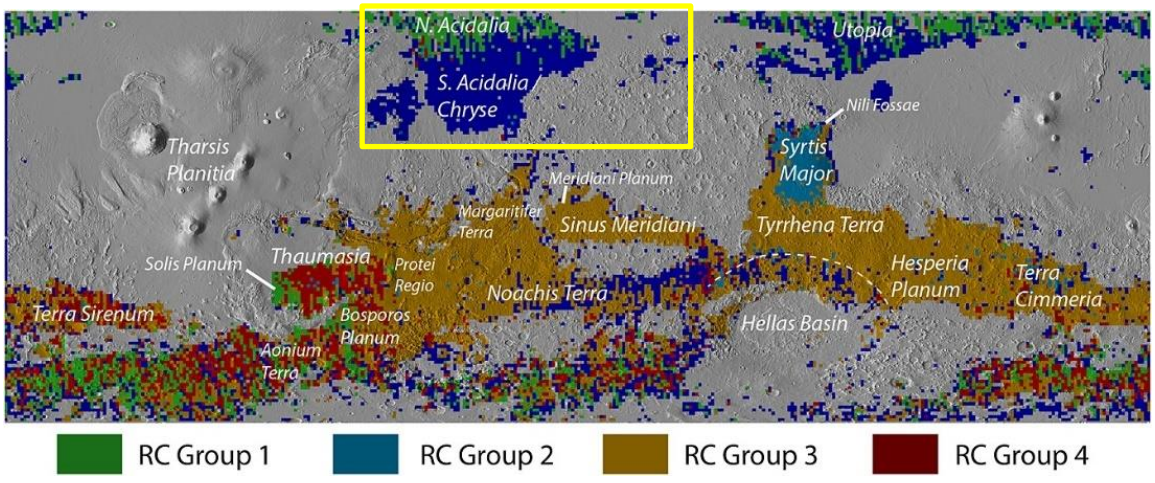

Figure 28:The regions classified in my study compared to the previously delineated surface type units. a) Surface Type classification by Kamps et al. (2019) with regions demarcated from my study overlain in dashed lines b) Surface type classification from TES modelled spectra by Rogers & Christensen (2007) with study area indicated by the yellow box. (RC stands for 'Roger Christensen' Group)

The study by Rogers & Christensen (2007) uses regional spectra derived from the TES instrument for various low albedo regions. The extracted regional spectra are then deconvolved using a spectral library to estimate the modal mineralogy in the low albedo regions. This study gave rise to two distinct units within Acidalia, i.e. North Acidalia and South Acidalia.

Region C from my study spatially relates to North Acidalia while Region A and B from my study fall within the area grouped as South Acidalia by Rogers & Christensen (2007). They characterise South Acidalia (RC Group 2) to be of higher albedo in comparison to North Acidalia, while North Acidalia is comprised of the high silica phase. The high silica phase of surface type 2 is comprised of plagioclase feldspar and glass(Bandfield et al., 2000). The study by Rogers & Christensen, (2007) attributes the increased albedo for South Acidalia (RC Group 2) to be due to a presence of dust which is seen for Region A in my study (Section 4.1.1).

4.1.1. Region A – South Acidalia

4.1.1.1. Mineralogical Composition – Mafic Mineralogy

The Transition Unit identified by Kamps et al. (2019) is spatially related to Region A as seen in Figure 28a (between 50W to 0W). Region A shows higher interpreted olivine content, as seen in Figure. 11a & 11b (also see distribution in Figure 29a). For a better understanding of the olivine index (OLINDEX3), the wavelengths utilised in this index are shown in Figure 29b.

It is important to note that in my study, higher values for a summary product is relative to the Northern Lowlands and not to Global Mars. However, the OLINDEX3 is a product that shows high values in Region A that is in range with global high values (see Figure 11a & 11b). The OLINDEX3 quantifies the broad 1μm absorptions due to ferrous iron, and this implies that the OLINDEX3 product can highlight not just olivines but could also indicate other mineral groups, e.g., Fe phyllosilicates (as seen for the region Mawrth Vallis – Figure 25a) if products indicating diagnostic phyllosilicate absorptions also show high values in the same region as OLINDEX3. It is difficult to interpret the exact composition of Region A since the 1 μm absorption could occur for other mineral groups, as mentioned earlier. The broad 1μm absorption is also identified in the spectrum of basaltic glass (Horgan, Smith, Cloutis, Mann, & Christensen, 2017) or glassy basalt (Salvatore, Mustard, Wyatt, & Murchie, 2010), that could also relate to the mineralogy of the study area in terms of the weathering process characterising Acidalia Planitia (Section 4.1.2.1).

As mentioned earlier, Region A shows globally high values for OLINDEX3 (Figure 11a and 11b) while no other products show an increased value in this region (except intermediate values for the dust products – discussed in Section 4.1.1.2). The OLINDEX3 values in Region A decrease progressively while moving towards higher latitudes (Figure 29a). As we move northward, with the decrease in the 1μm absorption, the spectral slope increases (Figure 33). The inverse relationship of the spectral slope and mafic absorption could be an indication that a weathering mechanism that decreases the 1μm signature (Salvatore et al., 2010).

In order to understand the localised patterns of OLINDEX3 (measures ~1μm absorption by ferrous minerals) in Region A, the summary product map was overlaid on the THEMIS daytime infrared image, as shown in Figure 30. A major drawback of the CRISM MSP mosaic is that the

levelling differences between the adjacent strips make interpretation and mapping of the regions quite difficult. The striping patterns of the summary products for the MSP strips are also seen in individual strips that make interpretation difficult. However, in the region shown in Figure 30, it is seen that high values are associated with crater ejecta.

The subtle patterns of higher values in the OLINDEX3 in the crater ejecta seen in Figure 30 could indicate that the material showing higher OLINDEX3 values might be from the sub-surface layer of mafic composition (Salvatore et al., 2010). Studies using OMEGA dataset to investigate olivine occurrences on the surface of Mars (Ody et al., 2013) have also identified localised high values for the olivine index parameter in the same region as Figure 30.

Although it seems like the region A does show elevated high calcium pyroxene content (Figure 13), on a closer look, the values for this index are consistently negative in this region while positive and relatively high values occur in the Southern Highland region. The HCPINDEX2 is a broadband parameter that accounts for the broad absorption at 2.12 μm and is calculated by a weighted sum of the absorption features at wavelengths within the range 2.12μm to 2.46μm. A negative broadband depth could be due to the significant contribution of noise or absence of absorption in the highest weighted wavelength or the majority of the wavelengths within the sampled range exhibit an absence in absorption. There could be various reasons for the negative band depths – noise, shifted absorption features, weightage of the wavelengths sampled. The negative values of the mafic parameters may have mineralogical meaning in terms of ferrous mixtures, and this relationship is studied by Horgan, Cloutis, Mann, & Bell, (2014) for the less complex Pelkey products. The Viviano-Beck products sample more wavelengths than the Pelkey products and the mineralogical implications for the negative values of these mafic parameters are not yet studied.

4.1.1.2. Mineralogical Composition – Dust Cover and Ferric Mineralogy

Concerning the fine-grained ferric minerals and dust cover/nanophase ferric oxides, it seems from my study that Region A shows intermediate values for the products indicating the same, i.e. BD530_2, RBR (Appendix 3). With respect to albedo, region A shows a higher albedo than regions B and C in the regional spectrum shown in Figure 33c. However, region A has a lower albedo than the dusty highland unit Region F (Figure 20). We know from the study of Ruff & Christensen, (2002) that the albedo is related to the dust cover in the Martian context (Section 4.1.2.1). From the spectral analysis, we see that the spectra of Region A are featureless, as seen in Figure 16 only exhibiting a downward sloping trend. As we move outward from Region A into F, the composition changes into more dusty highland terrain. The spectra of the dusty regions (Region F) show an absence of the downward slope, as shown in Figure 20. The dusty Region F is dominated by fine particle ferric dust as seen in the dust cover index map (Figure 8) otherwise addressed as nanophase ferric oxides (Ming & Morris, 2017).

Additionally, the SH600_2 that shows a significant influence in the PCA RGB (Figure 6b), also seems to highlight Region A. The product SH600_2 is designated by Viviano-Beck et al. (2014) to highlight ferric minerals (see Appendix 3). The global map of SH600_2 does show that the Region A (South Acidalia) shows slightly higher values. However, the non-averaged original resolution map of the SH600_2 parameter shows the extreme effects of levelling imbalance between strips. This levelling imbalance occurs due to the atmospheric and photometric correction applied to each MSP strips separately before they are mosaicked together (F. P. Seelos, Murchie, & Hopkins, 2018). Adjacent strips vary starkly and complicate interpretation.

a)

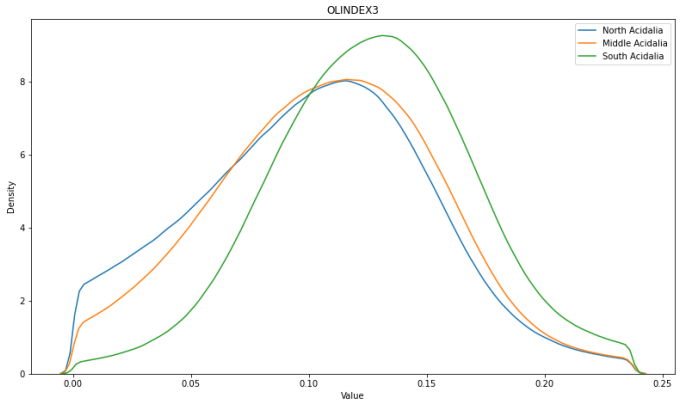

b)

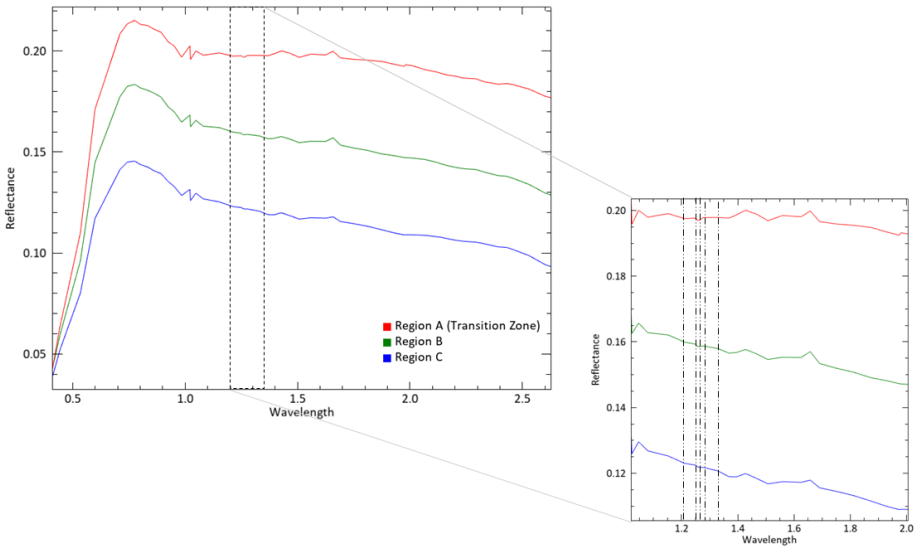

Figure 29 : a) Density plot showing the distribution of OLINDEX3 values for regions. It is seen that South Acidalia (Region A/Transition Zone) shows a tendency of higher values and a higher mean b) Formulation of the OLINDEX3 parameter indicated on the Regional Mean spectra (see section 4.1.2.1). Dotted lines in the zoomed-in spectra window indicate the wavelengths where the reflectance value is input for the OLINDEX3.

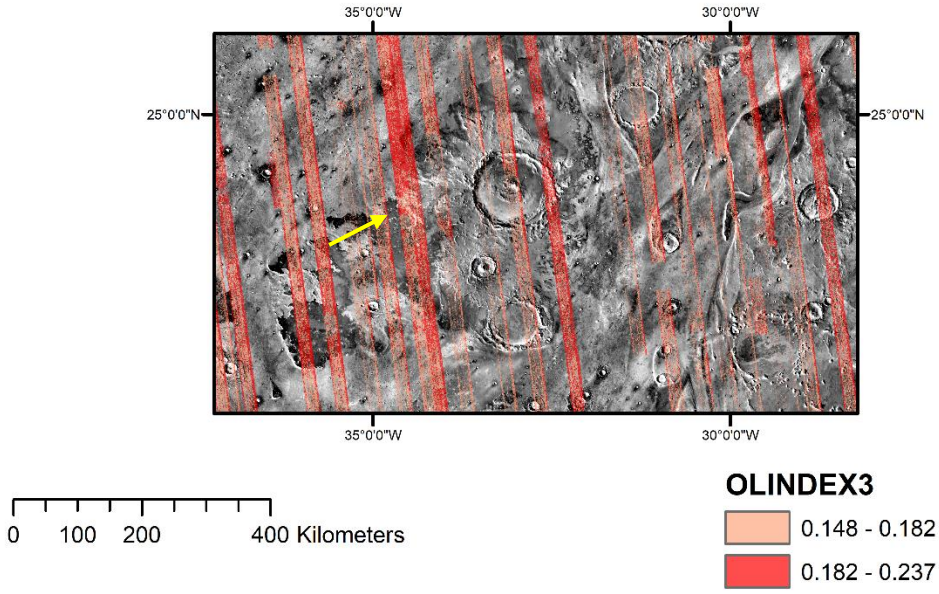

Figure 30 : Patterns shown in Region A showing high values of OLINDEX3 associated with the crater, overlain on THEMIS daytime IR.

Apart from mineralogy, the thermal inertia seems to be an interesting component in differentiating the regions of the Northern Lowlands. In the following section, I will discuss the observations from the Thermal Inertia maps generated by Christensen et al., (2001) using data from the TES instrument. The regions demarcated from my study were overlain on the TES derived Thermal Inertia map (Figure 31b) using JMARS.

4.1.1.3. Thermal Inertia

Region A also shows interesting patterns for the thermal inertia (TI) map (Figure 31b). With respect to the TES thermal inertia map (Mellon, Jakosky, Kieffer, & Christensen, 2000), as shown in Figure 31a and 31b, the patterns of TI values in Region A are complex. There are localised regions of high TI around 510-380 J m^{-2} K^{-1} $s^{-½}$ indicating larger particle size (Christensen et al., 2001) and these higher values occur roughly associated with the mouth and on the floor of the outflow channels northern Chryse Planitia (Region A). This pattern of thermal inertia values has been studied by Mellon, Jakosky, Kieffer, & Christensen, (2000). The aforementioned study attributed the TI values in region A to the boulders at the mouth of the outflow channels that may be indicative of the catastrophic flooding events transporting sediments, that would have taken place via these outflow channels during the Hesperian. The remainder of this transition zone shows intermediate thermal inertia values of 280-340 J m^{-2} K^{-1} $s^{-½}$.

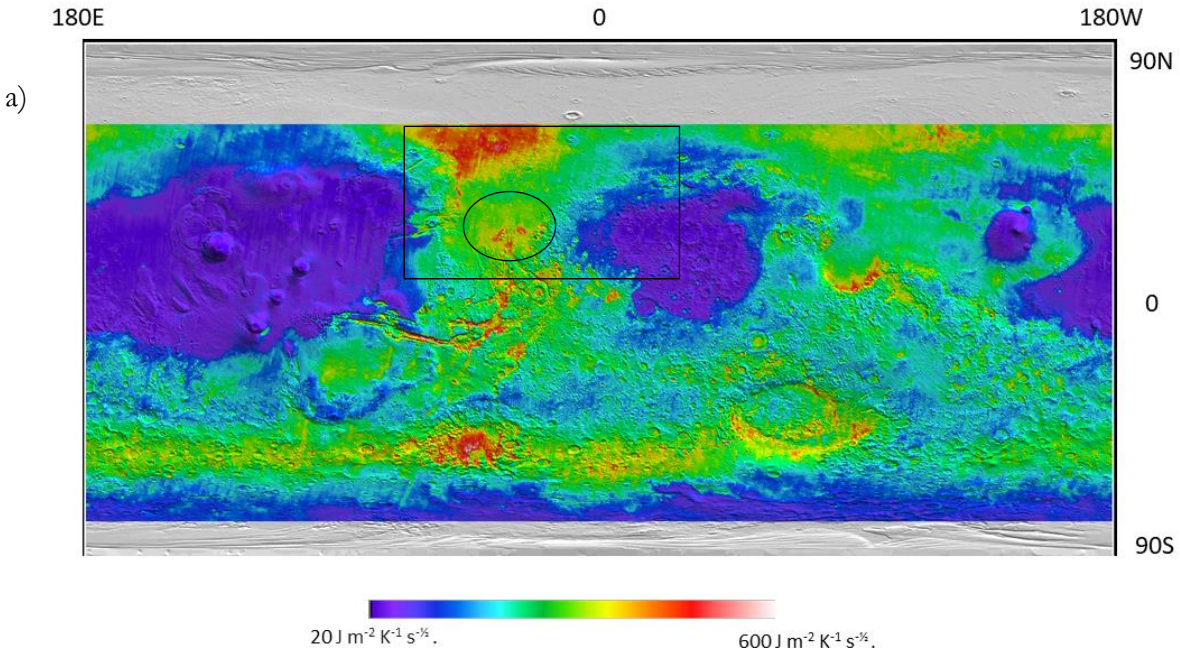

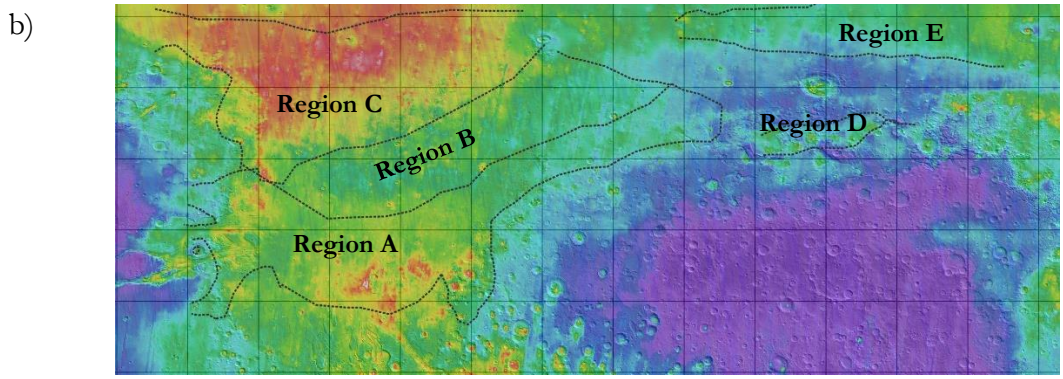

Figure 31 :Thermal Inertia Map by the TES Instrument (Christensen et al., 2001)with the study area indicated. The encircled region is the high TI values in Region A.

4.1.1.4. Geologic Context

With respect to the Geologic Map by Tanaka et al. (2014) shown in Figure 32, Region A relates to the Hesperian outflow unit. The Hesperian period is speculated to have been dominated by extensive deposition of sediment from the various Circum-Chryse outflow channels into the Northern Lowland basin (Salvatore et al., 2010). The Hesperian also contained episodes of volcanism (Salvatore et al., 2010). In the craters of Chryse Planitia (South Acidalia) , as shown in Figure 30, higher values for the OLINDEX3 MSP products occur associated with the ejecta of the crater, although the patterns are not very clearly discernible. The association of the observed olivine content with the crater ejecta could indicate the excavation of a mafic substratum that has also been noticed in the OMEGA data set by Ody et al. (2013) and said to have been indicative of volcanism in the Hesperian period. The study by Ody et al. (2013) also identified mafic signatures around larger craters further north within Acidalia, that would also indicate the occurrence of a mafic Hesperian substratum at larger depths. However, in my study, patterns around the craters in Region B and C are not identified, this could be because of the poor quality of the summary products and the general lack of defined patterns seen in the products.

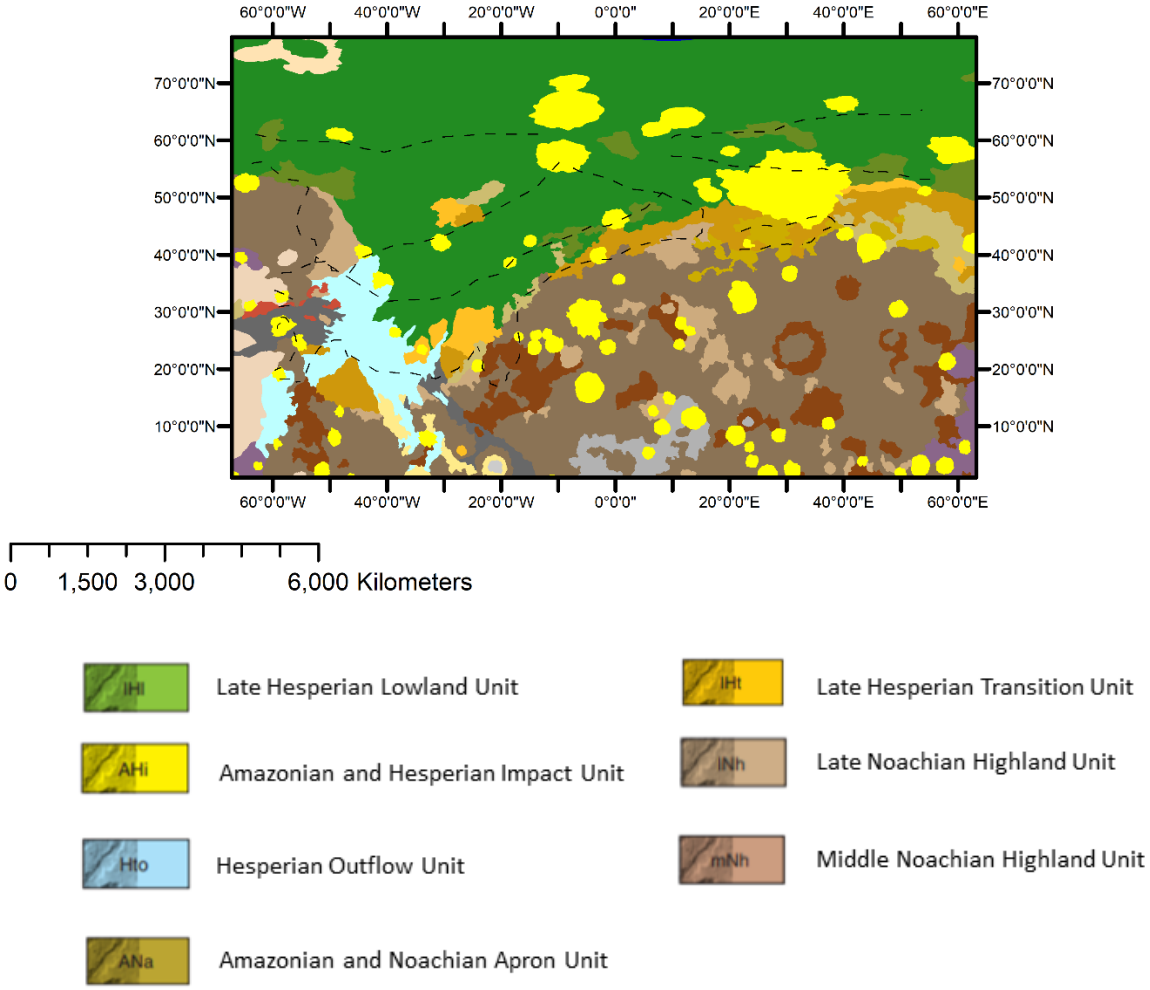

Figure 32 : Geologic Map by Tanaka et al. (2014) with the demarcated regions.

In summary, from my study Region A is indeed a 'transition zone' in terms of topography, Region A is more elevated than B and C (Figure 34a). In terms of regional composition, Region A shows higher indication of mafic mineralogy, i.e., the 1 μm absorption that could be interpreted as olivine content (or ferrous absorption in basaltic glass/glassy basalt) and intermediate dust cover compared to Region C, and F. The Region A also contains numerous outflow channels that seem to originate in the southern highlands. Additionally, Region A spatially relates to an extent to the transition unit identified by (Kamps et al., 2019). Its extension beyond 50N, and further east is not clearly identified in my study. The identified Region A is also in relation with the transition from ST1 and ST2 identified by Wyatt, McSween Jr., Moersch, & Christensen (2003) utilising the TES data, where ST 1 and 2 are described in section 1.1.1.

4.1.2. Region B (Middle Acidalia) and Region C (North Acidalia)

In the following sections I will elaborate on the characteristics of Regions B and C and put the variations in context with the characteristics of the Region A (South Acidalia).

4.1.2.1. Spectral Variation – Albedo, Spectral Slope

The spectral difference between Region B and C is quite subtle (Figure 33a) in comparison to the difference between these two regions and Region A as they are only seen as distinct units in the mafic browse product in Figure 9. The regional spectra for A, B and C are shown in Figure 33c along with the spectral angle between these observations (Figure 33a) and the absolute values of the slope (Figure 33b).

The spectral angle between Regions B and C is the lowest, which may imply that they are spectrally similar.

a)

Region	Angle
A and C	0.075
A and B	0.047
B and C	0.028

b)

Region	Mean Slope
Transition Zone /A	0.000502
Region B	0.000638
Region C	0.00071

c)

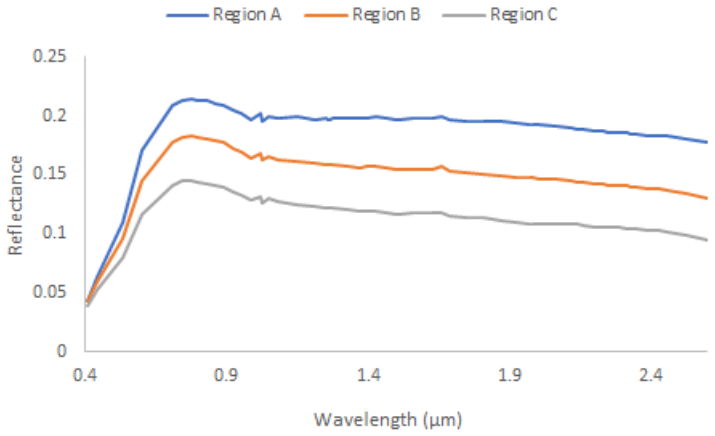

Figure 33: This figure set indicates the quantitative spectral differences between Region A,B and C a) Mean absolute spectral value b) Spectral angle between regional spectra c) Regional Spectra

The striking variation observed spectrally from Figure 33c between Regions A, B and C, is the difference in albedo. Typically the albedo is related to the fine particle dust cover in the Martian context (Ruff & Christensen, 2002), so it might be that this difference in albedo (the highest albedo in Region A), might be influenced by the presence of nanophase ferric oxides/dust, i.e., a northward decrease in dust from Region A to C.

The characteristic of high thermal inertia (Figure 31b) combined with low albedo might indicate the presence of duricrust in Region C (Jones, Caprarelli, Mills, Doran, & Clarke, 2014).

As seen in Figure 33c, the common characteristic of Regions A, B, C is the consistent downward, i.e. negative spectral slope from ~1 µm. The PCA composite Figure 6a shows regions B and C becoming more yellow-orange, indicating higher contributions from the product ISLOPE1 and SINDEX2 (section 4.1.2.2) . The product ISLOPE 1 is a characteristic product for the region Acidalia Planitia itself since this region shows a consistent negative downward spectral slope that seems to obscure other absorption features.

The existence of this slope makes it difficult to study in detail the mineralogy of the region Acidalia Planitia overall. In my study, a similar slope among these regions is identified. The strength of the slope is found to increase with increasing latitude in the CRISM MSP strips as we see in Figure 33b. Region C showed a slope that is close to 30% steeper than the regional spectral slope from

the Transition Unit, i.e. Region A. This spectral slope seems to be a defining ubiquitous characteristic of these low albedo lowlands. This negative slope has also been previously identified in the OMEGA dataset in this study (see Figure 22b) as well as in the study by Salvatore et al. (2010).

In my study using the mean spectra from the OMEGA scenes, Region A and B do show slopes in the spectra; however, the spectrum in Region C is rather flat from 1.6 μm to 2.5 μm as seen in Figure 22 b. This spectral flattening might be an artefact of this image scene 1000_4 since the region C as characterised by the CRISM data contains a steep downward slope and shows no signs of this spectral flattening.

The Northern Lowland regions that have been identified by my study to exhibit this negative spectral slope have also been modelled using data from the TES and interpreted to be andesitic (Bandfield et al., 2000) or weathered basalt (Wyatt & McSween, 2002).

The VNIR-SWIR negative slope has been earlier attributed to a thin bright Fe^{3+} coating that covers the dark basaltic material of the Northern Lowlands (Singer & Roush, 1983). The aforementioned study explains that the decreases in reflectance towards longer wavelengths (longward of 1μm) is due to the absorptions by the underlying dark basaltic substrate. However, this is might not likely be the favoured cause of the spectral slope in the case of my research since if such a ferric coating was present, high values for the BD530_2 parameter (Appendix 3) would be expected, and that is not seen in our data.

The lack of a strong ferric phase in the demarcated regions is supported by studies on the OMEGA dataset by Carrozzo et al. (2012). In the study by Carozzo et al. (2012), an index to highlight the absorptions due to ferric coasting is designed, this is known as COATINDEX. The COATINDEX values for the Northern Lowlands' regions show low values. This study by Carrozzo et al. (2012) attributes the downward slope of the northern lowland regions to a rind consisting of either pyroxene or glass. However, this composition of the rind must agree with the TES spectra that are highly dominated by silica (Bandfield et al., 2000). Taking into consideration, this thermal infrared constraint on the mineralogy of this region, Horgan & Bell (2012)propose that the Northern Lowlands regions are instead covered by glass-rich deposits that formed as a result of explosive volcanism.

The weathering rind is hypothesised by Horgan & Bell (2012) to be formed by the exposure of the iron-bearing glass to acidic solution where the acid penetrates the glass and leaches the cations and a rind consisting of silica is deposited on the glass. However, the origin of the acidic fluid necessary for this alteration is not very clear although there are a few hypotheses made in literature. Horgan & Bell (2012) hypothesise that fluid may have derived from ice sheets. The presence of ice sheets in the mid-latitudes has been attributed to the variations in the Martian obliquity that led to the presence of ice (Head, Mustard, Kreslavsky, Milliken, & Marchant, 2003). The small amounts of fluid rich in Fe^{2+} would have been acidified due to photooxidation or interaction with atmospheric oxygen (Horgan & Bell, 2012; Hurowitz, Fischer, Tosca, & Milliken, 2010). Another hypothesis is that the acidification of the fluid would have occurred with interaction from volcanic aerosols (Hurowitz et al., 2010). Additionally, Hurowitz et al. (2010) also place constraints regarding the 1 μm band position that is shifted to longer wavelength and exhibits itself in a broader manner that may be indicative of iron-bearing glass. Basaltic glass does show a mafic absorption signature at ~1μm (Horgan et al., 2017), which could also be a possible interpretation for the patterns exhibited by OLINDEX3 product values (section 4.1.1.1).

The CRISM MSP summary product map of Integrated Band Depth 1000nm (BDI1000VIS) that is designed to pick up iron-bearing glass shows relatively higher values ~ 0.023 (see Appendix 3) almost similar to the values exhibited by the Southern Highlands. Some studies interpret the underlying substrate as glassy basalt (Salvatore et al., 2010), while others characterise it as basaltic glass (Horgan & Bell, 2012), and the acidic alteration of both seem to produce spectral slopes identical to what has been identified in my study. Despite the patterns for the BDI1000VIS product, the interpretations for the OLINDEX3 1μm absorptions (Section 4.1.1.1), it is tricky to say the exact nature of the underlying substrate from my study – whether it is glassy basalt or basaltic glass. From my study and the literature, we can infer that the spectral downward slope is indicative of a distinct style (possibly acidic) of weathering in the northern lowland region thereby preferring the weathered basalt interpretation for surface type 2.

4.1.2.2. Summary Product Variations

The regions B and C show a relatively (to the global values) higher indication of occurrence for low calcium pyroxene. However, the patterns are quite faint, and the consequent absorption features around 1.8 μm are very faint in the mean spectra.

The regions B and C also shows lower elevation than Region A, where Region C shows the lowest values. This is seen in Figure 34a, which is an elevation profile across the traverse (red line) indicated in Figure 34 b.

Region C was demarcated preliminarily on viewing the PCA RGB composite (components 1,2,3) Figure 6a, where the colours became more yellow-orange northward moving from Region A to C. Yellow-orange tones imply an increase in values contributing to the Red and Green channel. In this case, these two channels have a significant positive contribution from the summary products SINDEX2 and ISLOPE1(see Section 4.1.2.1). The SINDEX2 parameter is engineered to highlight hydrated sulfate absorption at 2.4 μm (Viviano-Beck et al., 2014). However, the SINDEX2 parameter must be interpreted with caution as it also captures ice (Viviano-Beck et al., 2014)

Apart from the ISLOPE1 parameter, regions B and C shows elevated values for the band depth 1300 designed to detect Fe^{2+} substitutions in plagioclase but could also be highlighting Fe-Olivine (Viviano-Beck et al., 2014). However, the high values mentioned above are only in the range ~0.02.

The distributions of only the positive band depth values for hydrated summary products designed to pick up features indicating sulfates and carbonates, i.e. BD2210_2(phyllosilicates but also captures alunite, gypsum), BD2100_2, BD1750_2, BD3400_2 are visualised in Figure 14. Region C shows a higher probability to contain relatively high positive values for these products. Region B shows a very similar distribution to Region C.

The latitude dependent trend, as seen in Figure 14, in the probability of finding higher values for the evaporite products (in particular sulfates) in Region C (North Acidalia) identified by my study is in accordance with the higher values for the sulfate group identified by the TES instrument (Bandfield, 2002) where few pixels within Acidalia have been identified to show values beyond detection limit (Appendix 5).

Overall, on viewing the global averaged maps (Appendix 8) as well as the distributions of the positive values for the study area, the observation of higher probabilities of finding high values for the evaporite products, may support a weathered basalt (in acidic conditions) interpretation (Section 4.1.2.1) for the Northern Lowland regions. However, it is ambitious to state this as definitive evidence for acid weathering model since these products are affected by noise, and only

very few pixels show positive values. The product BD3400_2 must also be interpreted with caution since it lies in the wavelength region of very low signal to noise ratio for the CRISM instrument (Section 3.3). The trend in the product BD3400_2 does not ascertain the presence of carbonates. Moreover, widespread carbonates have not been identified previously (Ehlmann & Edwards, 2014). The positive values for the evaporites products also are very low. Additionally, upon zooming into these CRISM products, no prominent patterns are identified. Further investigation of this region is required to ascertain the abundance of sulfates.

a)

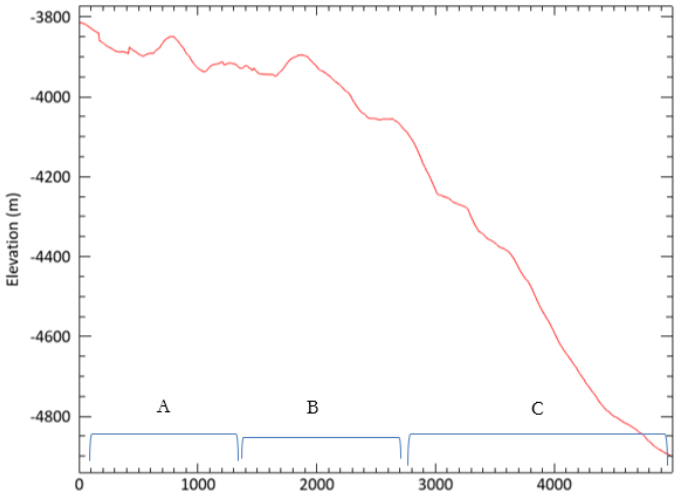

b)

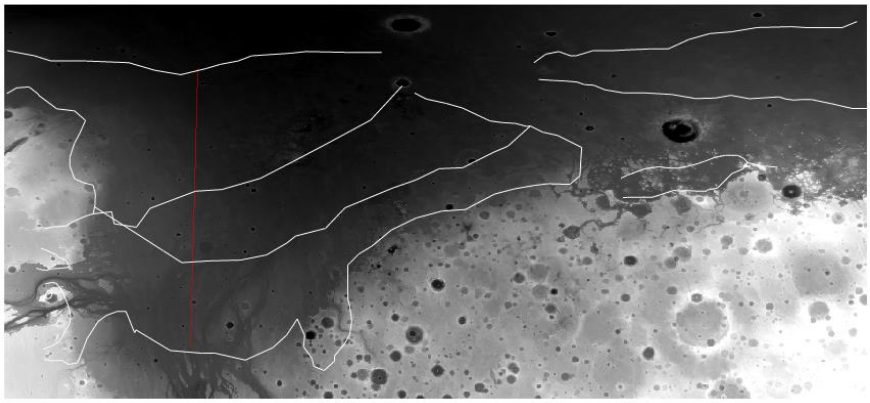

Figure 34 : a) Elevation Profile b) Traverse indicated in red across regions A, B and C overlain on MOLA DEM

In summary from section 4.1.2.1 and 4.1.2.2, the combination of the downward spectral slope and the indication of higher values for evaporite summary products in the Northern Lowlands might point towards acidic alteration. Despite the trend, I am reluctant to conclude that the identified high values for the evaporite products, ascertains their presence since the summary products are affected by noise in the spectra (as seen in Figure 16,17,18) and upon zooming in do not show very defined patterns associated with landforms. The CRISM MSP summary products also contain influences from aerosols - dust/ice since only the CO_2 atmospheric absorptions are corrected for by the volcano scan algorithm(Wiseman et al., 2014) .

4.1.3. Region D – Deuteronilus Mensae

Region D shows very similar properties in the PCA composite (components 1,2,3) as in Figure 6a to Region B and C, i.e. it appears magenta and contains significant contributions from the products ISLOPE1 and SH600_2 (both these products show relatively high values in this region). This region is precisely on the highland lowland dichotomy and is also known as the Deuteronilus Mensae region. Region D is characterised by its ice-related landforms encircling mesas (Baker & Head, 2015) and investigated in detail using the OMEGA image 4357_6 in my study, as shown in Figure 35.

The region D is encircled in black shown in Figure 35a, and the corresponding spectra are shown in Figure 35a. The spectra of the mesas and the embaying unit are similar i.e., they show the downward slope as well as absorption at 1.428μm (OH or ice feature) and ~2.6 μm (H_2O absorption). It is also seen that unit that embays the mesas show high values for the BD1435 that indicates CO2 ice. The geologic map by Chuang & Crown (2009) identifies this embaying unit as a debris apron material that was emplaced later compared to the mesas. The mesas being Noachian in age whereas the debris apron being the youngest, i.e. middle to late Amazonian (Figure 32).

Region D lies exactly on the northernmost extension of the Southern Highland-Northern Lowlands dichotomy (Watters et al., 2007). It is speculated to exhibit the characteristic features of the mesas and extensive ice-rich units around the mesas due to the glacial modification of the dichotomy in the Amazonian (Head, Nahm, Marchant, & Neukum, 2006) where mesas are remnants of the highland unit. The Region D, i.e. Deuteronilus Mensae is interesting as it lies on the proposed shoreline (Parker et al., 1993) as shown in Figure 35 a.

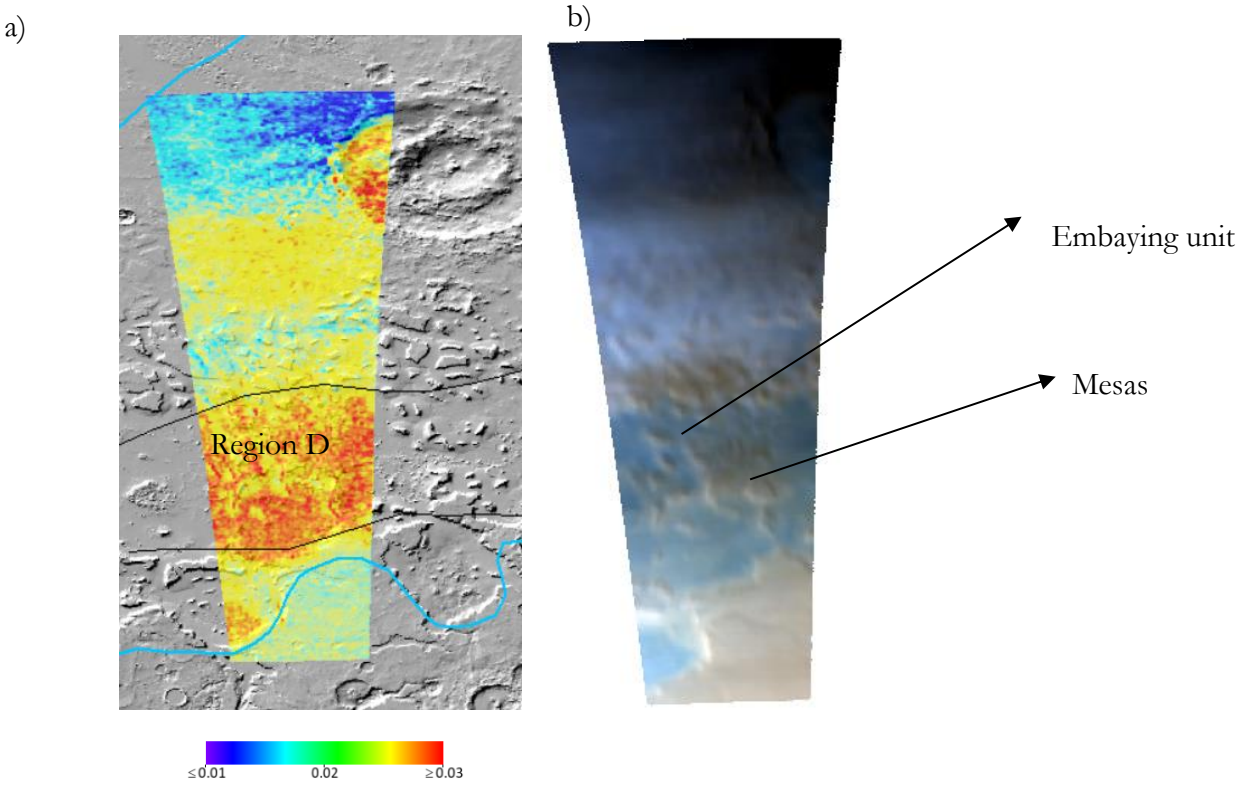

c)

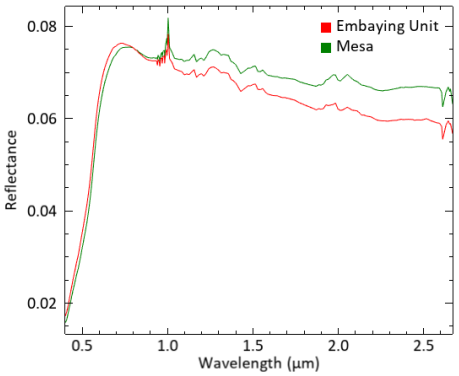

d)

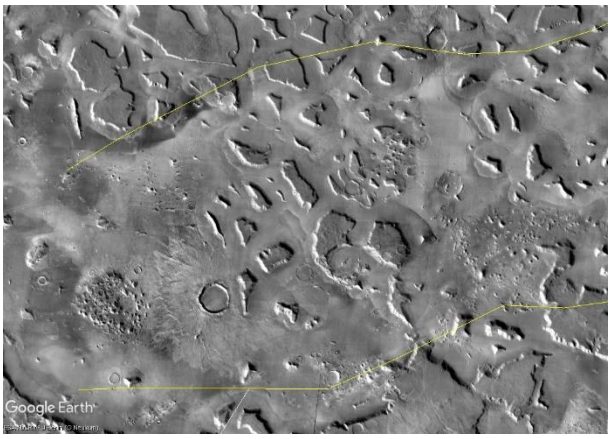

Figure 35 : a) Band Depth 1435 indicating CO2 ice absorption overlain on MOLA Hillshade with proposed shorelines (Parker et al., 1993) indicated in blue b) True colour image of the scene with mesas and embaying units indicated c)Mean Spectra of the units within Region D d) THEMIS daytime infrared image of the Region D encircled in yellow. Mesas in the region are clearly visible

If indeed a Noachian Ocean existed then it could have contributed to forming the mesas we see in this region following which the emplacement of the ice-rich debris apron could have occurred (Li, Robinson, & Jurdy, 2005). However, in my study, no indication of phyllosilicates was observed associated with the Noachian mesas. The lobate debris aprons surrounding the mesas are considered to form due to mass wasting processes involving ice (Head et al., 2006).

4.1.4. Region E – Eastern Acidalia

The region E also shows similar characteristics to Region A, B, C in the PCA composite (components 1,2,3) as shown in Figure 6a. Region E exhibits itself as an eastward extension of the principal lowland regions -A,B,C. The mean spectra in Figure 19b are also similar to Regions A, B, C in terms of the downward slope; however, region E shows deep absorptions at 1.5 μm and 2.0 μm. The 1.5 μm is indicative of water ice absorption (Viviano-Beck et al., 2014). My interpretation is that Region E is an eastward extension of the northern lowland formation with ice-rich terrains.This ice could be in the form of the Latitude Dependent Mantle that is formed by precipitation from the atmosphere and ground ice is speculated to be stable at the current obliquity of Mars (Orgel et al., 2019). According to the geologic map by Tanaka et al. (2014) show in Figure 32, this region is also covered by the Vastitas Borealis Formation that is hypothesised to be a veneer of sediments overlaying most of the principal lowlands formation, formed during the Amazonian (Head, Kreslavsky, & Pratt, 2002).

4.2. Local variations identified

Certain patterns in the PCA composites as well the mafic browse product were interesting but could not be studied in detail due to the noisy nature of the CRISM MSP data products; hence OMEGA scenes are used. These patterns were studied using the summary products calculated onto the OMEGA data and looking at the combination of the summary products, - i.e. browse products.

4.2.1. Mawrth Vallis

The region covered by OMEGA scene 353_3, as shown in Figure 25a, stood out during the data analysis as it showed extremely precise patterns even in the mafic browse product shown in Figure 9. This unit also is classified as a part of the Southern Highlands in the surface type classification by Kamps et al., (2019) (Figure 28a).

In the mafic browse product in Figure 25a, this region shows higher values for the OLINDEX3 product, i.e. indicating a broad 1 μm absorption in the region surrounding the Oyama crater. This is confirmed by a recurrence in the individual CRISM MSP strips (shown in Figure 25b). This region was further analysed using browse products on the OMEGA scene 353_3. This is the only region in my study of the Northern Lowlands, where clear indications of Fe/Mg and Al phyllosilicates are found in the OMEGA browse products. Smectite features identified in the yellow region are shown in Figure 26b and c. These smectites may have been remnants of aqueous alteration in this region. From the geological map in Figure 32, it is seen that Noachian units cover this area. The identification of phyllosilicates in the Noachian units may point towards the proposed aqueous alteration of the basaltic material during the Noachian (Loizeau et al., 2015; Gou, Yue, Di, & Wang, 2015).Although, this is a simplified version of the alteration history that may have characterised this region. The region Mawrth Vallis was also one of the candidate sites for the landing of the Exo Mars 2020 mission by the European Space Agency (Vago, 2014).

Stratigraphic patterns of Al-smectites overlying Fe-smectites in this region have been identified by higher-resolution CRISM Full Resolution Targeted data of pixel size ~18m (Loizeau et al., 2015); however, with the data used in my study where the pixel size is of the order 100-200m, it is difficult to discern the stratigraphy of the clay-bearing units. The study by Loizeau et al. (2015) attribute the formation of the Fe-Mg smectite layer to be due to aqueous alteration in the Early Noachian predating the Al-smectite unit, that is hypothesised to have been formed due to leaching of the Fe-Mg smectites. Since the stratigraphy is not visualised with the low resolution of the OMEGA and CRISM MSP data used in my study, only broad inferences of indications of aqueous alteration in the Noachian can be made.

It is noticed in my study that the wavelength map is shown in Figure 26a, that the floor of the Mawrth Vallis channel (indicated in Figure 26a) itself does not show indications of clay minerals but rather the regions near the Oyama crater do show these signatures. However, a large portion of the Mawrth Vallis channel is not imaged in the scene in Figure 26a

A study by Bibring et al. (2006) also indicated a similar pattern of absence of clay minerals in the Mawrth Vallis channel and attributed that the water that caused the alternation may not have been a part of the Hesperian outflow channels but another source earlier in the Martian history, thus lending further evidence to state that the alteration might have taken place by a source in the Noachian.

This region also served as a reference to understand the quality of the CRISM hydrated products (Appendix 4). Despite the clear mineral indication in Mawrth Vallis, the CRISM MSP strips are mostly noisy for the browse products and show very faint patterns.
Overall, the region Mawrth Vallis seems to hold a record of historical information regarding the ancient martian crust and is the only region in my study that shows distinct spectral absorption features indicative of Fe/Mg smectites.

4.2.2. Indications of Hydrated Minerals at the Dichotomy

As seen in section 3.4.4.2 OMEGA scene 314_4 shows a pattern of absorptions close to 2.18- 2.2 μm that might be indicating Al-OH absorptions (as shown in the Figure 27a) as well as pixels surrounding this region with absorptions at slightly longer wavelengths (yellow pixels) , i.e., ~2.28 μm (Fe/Mg-OH). The mean spectrum is shown in Figure 27b, shows very faint absorption features. This region was also detected and mapped using the CRISM full resolution targeted image and speculated to contain a complex assemblage of younger hydrated silica units containing phyllosilicate bearing knobs that were remnants of an altered Noachian crust just as the weathered unit at Mawrth Vallis (Pan & Ehlmann, 2014). However, the resolution of the dataset used in this research does not show the detailed patterns as done in the study by Pan & Ehlmann, (2014). The spatial association of this hydrated unit in this region, with a proposed shoreline (Carr & Head III, 2003) may be an argument in favour of a Noachian water body (paleo-ocean or a paleolake) that altered the old Noachian terrains.

4.3. Comparison with OMEGA Dataset

The density curve patterns are not uniform in the OMEGA dataset (Appendix 7) as they were observed to be in Figure 14 using the CRISM MSP strips. Although North Acidalia (region C) shows a higher probability of containing higher values for the summary product BD1750_2 and BD3400_2, the behaviour of Region C is similar to Region A as seen in the graphs for BD2210_2, BD2100_2. The disagreement could be because I have sampled regions of interest within the scenes and these are on the Eastern side of Acidalia(Figure 21). Also, the sampled pixels are not covering the whole of Regions A, B and C as they did in the mosaic density plots (Figure 14). It is recommended to make an extensive selection of OMEGA scenes covering the regions A, B and C thoroughly and then comparing the distribution.
Apart from the evaporites summary products, the products like ISLOPE1 and the mafic products also do not show a direct relation to the values from the CRISM MSP products. The scatterplots for the products ISLOPE1 and OLINDEX3, respectively, for the scene, 314_4 lying on the highland-lowland dichotomy are shown as an example in Appendix 7. The ISLOPE1 scatterplot shows clustering that indicates differences in spectral slope across the Highland Lowland dichotomy.
The spectral slope variations across the dichotomy identified in the CRISM MSP dataset is reproduced in the OMEGA dataset as well (section 3.4.2). Maps indicating the similar patterns between the ISLOPE1 on the CRISM and OMEGA data are attached in Appendix 7. However, the pattern of increasing slope steepness is not seen in the OMEGA dataset mainly due to the spectral flattening artefact in the scene 1000_4.

Patterns in areas with relatively clear absorption features, i.e., Mawrth Vallis showed clear relations between the OLINDEX3 values in both the OMEGA dataset as well as the CRISM dataset, as shown in Figure 25a.
A limitation of my study was the employment of a few selected OMEGA scenes which limited the comparison with the extensive CRISM MSP mosaic and MSP strips.
With respect to the global Olivine map produced using the OMEGA data (Appendix 2), it is seen that the Northern Lowlands itself do not contain any indications of Olivine. This is mainly due to the threshold defined by Ody et al. (2012) for the olivine highlighting parameters. Studies of olivine enrichment on a local scale (Ody et al., 2013) showed similar indications of olivine associated with crater ejecta as was observed in my study (section 4.1.1.1).

4.4. Implications for the Northern Lowlands

The Northern Lowlands could have formed due to a combination of various geological processes (Head et al., 2002). The lack of a clear spatial distribution, especially for summary products related to phyllosilicates or sulfates, complicates concluding on the timing and sequence of geological processes such as weathering. From my study, we see slight indications of the probable processes that led to the current state of the Northern Lowlands. In the following paragraphs, I elaborate on the context of the findings of this thesis.
The units I have investigated, span across different Martian geologic time scales with the local variations found in Mawrth Valles being the oldest, i.e. the Noachian terrain and the units B and C roughly coinciding with the Vastitas Borealis Formation that is the most recently deposited sedimentary layer during the Late Hesperian/ Early Amazonian (Tanaka, Skinner, & Hare, 2005).
The main characterisation of the studied units especially A, B, C are the spectral slope that is speculated to be affected by the presence of a weathering rind (see Section 4.1.2.1) and is similar to the spectra indicated by weathered glassy basalt in the study by Salvatore et al., (2010).
The formation of this rind is hypothesised to be formed due to weathering of basaltic glass or glassy basalt in acidic alteration in a study by Horgan & Bell (2012) (section 4.1.2.1).
If the steepness of the spectral slope in the CRISM MSP is an indication of the degree of weathering, then it may be that Region C was more pervasively altered due to increased interaction with ice (higher latitudes) (Wyatt, McSween, Tanaka, & Head, 2004) or with prolonged interaction due to the ponding acidic water (lower elevation than Region A, B). If such a regional acidic alteration did take place, it would be expected to find spectral indications of largescale deposits of evaporites. On a global scale, in the averaged maps generated by Kamps et al. (2019), relatively high values for evaporites products (especially sulfates) in the Lowlands compared to the Highlands is seen (Appendix 8). However, the values of the products are still quite low. On a local scale in the original resolution used by my study, no distinct patterns associated with landforms is identified with the evaporites summary products and their appearance is rather random. A faint latitude dependent trend of increasing probability of pixels with relatively higher values is seen in my study. The observed latitude dependent increase in evaporites especially sulfates is in accordance with the TES map (See Appendix 5) by (Bandfield, 2002) as shown in, with slightly higher values in the Northern Lowlands.
Regarding the origin of the substrate under the rind, interpretations from the TES instrument by Roger et al. (2007) (section 4.1), propose that it could originate from a basaltic influx from the

Southern Highlands that has been altered regionally in the Northern Lowlands. This regional alteration is in accordance with the interpretation of the possible acidic alteration (section 4.1.2.1), causing the spectral slope as discussed in the previous paragraphs. Roger et al. (2007) also provide an alternate speculation that the substrate beneath the weathering rind could originate from a different lithology altogether, due to the variation in pyroxene abundance in relation to highland units.

The study by Rogers & Hamilton (2015) use TES modelled spectra and global maps of the Gamma Ray Spectrometer along with Pelkey products to delineate provinces. Their study identified two classes within Acidalia, namely North Acidalia and South Acidalia. They indicate that North Acidalia shows an enhancement in the high silica phase but lower sulphate content than the Southern Acidalia. The latter result does not agree with the findings of my study that shows a higher probability of higher values withing the Northern Acidalia region (Region C) for the summary products indicating sulfates. However, Rogers & Hamilton (2015)were not able to explain the enrichment in south Acidalia.

This disagreement could be due to the fact that only a few pixels showed values beyond the detection limit for high sulfate content in Acidalia by the TES instrument (Bandfield, 2002b). Another probable cause of this disagreement would be that the summary products of the CRISM MSP may indicate patterns that are influenced by the atmosphere. Even though the strips are corrected for, the volcano scan algorithm only corrects for the carbon dioxide gas absorption and not for the effects of aerosols (Wiseman et al., 2014). The higher values for the evaporites may not be a definitive indication of their presence in the region.

In addition to the spectral slope, summary product patterns, my study also identified localised patterns as discussed in Section 4.2 that may relate to the remnants of an aqueously altered Noachian unit that is obscured in Region A, B and C by the overlying younger units. Region E is also covered by the younger Hesperian aged unit. From the alteration clay minerals identified in the OMEGA scene 353_3 covering the Mawrth Vallis unit, supports the hypothesis of the aqueous alteration of the Noachian crust. It is not clear if this aqueous alteration was largescale and under submarine conditions since extensive phyllosilicate signatures are absent throughout the study area due to the obscuration by Hesperian aged material in Region B and C. The identification of the Noachian altered remnants is also in accordance with the detection of clay minerals in scene 314_4 at the dichotomy boundary that may also indicate altered Noachian terrain (Pan & Ehlmann, 2014). In my study, I notice that the Noachian mesas in the region D (see Figure 35 and geologic map Figure 32), do not show the presence of any altered units.

In summary, as mentioned earlier, ascertaining one unified formation theory based on the results and interpretations of this research is tricky because the Northern Lowlands have formed because of different processes. However, instead of favouring one theory proposed by Wyatt et al., (2003), a complex combination of the three processes could explain the variations seen in the study area. A simplified interpretation could be that the ancient Noachian unit may have been aqueously altered. The aqueous alteration could have taken place through a paleolake or an ocean (associated with the shorelines). However, no widespread phyllosilicates are found mainly because most of the Noachian units are obscured by overlaying Hesperian material (Figure 32). Indications of volcanism during the Hesperian is also seen with the higher interpreted mafic mineralogy in the substratum in Acidalia Planitia (Salvatore et al., 2010). The Hesperian outflow channels with tear-shaped islands (Appendix 9) indicate there could have been a flow of sediment from the southern highlands

followed by widespread weathering processes in the Northern Lowlands basin. The medium of weathering could be due to acidic fluids (interaction with ice/acidic ocean) giving rise to the weathering rinds. It is speculated that the change from an alkaline to an acidic environment is in relation with the aridification of the surface (Bibring et al., 2006; Hurowitz et al., 2010).

5. CONCLUSIONS AND RECOMMENDATIONS

5.1. Conclusions

In this research, I investigate in detail the Region Acidalia Planitia and its immediate surroundings using the CRISM MSP orbital strips (summary products and reflectance) along with the OMEGA datasets. From this study, I conclude that:

- The Transition Unit described by Kamps et al. (2019) using the downsampled data (Figure 1), is retrieved in the non-downsampled, i.e. original summary product data as South Acidalia (Region A). This region appears to be a gradual transition in composition and in elevation. While the Northern Lowlands Unit identified in the study by Kamps et al. (2019) spatially relates to the regions North and Middle Acidalia. The spectral slope increases from South Acidalia to North Acidalia while the albedo decreases from South Acidalia to North Acidalia.
- Making mineralogical interpretations using the multispectral summary products is quite difficult since the products are severely affected by noise, atmosphere effects – aerosols, dust and ice since the volcano scan algorithm only accounts for CO_2 absorption. The observations of increased content of minerals indicated by the summary products are not definitive evidence and must be investigated with data of better quality. From my study, I do see an increase in mafic (interpreted olivine) content in South Acidalia (Region A) with faint patterns occurring associated with crater ejecta indicating the possible existence of a mafic subsurface. In the distributions of the positive band depths, the Middle Acidalia (Region B) and North Acidalia (Region C), do show a tendency to have a higher probability to contain relatively higher values for the products indicating sulfates and carbonates (BD1750_2, BD2210_2, BD2100_2, BD3400_2). On a global scale, Middle Acidalia (Region B) and North Acidalia (Region C) together forming the 'Northern Lowland Unit' show relatively higher values for these products (especially the products indicating sulfates) which may be indicative of a distinct style of weathering.However, as mentioned previously the relatively high values for the products are still very low and the nature of these products is quite random. So, the trend in the evaporite products is not definitve evidence of their presence.
- The region of the Northern Lowlands is dominated by the spectral slope that is designated to be highlighted by the product ISLOPE1 (Appendix 3) which is noisy and obscures patterns. In my study, we propose a refined parameter that calculates the slope of the fitted regression line between 1-2 μm. This product is much less noisy and clearly indicates the change in slope across the regions demarcated, especially across the Highland-Lowland dichotomy.
- Apart from the summary products, my study also shows that the spectral slope is a ubiquitous characteristic of the Northern Lowlands that seems to have an increasing trend with latitude in the CRISM MSP reflectance data. If the degree of steepness of the slope is an indication of the weathering process on Mars, it might be that the lowest-lying region – North Acidalia (Region C) has been more pervasively altered. The spectral slope is also

noticed in the OMEGA dataset however the spectra from North Acidalia (Region C) from scene 1000_4 exhibits a spectral flattening from 1.6 μm, that is more likely to be an artefact.

- From literature, we see that the spectral slope could be the by-product of weathering of basaltic glass/glassy basalt. This weathering rind could occur as a result of weathering under low pH acidic conditions. The fluid may have been acidified due to photo-oxidation, interaction with the volcanic aerosol. The fluid source may have been from ice sheets that would have been prevalent in the Amazonian or a short-lived acidic ocean. It is tricky to discern from my study what would have been the definite cause of the acidification of the fluid as well as the source of the fluid. On a broader scale, the patterns of higher values in the evaporites summary products (especially sulfates) in the Northern Lowlands seem to argue in favour of a weathering origin for ST2.
- Various uncertainties and sources of errors are present with respect to the CRISM summary product data, namely:
    1. Outlier definition was arbitrary and done to control noisy pixels
    2. Levelling imbalance in the CRISM data mosaic
    3. Striping effects in the CRISM data (mosaic and individual strips)
    4. Uncorrected effect of aerosols – ice, dust.
- The summary products show clearer patterns in the OMEGA scenes in comparison to the multispectral CRISM data. However, spatial misregistration is observed in the OMEGA scenes between different channels. Noise artefacts are observed in the spectra at the join of two detectors ~1 μm. Spectral flattening is also seen in scene 1000_4 covering the lowest albedo region, i.e. North Acidalia (Region C).
- The localised patterns in Mawrth Vallis show a clear indication of clay minerals associated with the ancient Noachian terrain. This might indicate an aqueously altered Noachian basement. Indications of hydrated features are also identified in the Highland-Lowland dichotomy in OMEGA scene 314_4. They are attributed to the remnant of a Noachian basement as seen in Mawrth Vallis. OMEGA scenes proved to be a very useful dataset in this study to view patterns in context and seem better suited for regional studies.
- Deuteronilus Mensae (Region D) is a characteristic 'fretted' terrain unit that is precisely at the Highland-Lowland dichotomy and shows indications of ice-rich units. Ice influence in the spectra are also identified in Eastern Acidalia (Region E).

In conclusion, it is seen from my study that the spectral slope is a ubiquitous feature characterising the Northern Lowlands. Literature interpretations of the spectral slope include the presence of weathering rind due to acidic alteration, over glassy basalt or basaltic glass. This interpretation favours the weathered basalt as an explanation for ST2 instead of andesite. Noachian units identified in my study exhibit signs of aqueous alteration that may be indicative of a Noachian paleo ocean or a paleolake. These phyllosilicate signatures are highly localised and obscured by younger Hesperian materials. The transition unit, i.e. South Acidalia (Region A), marks a gradual transition from highlands unit into the Acidalia basin, with higher elevations and a higher interpreted olivine content and intermediate dust cover.

5.2. Recommendations

The following recommendations are made based on the results and conclusions derived from this research:

- It is advised to always back up mineralogical analysis on the CRISM MSP strips with good quality data scenes from either OMEGA or the CRISM full resolution targeted images. OMEGA scenes proved effective in this study to visualise patterns that were difficult to recognise in the CRISM MSP strips. The CRISM MSP strips, although they provide global coverage, suffer from noise artefacts and effects of atmosphere that obscure patterns in the summary products that make mineralogical interpretations difficult. Additionally, for regional studies, the OMEGA scenes also have a larger field of view that may aid in studying patterns in context. For the purpose of studying the layering in many localised regions (eg: Mawrth Vallis, Highland-Lowland dichotomy indicating hydrated minerals, craters in South Acidalia showing olivine signatures) on Mars, the CRISM full resolution of 18m/pixel would be a useful dataset.
- I also recommend analysing mineralogical implications for the negative values in the mafic summary products of the Viviano-Beck products, as done by Carrozzo et al. (2012) for the Pelkey products. It would be interesting to characterise the values of the mafic products with Mars analogue samples and with mineral mixtures.
- I recommend studying the geomorphology of the study area in my research since it contains a range of landforms indicating complex past processes such as polygonally patterned grounds, mesas, mounds, tear-shaped island formations (Appendix 9) in the channels that may indicate various processes including periglacial processes (Rogers & Hamilton, 2015), mud volcanism (Oehler & Allen, 2010) widespread in the northern lowland.
- The spectral slope interpretations in this study were based on literature. However, I recommended supplementing the literature findings with laboratory spectral analysis on weathering rinds formed on mars analogue rocks and compare the resultant spectra with what is seen in my study.

LIST OF REFERENCES

Andrews-Hanna, J. C., Zuber, M. T., & Banerdt, W. B. (2008). The Borealis basin and the origin of the martian crustal dichotomy. *Nature*, *453*(7199), 1212–1215. https://doi.org/10.1038/nature07011

Baker, D. M. H., & Head, J. W. (2015). Extensive Middle Amazonian mantling of debris aprons and plains in Deuteronilus Mensae, Mars: Implications for the record of mid-latitude glaciation. *Icarus*, *260*, 269–288. https://doi.org/10.1016/j.icarus.2015.06.036

Bakker, W. H. (2018). HypPy User Manual. In *ITC - University of Twente*. Retrieved from http://www.itc.nl/personal/bakker/hyppy.html

Bakker, W. H., Van Ruitenbeek, F. J. A., Van Der Werff, H. M. A., Zegers, T. E., Oosthoek, J. H. P., Marsh, S. H., & Van Der Meer, F. D. (2014). Processing OMEGA/Mars Express hyperspectral imagery from radiance-at-sensor to surface reflectance. *Planetary and Space Science*, *90*, 1–9. https://doi.org/10.1016/j.pss.2013.11.007

Bandfield, J. L. (2002). Global mineral distributions on Mars. *Journal of Geophysical Research*, *107*(E6, 5042). https://doi.org/10.1029/2001JE001510

Bandfield, J. L., Hamilton, V. E., & Christensen, P. R. (2000). *A Global View of Martian Surface Compositions from MGS-TES* (Vol. 1626). https://doi.org/10.1126/science.287.5458.1626

Bibring, J. P., Langevin, Y., Altieri, F., Arvidson, R., Beilud, G., Bertheĺ, M., … Zasova, L. (2004). OMEGA: Observatoire pour la Minéralogie, l'Eau, les Glaces et l'Activité. *European Space Agency, (Special Publication) ESA SP*, *SP*(1291), 75–95.

Bibring, Jean Pierre, Langevin, Y., Mustard, J. F., Poulet, F., Arvidson, R., Gendrin, A., … Neukum, G. (2006). Global mineralogical and aqueous Mars history derived from OMEGA/Mars express data. *Science*, *312*(5772), 400–404. https://doi.org/10.1126/science.1122659

Carr, M. H., & Head III, J. W. (2003). Oceans on Mars: An assessment of the observational evidence and possible fate. *Journal of Geophysical Research*, *108*(E5), 5042. https://doi.org/10.1029/2002JE001963

Carr, M. H., & Head, J. W. (2010). Geologic history of Mars. *Earth and Planetary Science Letters*, *294*(3–4), 185–203. https://doi.org/10.1016/j.epsl.2009.06.042

Carrozzo, F. G., Altieri, F., Bellucci, G., Poulet, F., D'Aversa, E., & Bibring, J.-P. (2012). Iron mineralogy of the surface of Mars from the 1 μm band spectral properties. *Journal of Geophysical Research: Planets*, *117*(E11), n/a-n/a. https://doi.org/10.1029/2012JE004091

Carter, J., Poulet, F., Bibring, J. P., Mangold, N., & Murchie, S. (2013). Hydrous minerals on Mars

as seen by the CRISM and OMEGA imaging spectrometers: Updated global view. *Journal of Geophysical Research E: Planets*, *118*(4), 831–858. https://doi.org/10.1029/2012JE004145

Christensen, P. R., Bandfield, J. L., Hamilton, V. E., Ruff, S. W., Kieffer, H. H., Titus, T. N., … Greenfield, M. (2001). Mars Global Surveyor Thermal Emission Spectrometer experiment: Investigation description and surface science results. *Journal of Geophysical Research*, *106*, 823–846.

Chuang, F. C., & Crown, D. A. (2009). Geologic map of MTM 35337, 40337, and 45337 quadrangles, Deuteronilus Mensae region of Mars. In *US Department of the Interior, Geological Survey*.

Ehlmann, B. L., & Edwards, C. S. (2014). Mineralogy of the Martian Surface. *Annual Review of Earth and Planetary Sciences*, *42*(1), 291–315. https://doi.org/10.1146/annurev-earth-060313-055024

Ehlmann, B. L., Mustard, J. F., Swayze, G. A., Clark, R. N., Bishop, J. L., Poulet, F., … Murchie, S. L. (2009). Identification of hydrated silicate minerals on Mars using MRO-CRISM: Geologic context near Nili Fossae and implications for aqueous alteration. *Journal of Geophysical Research E: Planets*, *114*(10), 1–33. https://doi.org/10.1029/2009JE003339

Fishbaugh, K. E., Lognonné, P., Raulin, F., Des Marais, D. J., & Korablev, O. (2007). *Geology and Habitability of Terrestrial Planets*.

Frey, H. V, Roark, J. H., Shockey, K. M., Frey, E. L., & Sakimoto, S. E. H. (2002). *Ancient lowlands on Mars*. https://doi.org/10.1029/2001GL013832

Glotch, T. D., Bandfield, J. L., Tornabene, L. L., Jensen, H. B., & Seelos, F. P. (2010). Distribution and formation of chlorides and phyllosilicates in Terra Sirenum, Mars. *Geophysical Research Letters*, *37*(16), 1–5. https://doi.org/10.1029/2010GL044557

Head, J. W., Forget, F., Wordsworth, R., Turbet, M., Cassanelli, J., & Palumbo, A. (2018). Two Oceans on Mars?: History, Problems and Prospects. *49th Lunar and Planetary Science Conference*, 2194. https://doi.org/10.1016/j.icarus

Head, J. W., Kreslavsky, M. A., & Pratt, S. (2002). Northern lowlands of Mars: Evidence for widespread volcanic flooding and tectonic deformation in the Hesperian Period. *Journal of Geophysical Research E: Planets*, *107*(1), 3–1. https://doi.org/10.1029/2000je001445

Head, J. W., Mustard, J. F., Kreslavsky, M. A., Milliken, R. E., & Marchant, D. R. Recent ice ages on Mars. , 426 Nature § (2003).

Head, J. W., Nahm, A. L., Marchant, D. R., & Neukum, G. (2006). Modification of the dichotomy boundary on Mars by Amazonian mid-latitude regional glaciation. *Geophysical Research Letters*, *33*(L08S03). https://doi.org/10.1029/2005GL024360

Horgan, B. H. N., & Bell, J. F. (2012). Widespread weathered glass on the surface of Mars. *Geology*, *40*(5), 391–394. https://doi.org/10.1130/G32755.1

Horgan, B. H. N., Cloutis, E. A., Mann, P., & Bell, J. F. (2014). Near-infrared spectra of ferrous mineral mixtures and methods for their identification in planetary surface spectra. *Icarus*, *234*, 132–154. https://doi.org/10.1016/j.icarus.2014.02.031

Horgan, B. H. N., Smith, R. J., Cloutis, E. A., Mann, P., & Christensen, P. R. (2017). Acidic weathering of basalt and basaltic glass: 1. Near-infrared spectra, thermal infrared spectra, and implications for Mars. *Journal of Geophysical Research: Planets*, *122*(1), 172–202. https://doi.org/10.1002/2016JE005111

Hurowitz, J. A., Fischer, W. W., Tosca, N. J., & Milliken, R. E. (2010). Origin of acidic surface waters and the evolutionof atmospheric chemistry on early Mars. *Nature Geoscience*, *3*(5), 323–326. https://doi.org/10.1038/ngeo831

Jones, E., Caprarelli, G., Mills, F., Doran, B., & Clarke, J. (2014). An Alternative Approach to Mapping Thermophysical Units from Martian Thermal Inertia and Albedo Data Using a Combination of Unsupervised Classification Techniques. *Remote Sensing*, *6*(6), 5184–5237. https://doi.org/10.3390/rs6065184

Kamps, O. M., Hewson, R. D., Ruitenbeek, F. J. A. Van, & Meer, F. D. Van Der. (2019). *Defining Surface Types of Mars using Global CRISM Summary Product Maps*.

Li, H., Robinson, M. S., & Jurdy, D. M. (2005). Origin of martian northern hemisphere mid-latitude lobate debris aprons. *Icarus*, *176*, 382–394. https://doi.org/10.1016/j.icarus.2005.02.011

Lillesand, T. M., & Kiefer, R. W. (1979). *Remote sensing and image interpretation*. John Wiley and Sons, New York. https://doi.org/10.2307/634969

Loizeau, D., Mangold, N., Poulet, F., Bibring, J.-P., Bishop, J. L., Michalski, J., & Quantin, C. (2015). History of the clay-rich unit at Mawrth Vallis, Mars: High-resolution mapping of a candidate landing site. *Journal of Geophysical Research: Planets*, *120*(11), 1820–1846. https://doi.org/10.1002/2015JE004894

Marinova, M. M., Aharonson, O., & Asphaug, E. (2008). Mega-impact formation of the Mars hemispheric dichotomy. *Nature*, *453*(7199), 1216–1219. https://doi.org/10.1038/nature07070

Mellon, M. T., Jakosky, B. M., Kieffer, H. H., & Christensen, P. R. (2000). High-Resolution Thermal Inertia Mapping from the Mars Global Surveyor Thermal Emission Spectrometer. *Icarus*, *148*, 437–455. https://doi.org/10.1006/icar.2000.6503

Ming, D. W., & Morris, R. V. Chemical, mineralogical, and physical properties of Martian dust

and soil. , Dust in the Atmosphere of Mars § (2017).

Murchie, S., Arvidson, R., Bedini, P., Beisser, K., Bibring, J. P., Bishop, J., … Wolff, M. (2007). Compact Connaissance Imaging Spectrometer for Mars (CRISM) on Mars Reconnaissance Orbiter (MRO). *Journal of Geophysical Research E: Planets*, *112*(5), 1–57. https://doi.org/10.1029/2006JE002682

Murchie, S., Guinness, E., & Slavney, S. (2016). *Mars Reconnaissance Orbiter CRISM Data Product Software Interface Specification Version 1.3.7.4*.

Ody, A., Poulet, F., Bibring, J.-P., Loizeau, D., Carter, J., Gondet, B., & Langevin, Y. (2013). Global investigation of olivine on Mars: Insights into crust and mantle compositions. *Journal of Geophysical Research: Planets*, *118*(2), 234–262. https://doi.org/10.1029/2012JE004149

Ody, A., Poulet, F., Langevin, Y., Bibring, J. P., Bellucci, G., Altieri, F., … Manaud, N. (2012). Global maps of anhydrous minerals at the surface of Mars from OMEGA/MEx. *Journal of Geophysical Research E: Planets*, *117*(9), 1–14. https://doi.org/10.1029/2012JE004117

Oehler, D. Z., & Allen, C. C. (2010). Evidence for pervasive mud volcanism in Acidalia Planitia, Mars. *Icarus*, *208*(2), 636–657. https://doi.org/10.1016/j.icarus.2010.03.031

Orgel, C., Hauber, E., Gasselt, S., Reiss, D., Johnsson, A., Ramsdale, J. D., … Teodoro, L. F. A. (2019). Grid Mapping the Northern Plains of Mars: A New Overview of Recent Water- and Ice-Related Landforms in Acidalia Planitia. *Journal of Geophysical Research: Planets*, *124*(2), 454–482. https://doi.org/10.1029/2018JE005664

Pan, L., & Ehlmann, B. L. (2014). Phyllosilicate and hydrated silica detections in the knobby terrains of Acidalia Planitia, northern plains, Mars. *Geophysical Research Letters*, *41*(6), 1890–1898. https://doi.org/10.1002/2014GL059423

Pan, L., Ehlmann, B. L., Carter, J., & Ernst, C. M. (2017). The stratigraphy and history of Mars' northern lowlands through mineralogy of impact craters: A comprehensive survey. *Journal of Geophysical Research: Planets*, *122*(9), 1824–1854. https://doi.org/10.1002/2017JE005276

Parker, T. J., Gorsline, D. S., Saunders, R. S., Pieri, D. C., & Schneeberger, D. M. (1993). Coastal geomorphology of the Martian northern plains. *Journal of Geophysical Research*, *98*(E6), 11061–11078. https://doi.org/10.1029/93je00618

Pelkey, S. M., Mustard, J. F., Murchie, S., Clancy, R. T., Wolff, M., Smith, M., … Gondet, B. (2007). CRISM multispectral summary products: Parameterizing mineral diversity on Mars from reflectance. *Journal of Geophysical Research E: Planets*, *112*(8), 1–18. https://doi.org/10.1029/2006JE002831

Poulet, F., Gomez, C., Bibring, J. P., Langevin, Y., Pinet, P., Belluci, G., & Mustard, J. (2007). Martian surface mineralogy from Observatoire pour la Minéralogie, l'Eau, les Glaces et

l'Activité on board the Mars Express spacecraft (OMEGA/MEx): Global mineral maps. *Journal of Geophysical Research E: Planets*, *112*(8). https://doi.org/10.1029/2006JE002840

Riu, L., Poulet, F., Bibring, J. P., & Gondet, B. (2019). The M3 project: 2 - Global distributions of mafic mineral abundances on Mars. *Icarus*, *322*, 31–53. https://doi.org/10.1016/j.icarus.2019.01.002

Rogers, A. D., & Christensen, P. R. (2007). Surface mineralogy of Martian low-albedo regions from MGS-TES data: Implications for upper crustal evolution and surface alteration. *J. Geophys. Res*, *112*, 1003. https://doi.org/10.1029/2006JE002727

Rogers, A. D., & Hamilton, V. E. (2015). Compositional provinces of Mars from statistical analyses of TES, GRS, OMEGA and CRISM data. *Nature*, *175*(4449), 238. https://doi.org/10.1038/175238c0

Ruff, S. W., & Christensen, P. R. (2002). Bright and dark regions on Mars: Particle size and mineralogical characteristics based on thermal emission spectrometer data. *Journal of Geophysical Research E: Planets*, *107*(12), 10–11. https://doi.org/10.1029/2001je001580

Salvatore, M. R., Mustard, J. F., Wyatt, M. B., & Murchie, S. L. (2010). Definitive evidence of Hesperian basalt in Acidalia and Chryse planitiae. *Journal of Geophysical Research*, *115*(E7). https://doi.org/10.1029/2009je003519

Seelos, F. P., Murchie, S. L., & Hopkins, J. (2018). CRISM Mapping Data Empirical Radiometric Reconciliation for the Next-Generation Mars Global Multispectral Map. *49th Lunar and Planetary Science Conference*.

Seelos, K. D., Viviano, C. E., Ackiss, S. E., Kremer, C. H., & Murchie, S. L. (2019). The MICA Files: A Compilation and Reference Document for Minerals Identified Through CRISM Analysis. *50th Lunar and Planetary Science Conference*.

Singer, R., & Roush, T. (1983). Spectral reflectance properties of particulate weathered coatings on rocks: Laboratory modeling and applicability to Mars. *Proc. Lunar Planet. Sci. XIV*, 708–709. Retrieved from http://articles.adsabs.harvard.edu/pdf/1983LPI....14..708S

Smith, D. E., Zuber, M. T., Solomon, S. C., Phillips, R. J., Head, J. W., Garvin, J. B., … Duxbury, T. C. (1999). The global topography of Mars and implications for surface evolution. *Science*, *284*(5419), 1495–1503. https://doi.org/10.1126/science.284.5419.1495

Tanaka, K. L., Robbins, S. J., Fortezzo, C. M., Skinner, J. A., & Hare, T. M. (2014). The digital global geologic map of Mars: Chronostratigraphic ages, topographic and crater morphologic characteristics, and updated resurfacing history. *Planetary and Space Science*, *95*, 11–24. https://doi.org/10.1016/j.pss.2013.03.006

Tanaka, K. L., Skinner, J. A., Dohm, J. M., Irwin, R. P., Kolb, E. J., Fortezzo, C. M., … Hare, T.

M. (2014). *USGS Scientific Investigations Map 3292, pamphlet*.

Tanaka, K. L., Skinner, J., & Hare, T. (2005). *Geologic map of the northern plains of Mars*. Retrieved from ftp://pdsimage2.wr.usgs.gov/pub/pigpen/mars/geology/NPlains_geology_SIM2888_2005_pamphlet.pdf

Tukey, J. W. (1977). *Exploratory data analysis*. Reading, Mass. : Addison-Wesley Pub. Co.

Vago, J. L. (2014). *Recommendation for the Narrowing of ExoMars 2018 Landing Sites*.

Viviano-Beck, C. E., Seelos, F. P., Murchie, S. L., Kahn, E. G., Seelos, K. D., Taylor, H. W., … Morgan, M. F. (2014). Revised CRISM spectral parameters and summary products based on the currently detected mineral diversity on Mars. *Journal of Geophysical Research E: Planets*, *119*(6), 1403–1431. https://doi.org/10.1002/2014JE004627

Watters, T. R., Mcgovern, P. J., & Iii, R. P. I. (2007). *Hemispheres Apart: The Crustal Dichotomy on Mars*. https://doi.org/10.1146/annurev.earth.35.031306.140220

Wiseman, S. M., Arvidson, R. E., Wolff, M. J., Smith, M. D., Seelos, F. P., Morgan, F. L., … Mcguire, P. C. (2014). Characterization of Artifacts Introduced by the Empirical Volcano-Scan Atmospheric Correction Commonly Applied to CRISM and OMEGA Near-Infrared Spectra. *Icarus*. https://doi.org/10.1016/j.icarus.2014.10.012

Wold, S., Esbensen, K., & Geladi, P. (1987). Principal Component Analysis. *Chemometrics and Intelligent Laboratory Systems*, *2*, 37–52.

Wyatt, M. B., & McSween, H. Y. (2002). Spectral evidence for weathered basalt as an alternative to andesite in the northern lowlands of Mars. *Nature*, *417*(6886), 263–266. https://doi.org/10.1038/417263a

Wyatt, M. B., McSween, H. Y., Tanaka, K. L., & Head, J. W. (2004). Global geologic context for rock types and surface alteration on Mars. *Geology*, *32*(8), 648–654. https://doi.org/10.1130/G20527.1

Wyatt, M. B., McSween Jr., H. Y., Moersch, J. E., & Christensen, P. R. (2003). Analysis of surface compositions in the Oxia Palus region on Mars from Mars Global Surveyor Thermal Emission Spectrometer Observations. *Journal of Geophysical Research*, *108*(E9), 1–16. https://doi.org/10.1029/2002je001986

Zuber, M. T. (2000). Internal structure and early thermal evolution of Mars from Mars global surveyor topography and gravity. *Science*, *287*(5459), 1788–1793. https://doi.org/10.1126/science.287.5459.1788

APPENDICES

Appendix 1. Principal Component Maps

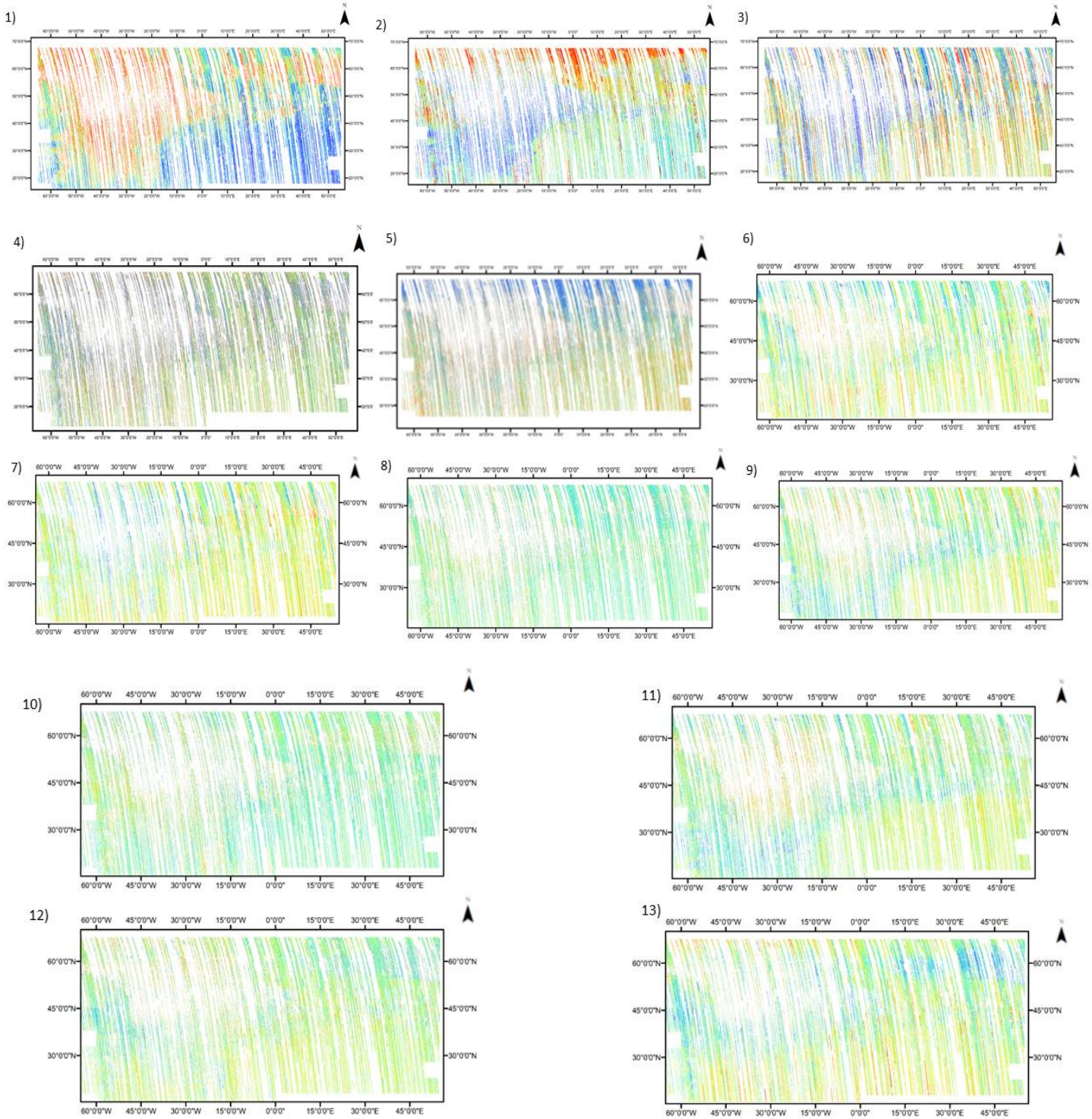

Appendix 2. OMEGA Global Maps

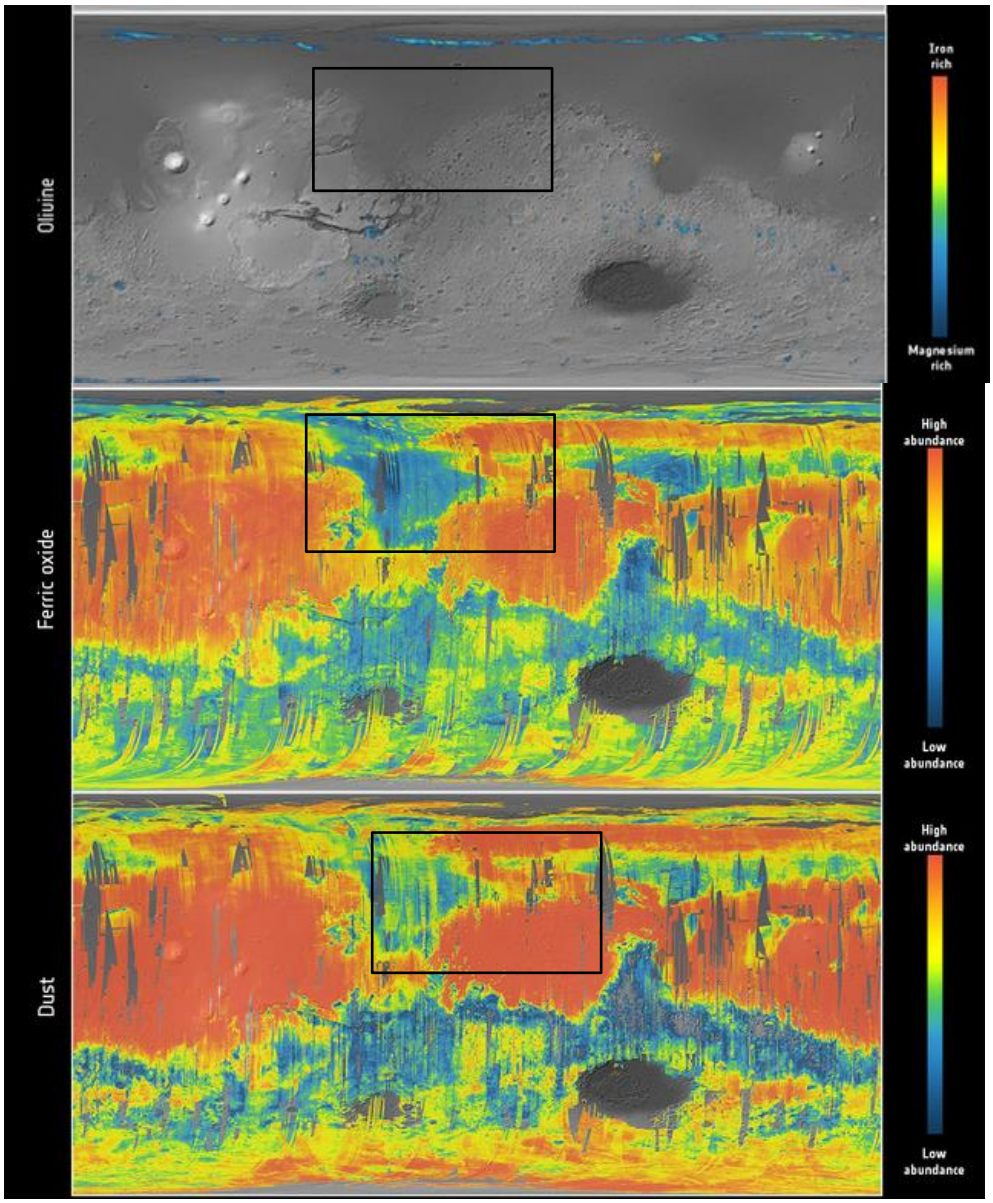

Global Maps indicating a)Olivine,b)Ferric Oxide and c)Dust cover (Ody et al., 2013; Ody et al., 2012) with the study area indicated in the black rectangle.

Appendix 3 : Summary Product Maps

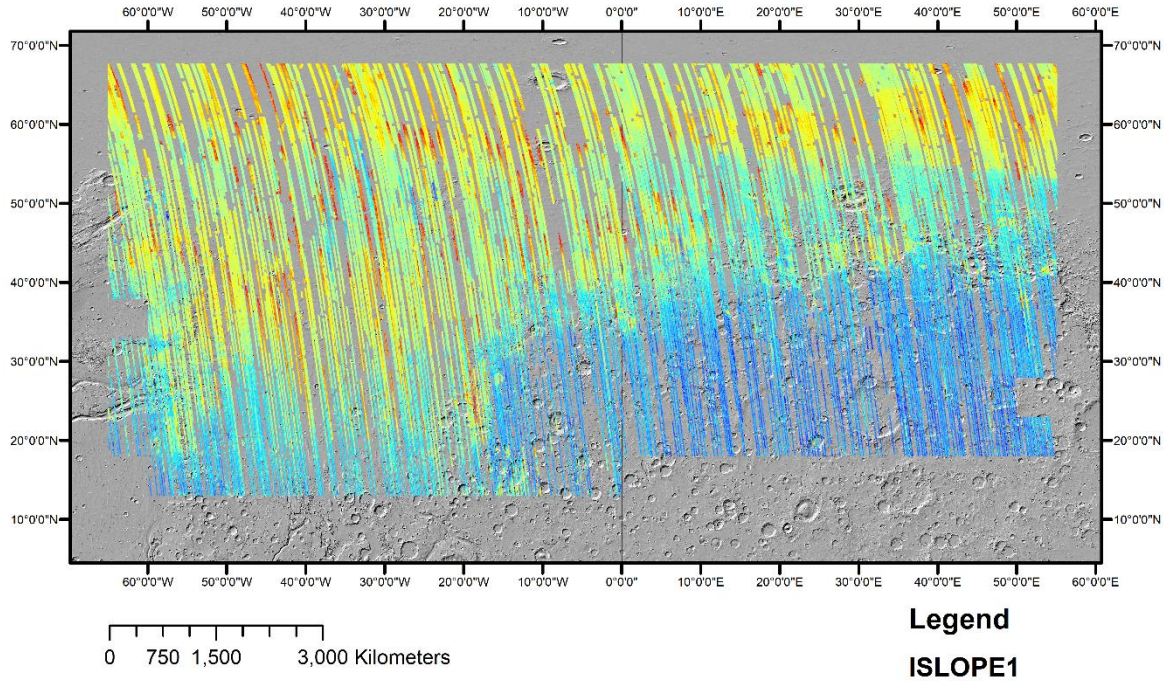

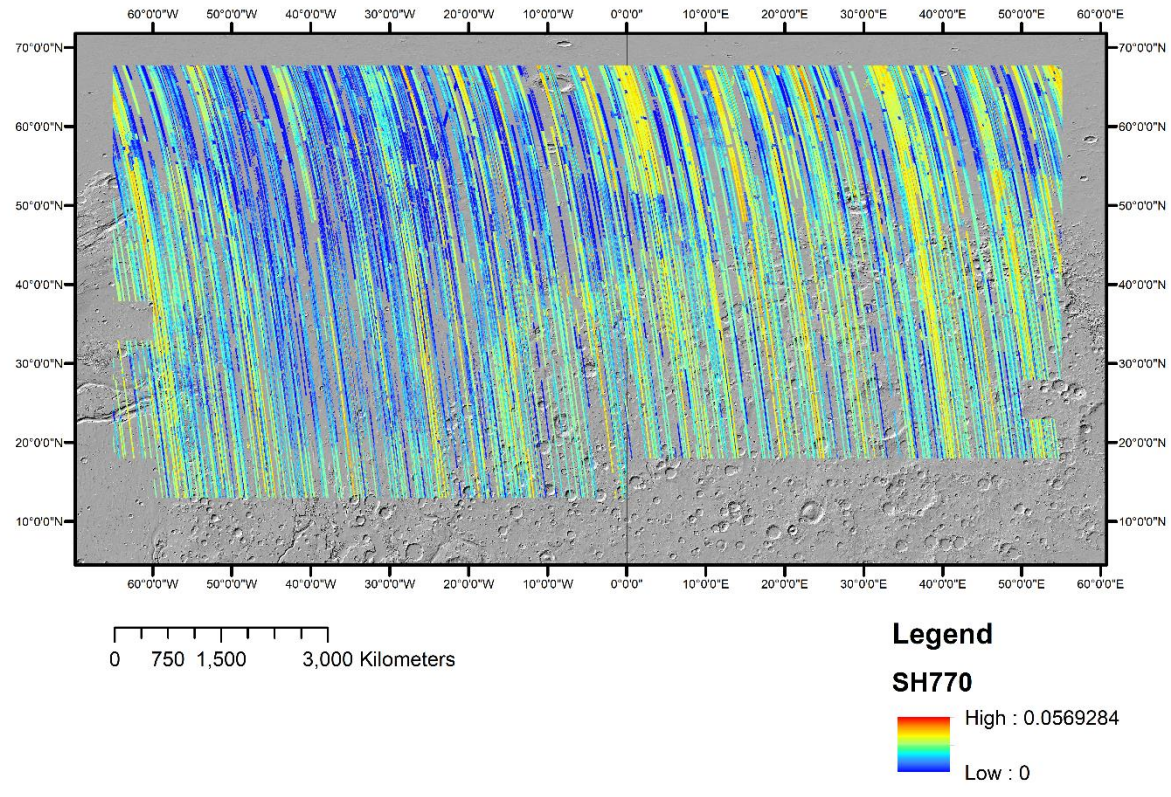

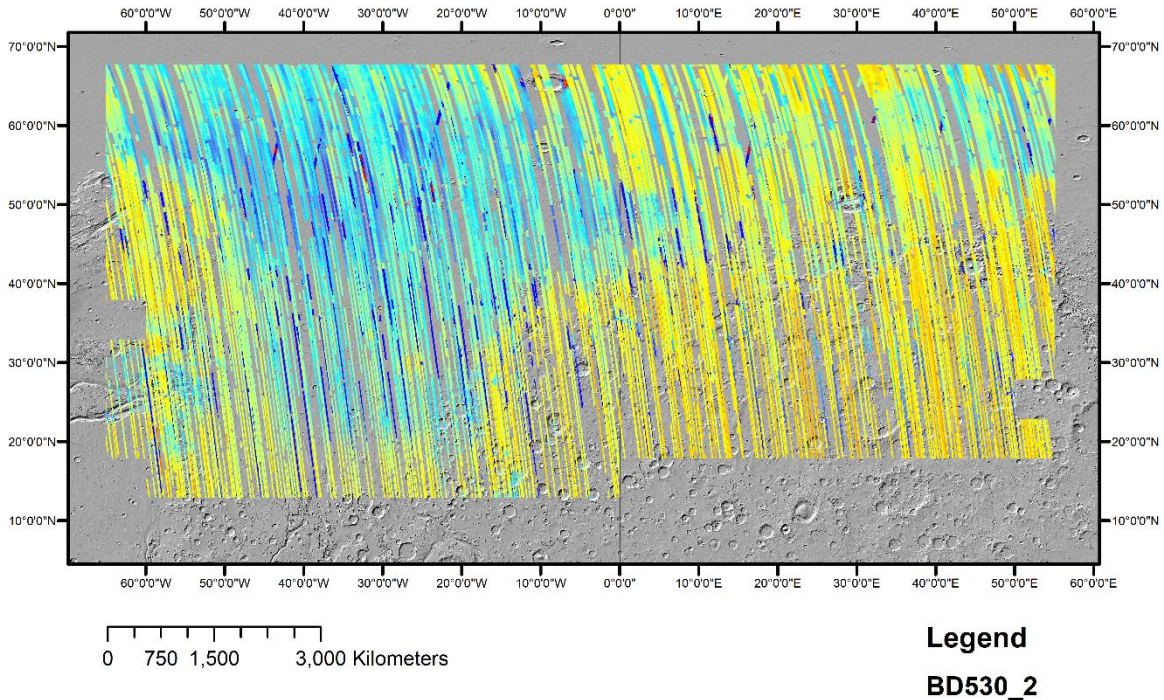

0 750 1,500 3,000 Kilometers

Legend

BD530_2

High : 0.403

Low : 0

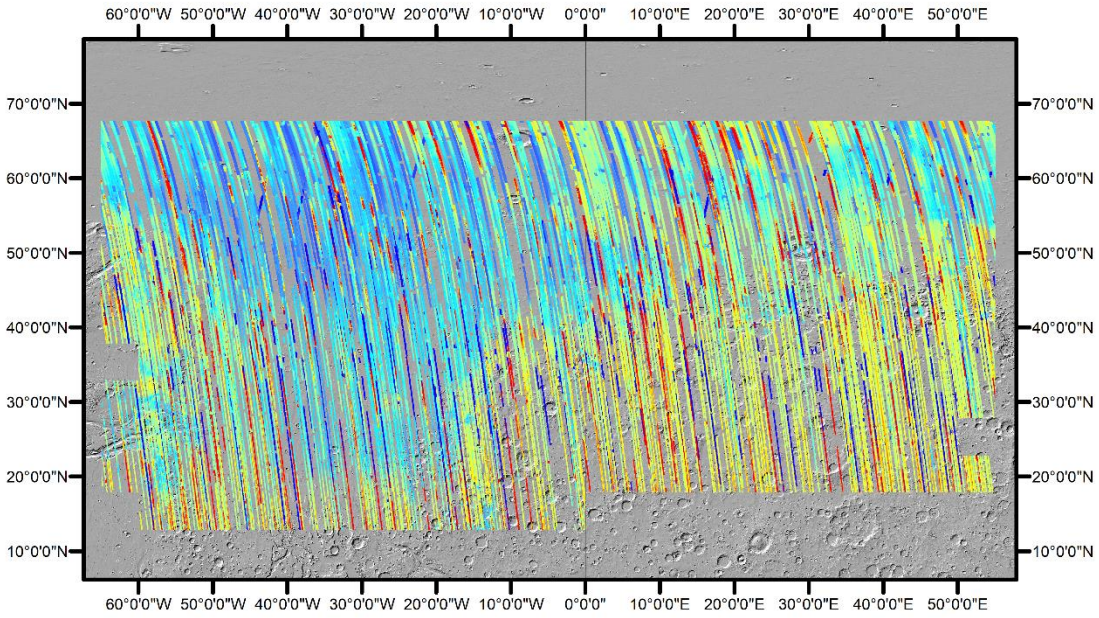

0 1,000 2,000 4,000 Kilometers

Legend

RBR

High : 16

Low : 0

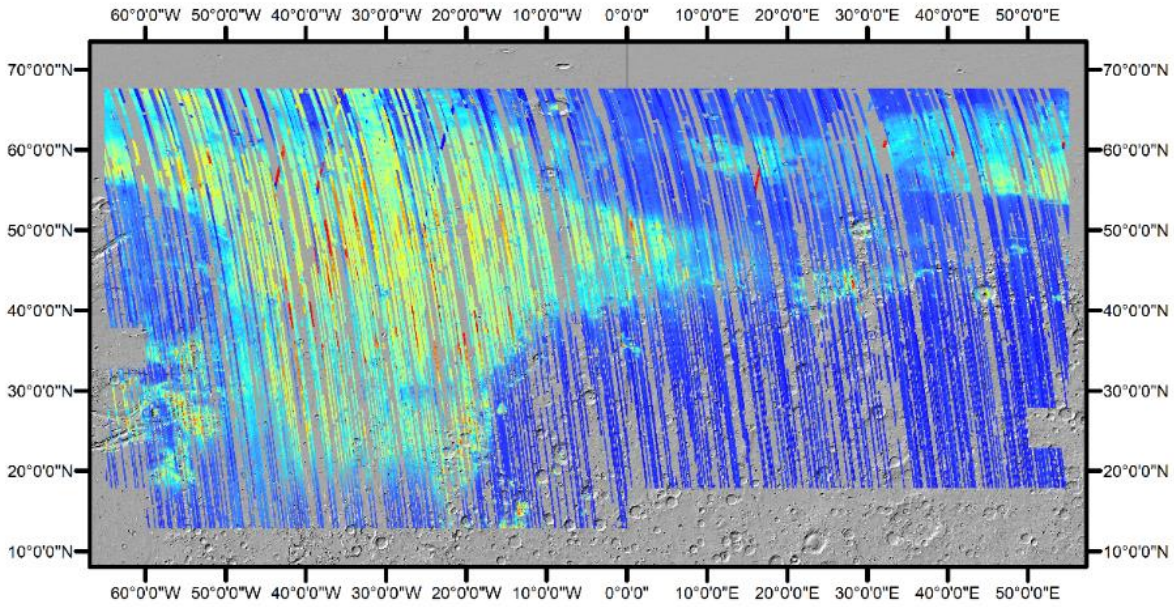

Legend

BDI1000VIS

High : 0.03

Low : 0

0 1,000 2,000 4,000 Kilometers

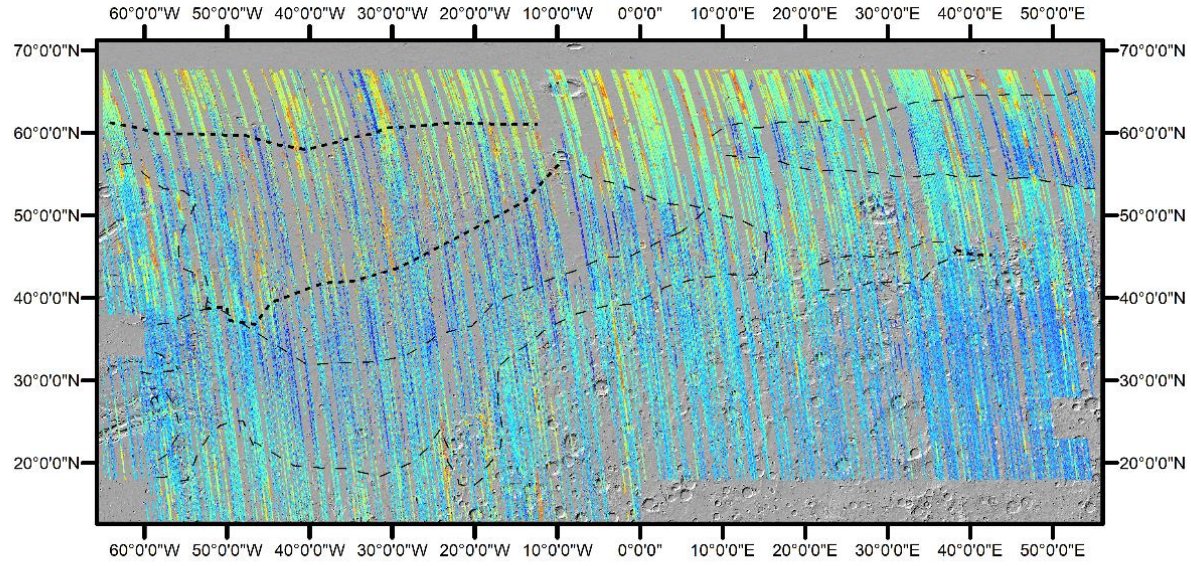

Legend

BD1900_2

High : 0.067

Low : 0

0 1,000 2,000 4,000 Kilometers

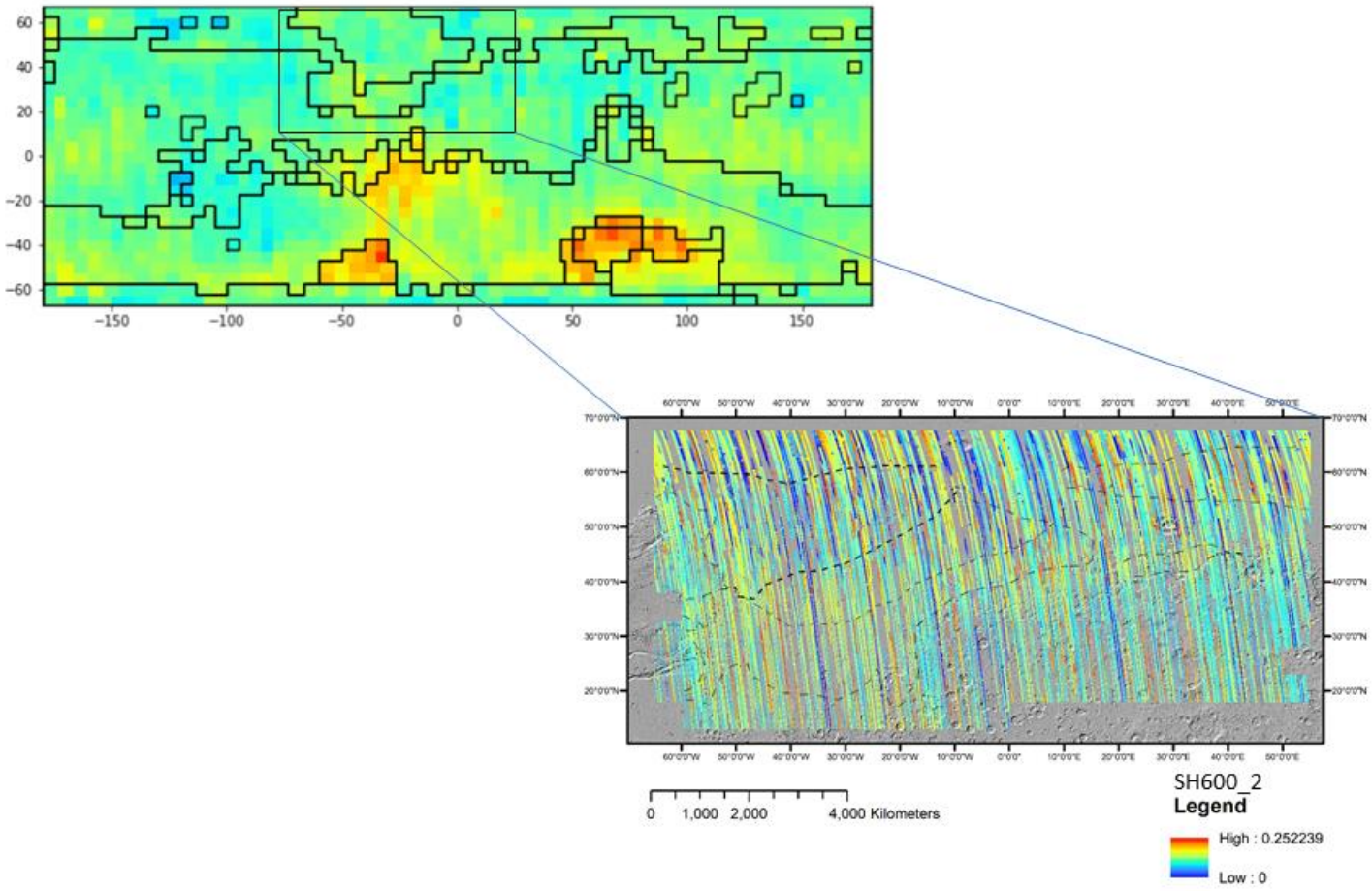

Global map (Kamps et al., 2019) and study area map of the Viviano-Beck et al. (2014) SH600_2

Appendix 4 : CRISM MSP Browse products for Mawrth Vallis

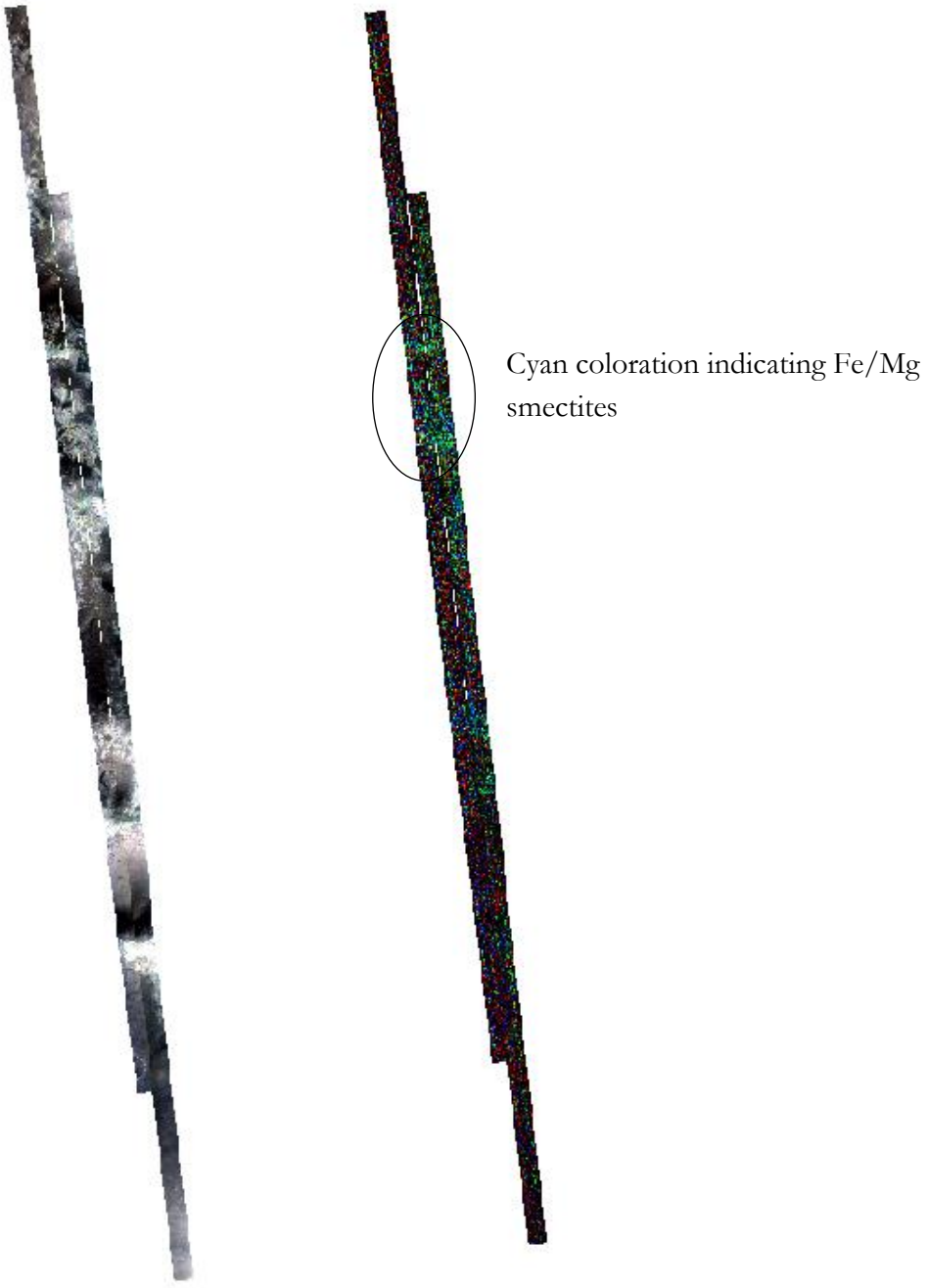

CRISM MSP Browse Products a) FAL b) PFM showing subtle patterns but mostly noisy.

Appendix 5 : TES Sulfate Map

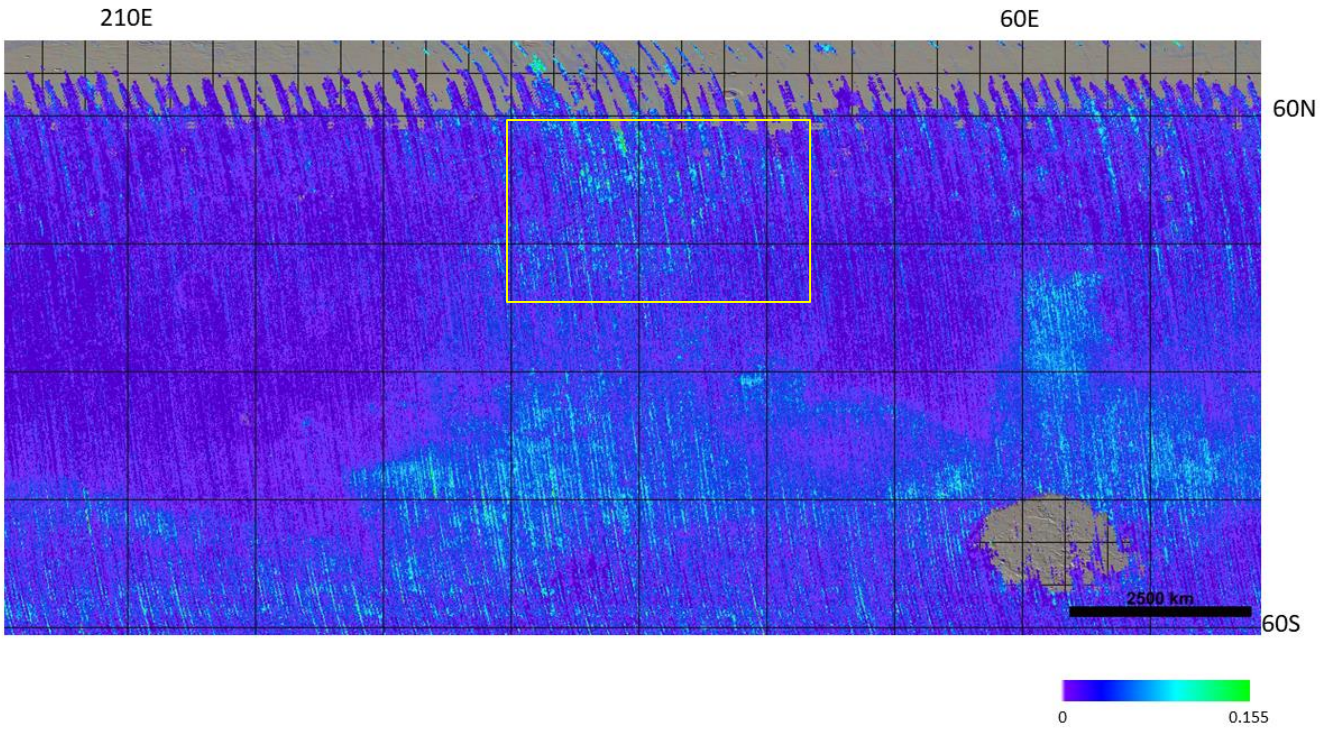

TES Sulfate Abundance Map (Bandfield et al., 2000) with study area indicated

Appendix 6 : List of processed CRISM MSP image IDs

Product ID
msp00002845_07_if214*_trr3
msp00003043_07_if214*_trr3
msp000033a3_07_if214*_trr3
msp0000350c_05_if214*_trr3
msp000084df_01_if214*_trr3
msp00026b69_07_if214*_trr3
msp0002aa9c_01_if214*_trr3
msp00008898_05_if214*_trr3
msp0002ca8e_01_if214*_trr3
msp0000d66d_03_if214*_trr3
msp00041851_01_if214*_trr3
msp00003351_07_if214*_trr3
msp00003fce_07_if214*_trr3
msp000089fe_01_if214*_trr3
msp0000b08b_03_if214*_trr3
msp00018fcc_01_if214*_trr3
msp00019ef1_01_if214*_trr3
msp000260fe_05_if214*_trr3
msp0002df06_03_if214*_trr3
msp00030139_01_if214*_trr3
msp0003a9c5_05_if214*_trr3
msp000418da_01_if214*_trr3
msp00002f49_07_if214*_trr3
msp000048f1_01_if214*_trr3
msp0000d76c_03_if214*_trr3
msp000105f1_01_if214*_trr3
msp000121a9_01_if214*_trr3
msp000144d3_01_if214*_trr3
msp00014c00_01_if214*_trr3
msp000235e6_01_if214*_trr3
msp00026ee7_07_if214*_trr3
msp00029017_01_if214*_trr3

Appendix 7 : Comparison with OMEGA

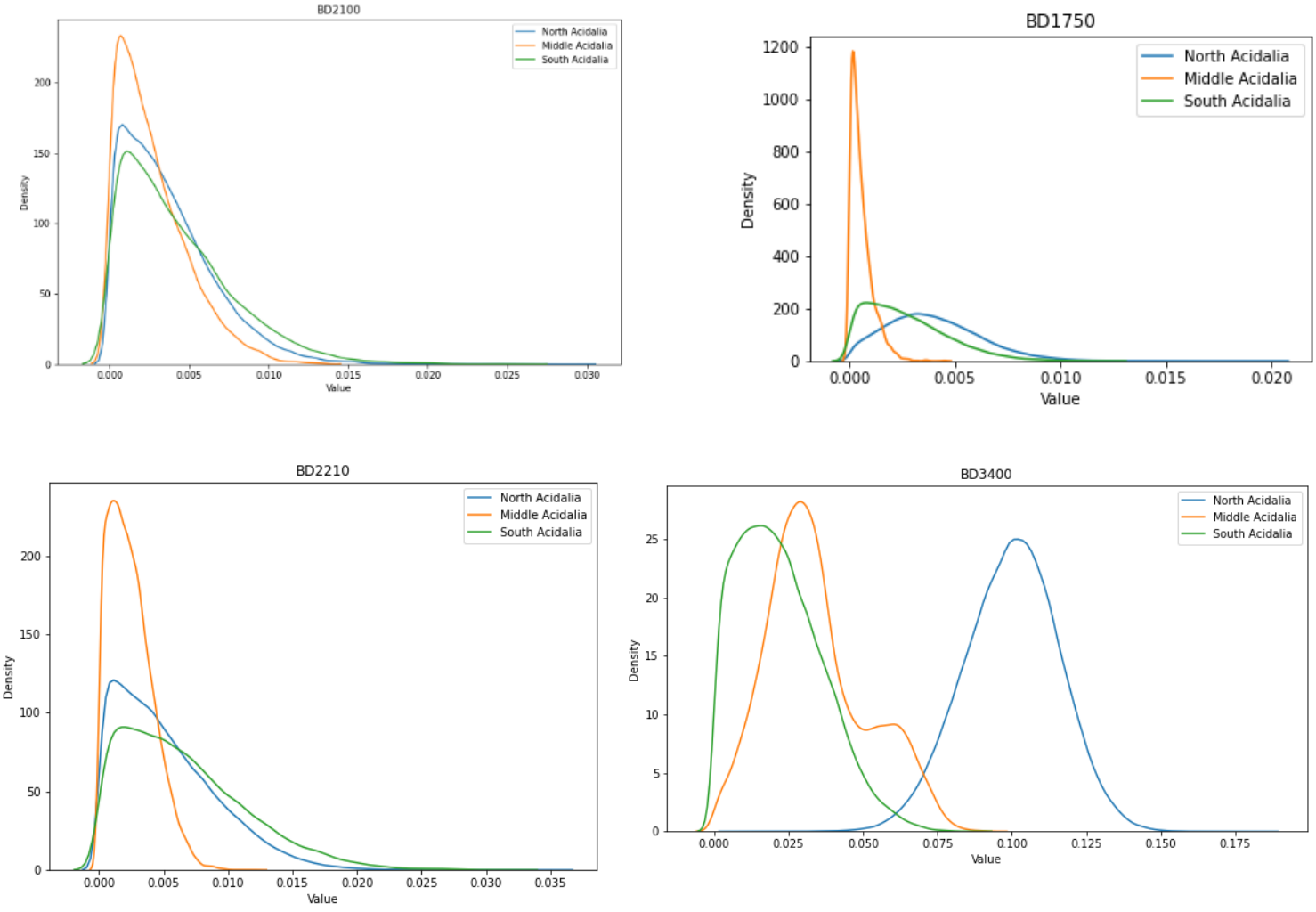

Density plot indicating distribution of pixels having high values for a) BD1750_2 b)BD3400_2 c)BD2100_2 and d) BD2210_2 for regions South Acidalia – Region A, Middle Acidalia -Region B, North Acidalia – Region C.

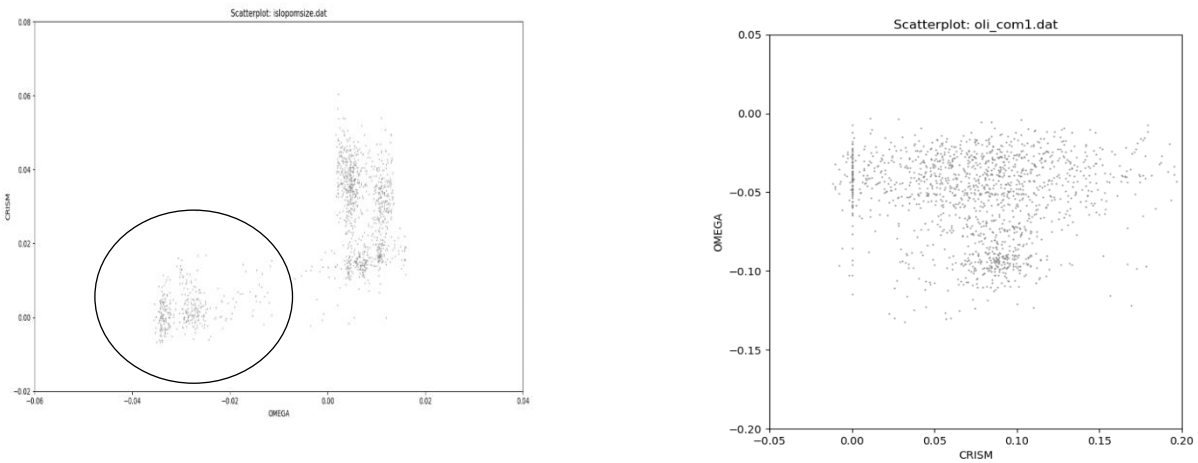

Scatterplots between CRISM and OMEGA summary products a) ISLOPE1 with the Region F pixels circled showing low values indicating an upward slope b) OLINDEX3

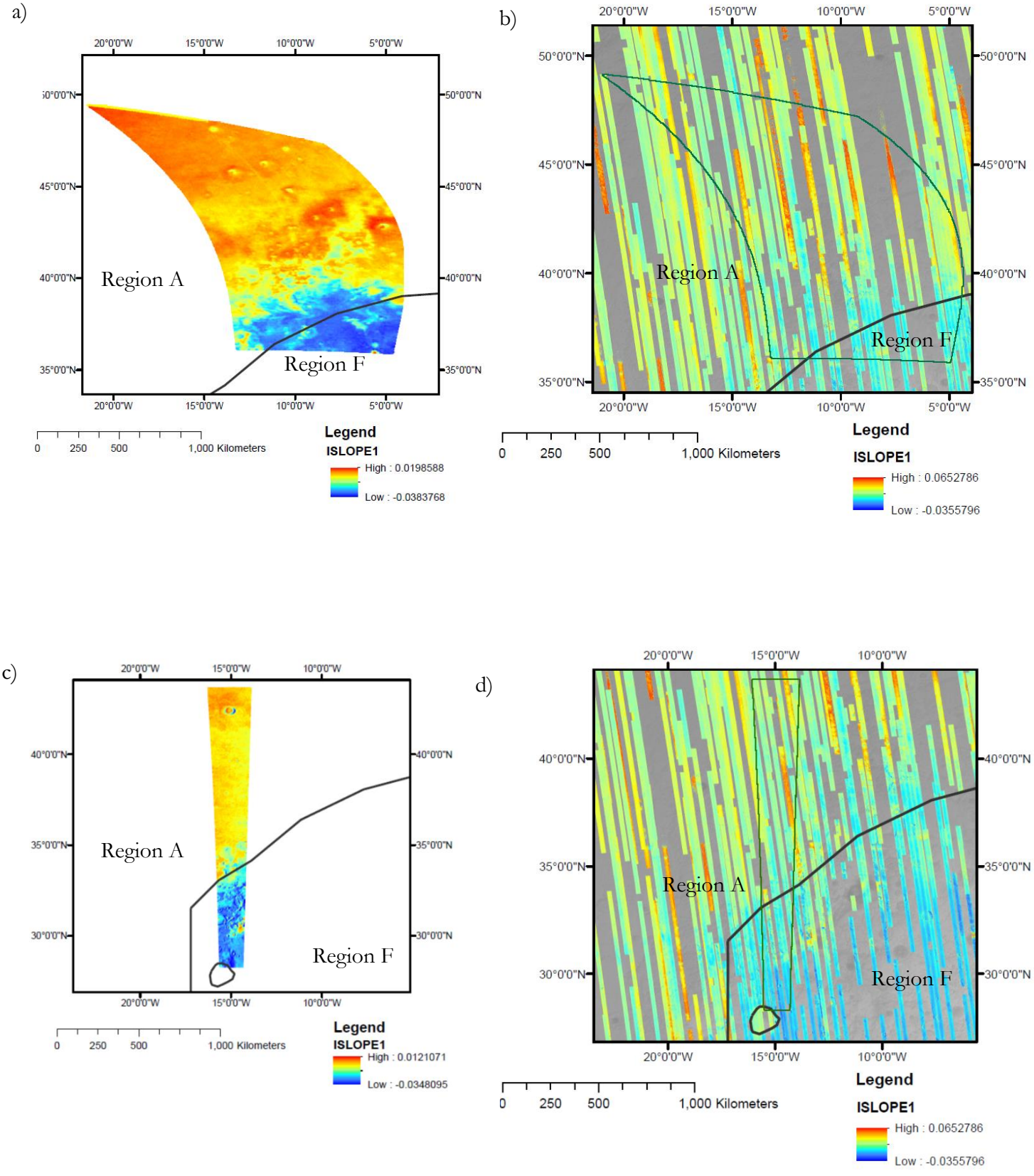

Comparison between ISLOPE1 products on the OMEGA scenes a) 314_4 c) 2398_4 and b) & d) corresponding CRISM mosaic with the OMEGA scene outlined.

Appendix 8 : Global Maps (Kamps et al., 2019) for the evaporites summary products

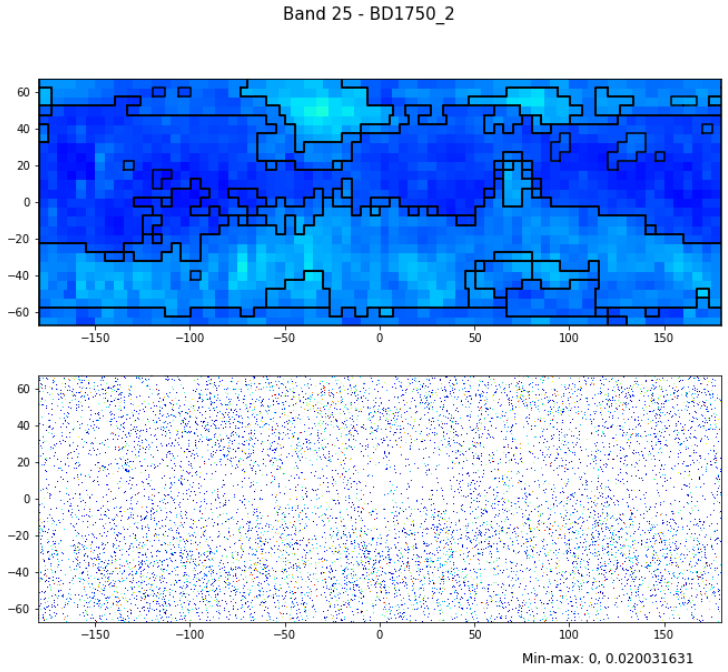

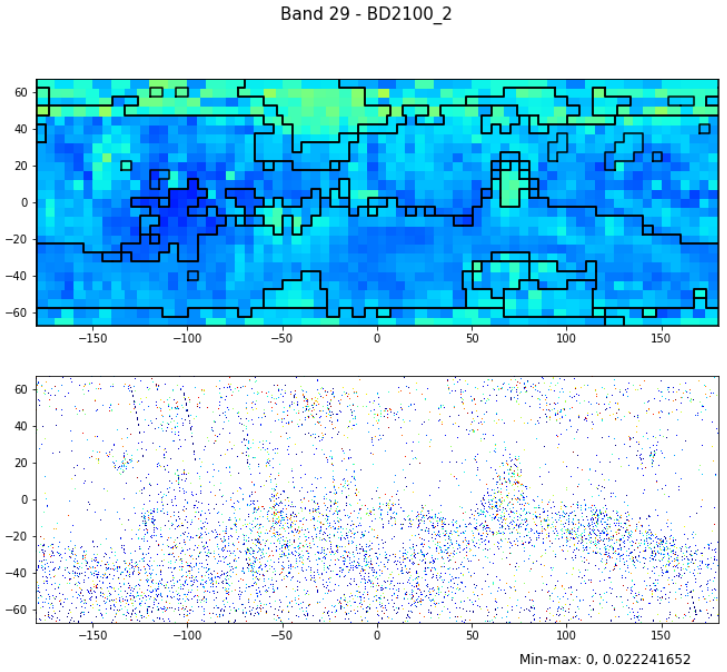

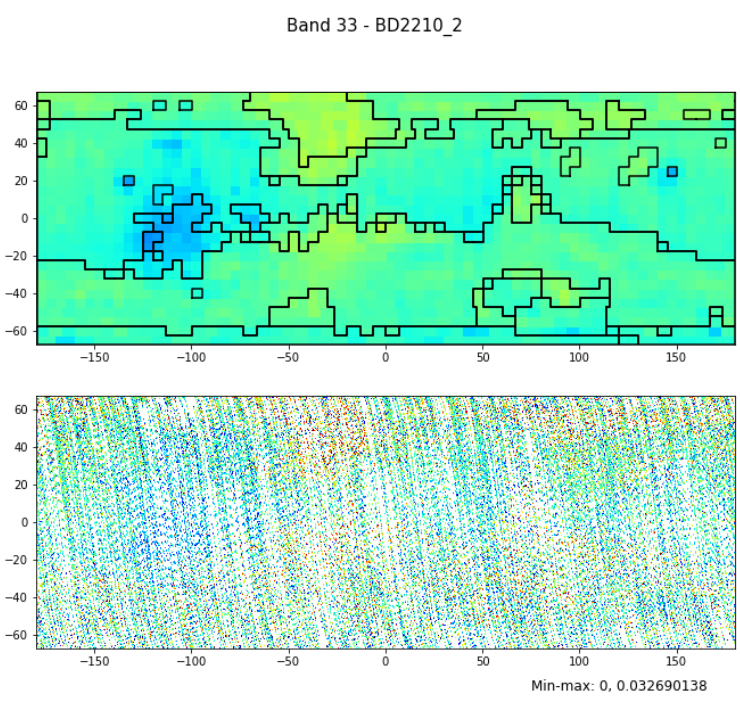

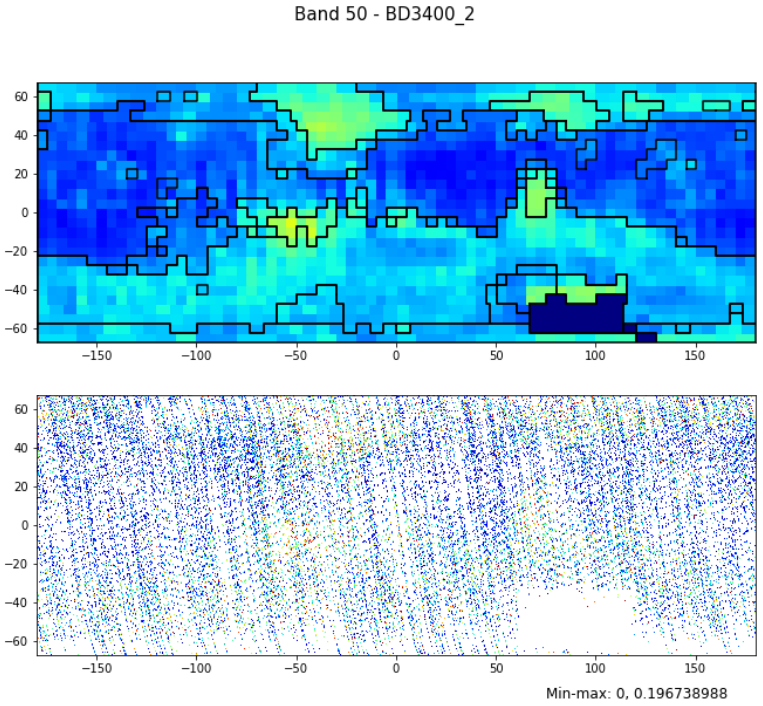

Global averaged and non averaged maps of evaporites summary products generated by Kamps et al. (2019)

Appendix 9 : Interesting landforms in Acidalia Planitia

a)

b)

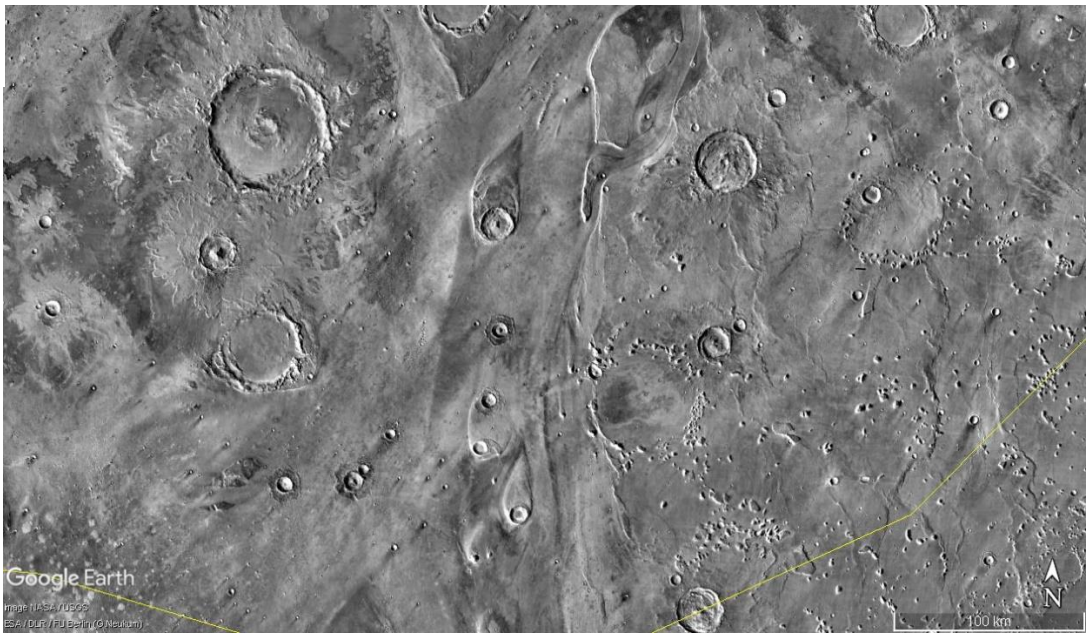

a) Polygonally Patterned ground in Northern Acidalia – Region C b) Tear drop shaped landforms indicating flow of materials in the Hesperian outflow channels in Region A.